SIMULATION OF ORTHOGONAL METAL CUTTING BY FINITE ELEMENT ANALYSIS

A THESIS SUBMITTED TO
THE GRADUATE SCHOOL OF NATURAL AND APPLIED SCIENCES
OF
THE MIDDLE EAST TECHNICAL UNIVERSITY

BY

HALİL BİL

IN PARTIAL FULFILLMENT OF THE REQUIREMENTS FOR THE DEGREE OF

MASTER OF SCIENCE

IN

THE DEPARTMENT OF MECHANICAL ENGINEERING

AUGUST 2003

Approval of the Graduate School of Natural and Applied Sciences.

Prof. Dr. Canan ÖZGEN
Director

I certify that this thesis satisfies all requirements as a thesis for the degree of Master of Science.

Prof. Dr. Kemal İDER
Head of Department

This is certify that we have read this thesis and that in our opinion it is fully adequate, in scope and quality, as a thesis for the degree of Master of Science.

Prof. Dr. A. Erman Tekkaya
Co-Supervisor

Prof. Dr. S. Engin Kılıç
Supervisor

Examining Committee Members:

Prof. Dr. Alp ESİN (Chairperson)

Prof. Dr. S. Engin KILIÇ (Supervisor)

Prof. Dr. A. Erman TEKKAYA (Co-Supervisor)

Asst. Dr. Serkan DAĞ

Prof. Dr. Turgut TOKDEMİR

ABSTRACT

SIMULATION OF ORTHOGONAL METAL CUTTING BY FINITE ELEMENT ANALYSIS

Halil BİL
M.Sc., Department of Mechanical Engineering
Supervisor: Prof. Dr. S. Engin KILIÇ
Co-Supervisor: Prof. Dr. A. Erman TEKKAYA

August 2003, 115 pages

The aim of this thesis is to compare various simulation models of orthogonal cutting process with each other as well as with various experiments. The effects of several process parameters, such as friction and separation criterion, on the results are analyzed. As simulation tool, commercial implicit finite element codes MSC.Marc, Deform2D and the explicit code Thirdwave AdvantEdge are used. Separation of chip from the workpiece is achieved either only with continuous remeshing or by erasing elements according to the damage accumulated. From the results cutting and thrust forces, shear angle, chip thickness and contact length between the chip and the rake face of the tool can be estimated. For verification of results several cutting experiments are performed at different cutting conditions, such as rake angle and feed rate. Results show that commercial codes are able to simulate orthogonal cutting operations within reasonable limits.

Friction is found to be the most critical parameter in the simulation, since good agreement can be achieved for individual process variables by tuning it. Therefore, simulation results must be assessed with all process variables and friction parameter should be tuned according to the shear angle results.

Plain damage model seems not appropriate for separation purposes of machining simulations. On the other hand, although remeshing gives good results, it leads to the misconception of crack generation at the tip of the tool. Therefore, a new separation criterion is necessary to achieve both good physical modeling and prediction of process variables.

Keywords: Finite Element Method, Orthogonal Metal Cutting, Remeshing, Damage, Friction.

ÖZ

DİK KESME İŞLEMLERİNİN SONLU ELEMAN ANALİZİ İLE SİMULASYONU

Halil BİL
Yüksek Lisans, Makine Mühendisliği Bölümü

Tez Yöneticisi: Prof. Dr. S. Engin KILIÇ
Yardımcı Tez Yöneticisi: Prof. Dr. A. Erman TEKKAYA

Ağustos 2003, 115 sayfa

Bu tezin amacı, dik kesme işlemleri için geliştirilmiş çeşitli sonlu eleman modellerinin birbirleriyle ve deneyler ile karşılaştırılmasıdır. Sürtünme koşulları ve ayrılma kriterleri gibi parametrelerin sonuçlar üzerindeki etkisi incelenmiştir. Simülasyon aracı olarak, kapalı kodlar olan MSC.Marc ve Deform2D ile açık bir kod olan Thirdwave AdvantEdge kullanılmıştır. Talaşın iş parçasından ayrılması, sürekli yeni ağ tanımlanması veya elemanların toplam hasara göre silinmesi ile elde edilmiştir. Sonuçlardan, kesme ve ilerleme kuvvetleri, kayma açısı, talaş kalınlığı ve kalem ile talaş arasındaki temas uzunluğu tahmin edilebilmektedir. Sonuçların doğrulanması için değişik kesme koşullarında (kesme açısı ve ilerleme hızı) deneyler yapılmıştır. Sonuçlar, ticari yazılımlarının dik kesme işlemlerini kabul edilebilir sınırlar içerisinde simüle edebileceğini göstermiştir.

Sürtünme koşullarının simülasyonu etkileyen en önemli parametre olduğu bulunmuştur. Çünkü, bu parametrenin ayarlanması ile her işlem değişkeni için ayrı ayrı iyi sonuçlar elde edilebilmektedir. Dolayısıyla, simülasyon sonuçları

bütün işlem değişkenleri ile değerlendirilmelidir. Ayrıca, sürtünme koşulları kayma açısına göre ayarlanmalıdır.

Hasar modellerinin talaşın iş parçasından ayrılması amacı ile kullanılması uygun değil gibi görünmektedir. Yeni ağ tanımlanması ise iyi sonuçlar vermesine rağmen, iş parçası malzemesinde çatlak oluşması gibi bir kavram hatasına yol açmaktadır. Dolayısıyla, hem iyi bir fiziksel modelleme yapılması hem de işlem değişkenlerinin doğru tahmin edilebilmesi için yeni bir ayrılma kriterine ihtiyaç vardır.

Keywords: Finite Element Method, Orthogonal Metal Cutting, Remeshing, Damage, Friction.

To my family and Dilek Başaran.

ACKNOWLEDGEMENTS

I would like to express my appreciation to my supervisor Prof. Dr. S. Engin KILIÇ and my co-supervisor Prof. Dr. A. Erman TEKKAYA for their help and inspiration through out my thesis.

I am also grateful to the Femlab members: Kurşad Kayaturk, Ahmet Kurt, Özgür Koçak, Bahadır Koçaker, Muhsin Öcal and Mete Egemen for making the working days and nights in the laboratory a joy.

The support of Mechanical Engineering Department and Graduate School of Natural and Applied Sciences is also very much appreciated. I am also thankful to Ercenk Aktay from Figes Company, who made Thirdwave AdvantEdge available to use.

Lastly, I would like to express my deepest gratitude and respect to my family who made all the things possible. Their support and patience are just making me feel better.

TABLE OF CONTENTS

CHAPTERS

LIST OF TABLES

LIST OF FIGURES

LIST OF SYMBOLS AND ABBREVIATIONS

θ	Angle of Obliqueness
a_c	Uncut Chip Thickness
a_0	Chip Thickness
γ	Rake Angle
φ	Shear Angle
α	Clearance Angle
V	Relative Velocity Between Tool and Workpiece
V_c	Cutting Speed
B.U.E.	Built-Up Edge
β	Friction Angle
F_f	Frictional Force
F_n	Normal Force
F	Equivalent Force
μ	Friction Coefficient
h_1	Length of Sticking Region
h_2	Length of Sliding Region
δ	ratio of the plastic zone thickness to the cut chip thickness
l_c	Contact Length
V_s	Shearing Speed at Shear Zone
q	Heat
h	Convection Heat Transfer Coefficient
T_w	Workpiece Surface Temperature
T_0	Ambient Temperature
F_{fr}	Frictioanl Force
v_r	Relative Sliding Velocity Between Tool and Chip

M	Mechanical Equivalent of Heat
R	Rate of Specific Volumetric Flux
f	Fraction of Plastic Work Converted into Heat or Feed Rate
W^p	Rate of Plastic Work
ρ	Density
$\dot{\varepsilon}$	Strain-Rate
m	Friction Factor
k_y	Shear Yield Stress
t	Tangential Vector
$\overline{\sigma}$	Equivalent Stress
C	Critical Damage Value
Q_{chip}	Heat Given to Chip
Q_{tool}	Heat Given to Tool
$Q_{friction}$	Heat Genetared due to Friction
σ_f	Flow Stress
ε^p	Accumulated Plastic Strain
$\dot{\varepsilon}_0^p$	Reference Plastic Strain-Rate
m_1	Low Strain-Rate Sensitivity Exponent
m_2	High Strain-Rate Sensitivity Exponent
$\dot{\varepsilon}_t$	Treshold Strain Rate
T	Current Temperature
σ_0	Initial Yield Stress
T_0	Reference Temperature
ε_0^p	Reference Plastic Strain
$T(T)$	Thermal Softening Factor
r_c	Chip Thickness Ratio
d_c	Depth of Cut
F_c	Cutting Force
F_t	Thrust Force
T_{max}	Maximum Temperature

CHAPTER 1

INTRODUCTION

1.1 Introduction

Manufacturing technology has been the driving force behind modern economics since the Industrial Revolution (1770). Metal shaping processes, in particular, have created machinery and structures that permeate almost every aspect of human life today. Although manufacturing techniques have become more sophisticated, many processes and tool designs are still based on experience and intuition.

There are mainly two distinct classes of solid-state manufacturing processes. Deformation processes produce the required shape, with the necessary mechanical properties, by plastic deformation in which the material is moved and its volume is conserved. Machining processes produce the required shape by removal of selected areas of the workpiece through a machining process. Most machining is accomplished by straining a local region of the workpiece by the relative motion of the tool and the workpiece. Although mechanical energy is the usual input to most machining processes, some of the newer metal removal processes employ chemical, electrical and thermal energy. Machining is usually employed to produce shapes with high dimensional tolerance, good surface finish and often with complex geometry. Machining is a secondary processing operation since it is usually conducted on a workpiece that was produced by a primary

process such as hot rolling, forging or casting, etc. More than almost 80 percent of all manufactured parts must be machined before they are completed. There is a wide variety of machining processes and machine tools that can be utilized. Since the development of machine tools is parallel to the industrialization of the society, it is an old field with much specialized terminology and jargon.

Metal cutting processes are widely used to remove unwanted material and achieve dimensional accuracy and desired surface finish of engineering components. In metal cutting processes, the unwanted material is removed by the cutting tool, which is significantly harder than the workpiece. The width of cut is usually much larger than the depth of cut and thus, the chip is produced in a nearly plane strain condition

Importance of metal cutting operations may be understood by considering the total cost associated with this activity. For example, in the USA, the yearly cost associated with metal removal has been estimated at about 10 percent of the gross national product. The importance of the cutting process may be further appreciated by the observation that nearly every device in use in our complex society has one or more machined surface. Therefore, there are several reasons for developing a rational approach to material cutting:

1. Improve cutting: Even minor improvements in productivity are of major importance in high volume production.
2. Produce products of greater precision and of greater useful life.
3. Increase the rate of production and produce a greater number and variety of products with the tools available.

Metal cutting is a typical irreversible process, comprising large plastic deformation coupled with temperature rise at high strain rates. From a continuum mechanics point of view, suitable constitutive or governing equations that can describe this phenomenon are needed to predict chip flow, cutting forces, cutting

temperature, tool wear, etc. However, the solutions of displacement or velocity, stress, strain and temperature fields in metal cutting processes have not easily been obtained since large deformations and temperature rise lead to highly non-linear and time dependent mechanics of the process.

Cutting processes are quite complex, largely due to the fact that two basic operations occur simultaneously in a close proximity with strong interaction.

1. Large strain and partly extremely large strain-rate plastic deformation in a zone of concentrated shear
2. Material transport along a heavily loaded region of relative motion between chip and tool.

In general, several simplified models which emphasize different aspects of the problem such as thermal, material and surface considerations are operative simultaneously with varying degrees of importance depending on specific machining conditions. Due to complexities of the problem, a general predictive theory is not possible. Thus, an easier method was to illustrate how fundamental concepts may be used to explain observed results from carefully planned experiments and how solutions to new machining situations may be achieved by application of scientific principles.

The plane-strain orthogonal metal cutting process, for which, the direction of relative movement of wedge-shaped cutting tool is perpendicular to its straight cutting edge, has been extensively studied since it provides a reasonably good modeling of the chip formation on the major cutting edge of many metal removal processes such as turning, milling, drilling, etc.

A computational approach using the finite element method soon became a mainstream for the analysis of machining after it has been developed. Because, it provides a nearly exact displacement and/or velocity field depending on the

assumptions made while building the model for orthogonal metal cutting operation. Of course, it is continuing to find even more usage in response to quick and revolutionary developments in computer hardware.

1.2 Aim and Scope of the Study

This work is motivated by the fact that machining is a very common process in the industry and experimental observations with trial and error periods are still needed for the process optimization. Hence, the availability of a successful finite element model for the prediction of process variables is very promising in decreasing experimentation, which is quite time consuming and expensive. In addition, simultaneous engineering of product and its machining operations can be achieved by optimizing cutting conditions through simulations.

Thus the aim of this work is to develop two dimensional finite element models of orthogonal metal cutting operations with several commercial codes. Then, observations of the effects of several parameters on the results will be done. These parameters can be divided into two as the variables related with cutting conditions and the variables related with finite element model. Cutting conditions can be changed by altering the rake angle of the tool, feed rate, cutting speed, etc. On the other hand, friction model, friction parameter, separation criterion and material modeling are related with finite element model.

At the end of simulations, cutting and thrust forces, shear angle, chip thickness and contact length as well as stress, strain, strain-rate and temperature distributions can be estimated.

The results are going to be verified with experimental results. In addition to experiments included in this work, more results will be collected from literature and will be compared with simulations.

Therefore, the scope of the thesis can be concluded as the following.

1. Developing finite element models of two dimensional orthogonal metal cutting operations.
2. Using different commercial codes for the purpose of comparison.
3. Observing the effects of friction model, friction parameter, separation criterion and material modeling on the results.
4. Designing orthogonal cutting experiments to verify the results of simulations.
5. Performing the experiments for several cutting conditions like different rake angles and feed rates.
6. Comparing the results of simulations with experiments.

1.3 Finite Element Models and Experiments

In this present work, the commercial codes MSC.Marc, DEFORM2D and ThirdWave AdvantEdge have been used to create thermo-mechanically coupled finite element models of plane-strain orthogonal metal cutting operations. Material is modeled as elastic-plastic, with flow stress being dependent on strain, strain-rate and temperature. The friction between the tool and chip is of shear type for MSC.Marc and DEFORM2D; however Thirdwave AdvantEdge uses Coulomb friction model. In simulations with MSC.Marc and AdvantEdge no damage or failure criteria are defined assuming the formation of chip due to totally plastic flow. However, the Cockroft-Latham damage criterion has been used in simulations with DEFORM2D to see the effects.

Experiments have also been performed to verify the results. Purely orthogonal cutting operations are conducted on a lathe by cutting the end of hollow cylinders with large diameter and small wall thickness. Cutting and thrust forces are measured by means of a dynamometer. In addition, shear plane angles are calculated from the chip thicknesses which are measured by means of a tool maker’s microscope.

1.4 Content of this Study

The importance of the metal cutting in our life is explained after an introduction. The difficulties involved in analytical solution of the cutting processes are also added in this chapter.

In Chapter 2, the general well known theories in metal cutting are discussed. The purpose of that chapter is to well understand the mechanics of metal cutting and to get some usable equations in solving the problem. This information will be used in comparison with the results obtained by the finite element method. Current literature available on finite element simulation of metal cutting processes is also reviewed in Chapter 2.

The experimental test procedure and test equipments are mentioned in Chapter 3. The modeling of the metal cutting and the solution procedure are explained in Chapter 4. All results, both from experiments and simulations by three commercial codes are given in Chapter 5. Simulation results are compared both with the experimental results of this work and with the ones from literature in this chapter. In addition, comparisons with analytical solutions are also available.

This work is discussed and concluded in Chapter 6. Some recommendations for future work are given in that chapter as well.

CHAPTER 2

LITERATURE SURVEY

2.1 Introduction

In this chapter, an overview of the literature related with analytical and numerical solutions of metal cutting and chip formation will be given.

This chapter starts with a section in which nomenclature and mechanics of chip formation is explained. In the second section, analytical solutions of shear angle relationships are given.

Third section explains the friction phenomena on the rake face of the tool which is in contact with the chip. Then, in fourth section, shear stresses observed in the shear zone are mentioned and discussed.

In the last section, numerical models of orthogonal metal cutting are given. The development of models is explained in a historical order.

2.2 Chip Formation and Nomenclature

Since the cutting process involves separation of metal, historically it was first believed to be a fracture process, involving crack formation and propagation.

Later there was doubt whether or not a crack existed ahead of the tool. Mallock [1] and Reuleaux [2], who took some of the first photomicrographs of chip formation, claimed that a crack could be observed. However, Kick [3] opposed the interpretation of the original photographic evidence and claimed that no crack existed. Improved photomicrograph techniques have indicated that metal cutting is basically a plastic-flow process and there is no crack formation at the tool tip.

Most practical cutting operations, such as turning or milling, involve two or more cutting edges inclined at various angles to the direction of cut. However, the basic mechanism of cutting can be explained by analyzing cutting with a single cutting edge. The simplest case of this is known as orthogonal cutting, in which the cutting edge is perpendicular to the relative cutting velocity between tool and workpiece, as shown in Figure 2.1-a. A single cutting edge inclined to the cutting velocity as in Figure 2.1-b gives oblique cutting.

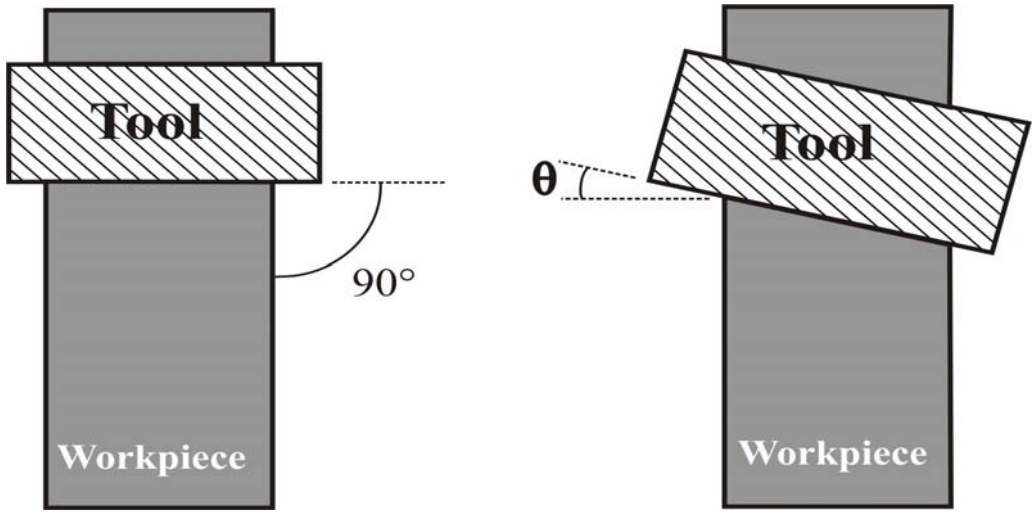

(a) (b)

Figure 2.1 (a) Orthogonal cutting (b) Oblique cutting

The nature of chip formation is approximately the same for orthogonal or oblique cutting with one or more cutting edges. Three basic types of chip formation are generally recognized:

1. Discontinuous-chip formation, which involves periodic rupture so that the chip forms as small separate segments
2. Continuous-chip formation
3. Continuous chip with built-up edge, where, a strain-hardened nose of material periodically builds up and breaks away from the cutting edge of the tool.

Figure 2.2 shows the photo-micrographs of chip samples produced by quick-stop techniques. The mentioned chip forms can be seen clearly.

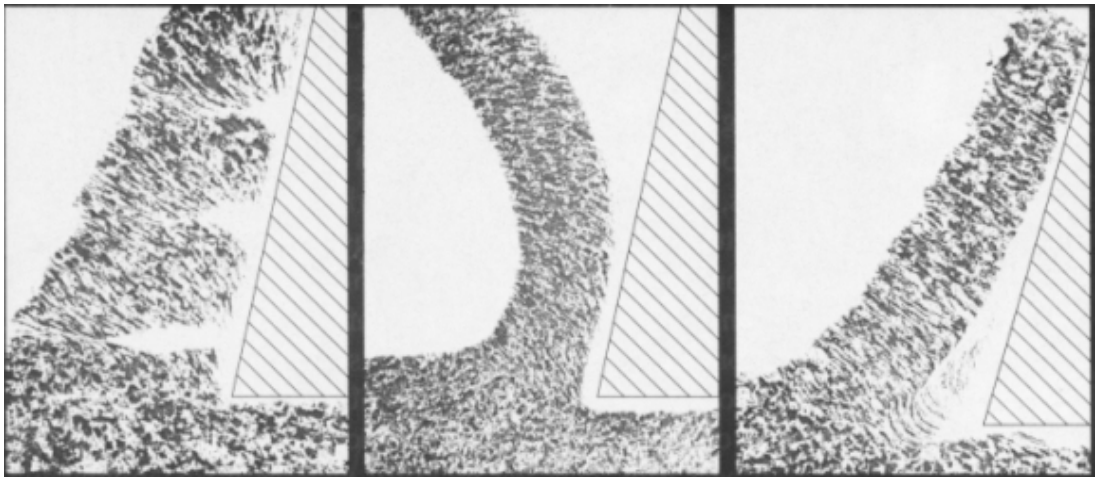

(a) (b) (c)

Figure 2.2: Chip samples produced by quick stop techniques. (a) Discontinuous (b) Continuous chip (c) Continuous chip with build-up edge [4]

In Figure 2.3, rake angle γ, undeformed chip thickness a_0, and chip thickness a_c are indicated for an orthogonal cut.

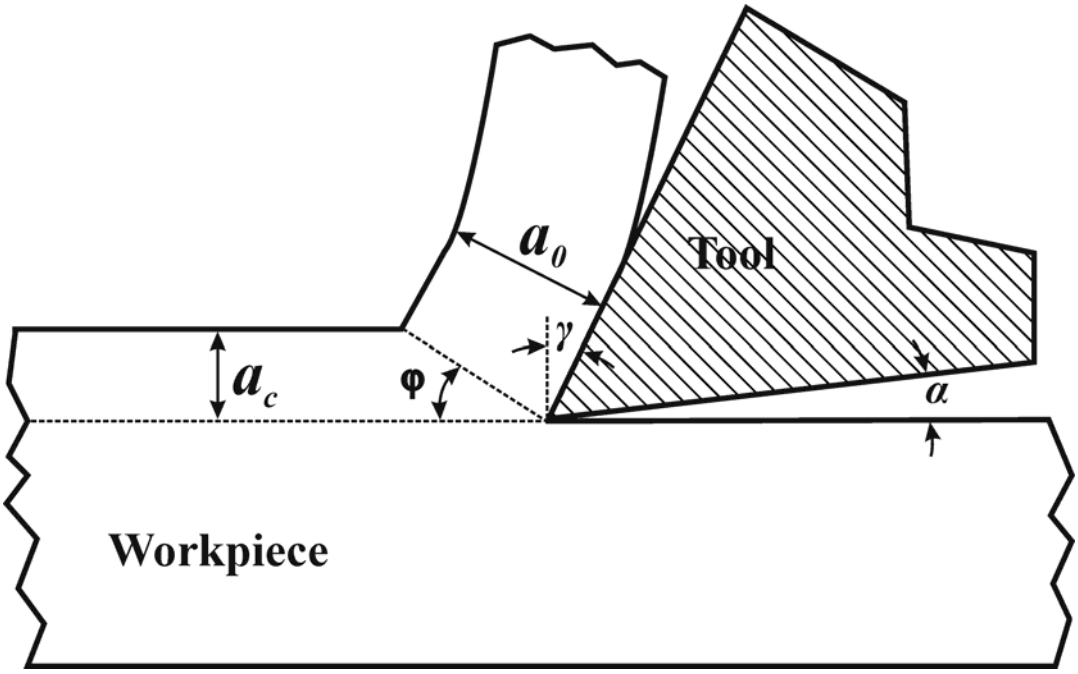

Figure 2.3 Some of the variables in orthogonal cutting: a is the rake angle, t is the undeformed chip thickness, t_c is the chip thickness and c is the clearance angle

Chip formation, at least with a continuous chip, is a plastic-flow process due to shear. There is, and has been for some time, considerable controversy about the shape of the plastic-flow region. Piispannen [5], Ernst [6] and Merchant [7] proposed a cutting model as in Figure 2.4-a. They claimed that the chip is formed by simple shear on a plane running from the tool tip to a point on the free surface workpiece. No plastic flow takes place on either side of this shear plane. Palmer and Oxley [8], Okisima and Hitomi [9] and others, have suggested the deformation zone somewhat like that shown in Figure 2.4-b.

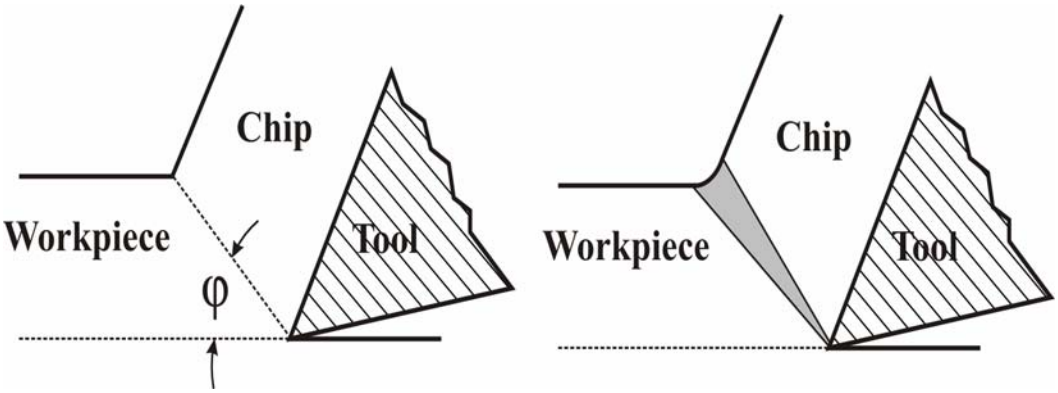

(a) (b)

Figure 2.4. Assumed shape of deformation zone in cutting:
(a) thin shear-plane model, where φ is known as shear angle (b) thick shear zone.

Careful examination of motion picture films and photomicrographs indicates that under different conditions the deformation approximates to one or the other of the above shear models. At low cutting speeds, particularly when cutting metals which are in the annealed condition, the thick-zone model is usually the most realistic. At high speeds, the thin-shear-plane model is approached (Figure 2.5).

The dependence of the plastic zone on cutting conditions can be illustrated by cutting wax. In tests with wax, it has been shown that at small, or negative, rake angles the plastic zone is very thin with a sharp transition between the top of the workpiece and the chip. On the other hand, at very large rake angles there is a gradual curvature from the workpiece into the chip, and a thick plastic zone.

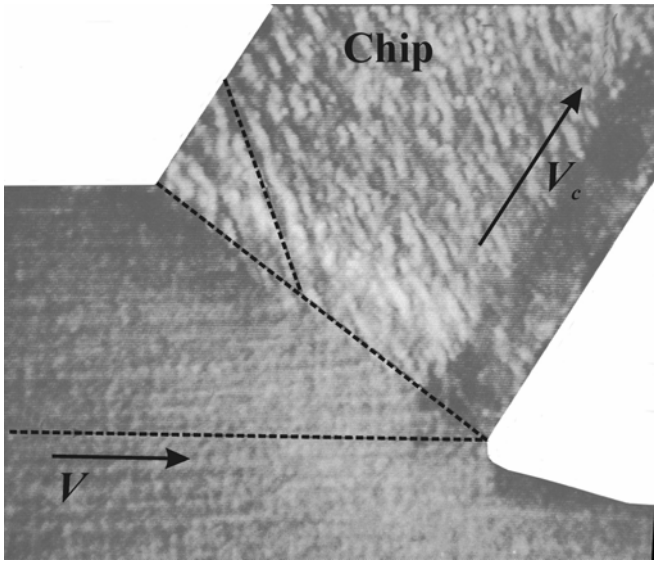

Figure 2.5: A photomicrograph of orthogonal cutting operation where thin shear plane is approached. [4]

Discontinuous chip formation, on the other hand, does involve some fracture. However, it is a non-steady-state process and between the fracture cycles there is some plastic flow as in continuous chip formation. This probably takes on a form as indicated in Figure 2.6. No doubt the plastic zone may at times approach to a thin plane. As the plastic zone spreads forward, the shear strain increases and fracture occurs. The properties of the material, as well as the cutting conditions, play a part in causing discontinuous chip formation.

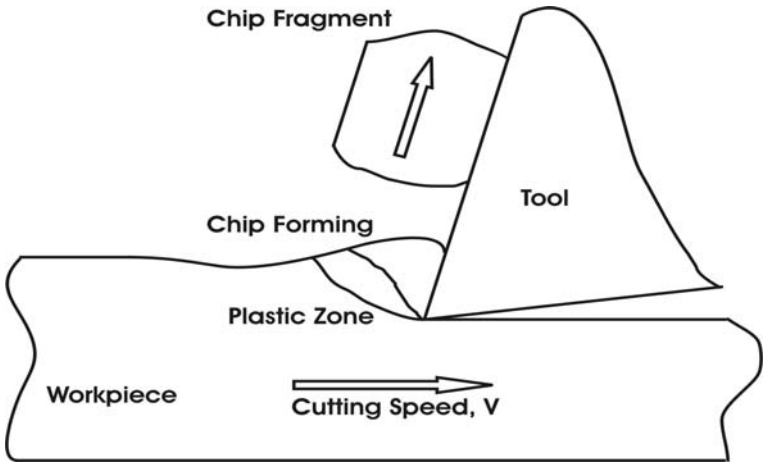

Figure 2.6: An illustration of the mechanism of discontinuous chip formation.

It must be realized that the change from one type of chip to the other is gradual and sometimes the chip fragments may not be completely separated. This is sometimes referred to as a semi-discontinuous chip, but it may be classified as discontinuous.

The formation of a built-up edge on the tool is brought about by high normal loads on the tool rake face, leading to adhesion between the chip and tool. This adhesion may be so severe that instead of sliding of chip over the tool rake face, rapture occurs within the chip after a considerable amount of plastic flow. Further layers build up, until a large nose of material may project from the cutting edge as shown in Figure 2.7.

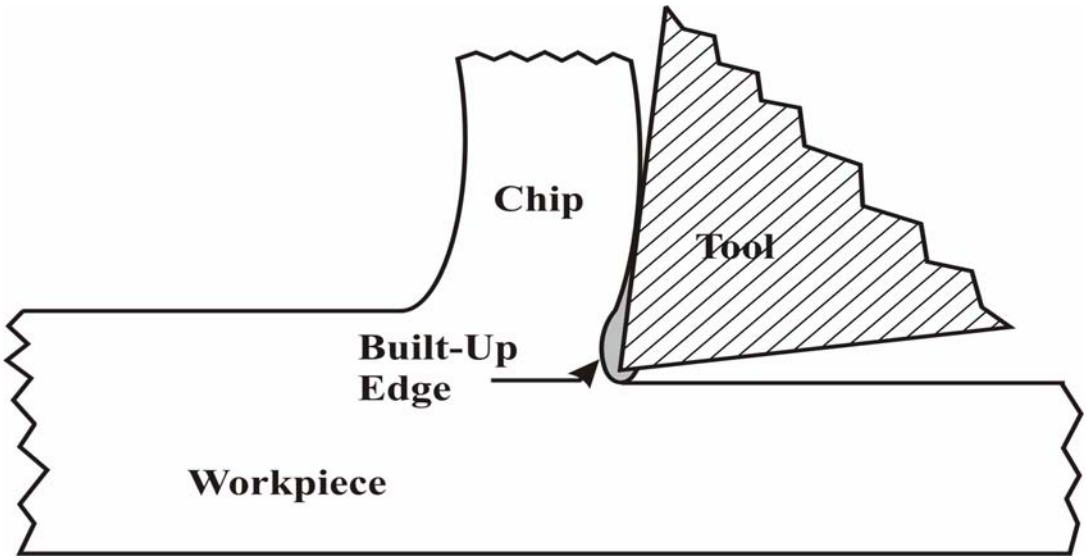

Figure 2.7. Idealized picture of built-up edge (B.U.E) formation.

Periodically, this nose fractures and the fragments are welded onto the chip and the workpiece. This mechanism is repeated with a frequency of the order of several cycles per a second.

The conditions in metal cutting are more extreme than in most of other deformation processes. The distinguishing features of the metal cutting process are the following:

1. It is a plastic-flow process with exceptionally large strains. There is a high compressive stress acting on the plastic zone and this prevents rupture from occurring until the strain is well above the rupture value in, say, a tensile test.
2. The deformation is localized to an extremely small plastic zone. Thus, the strain rate is unusually high.

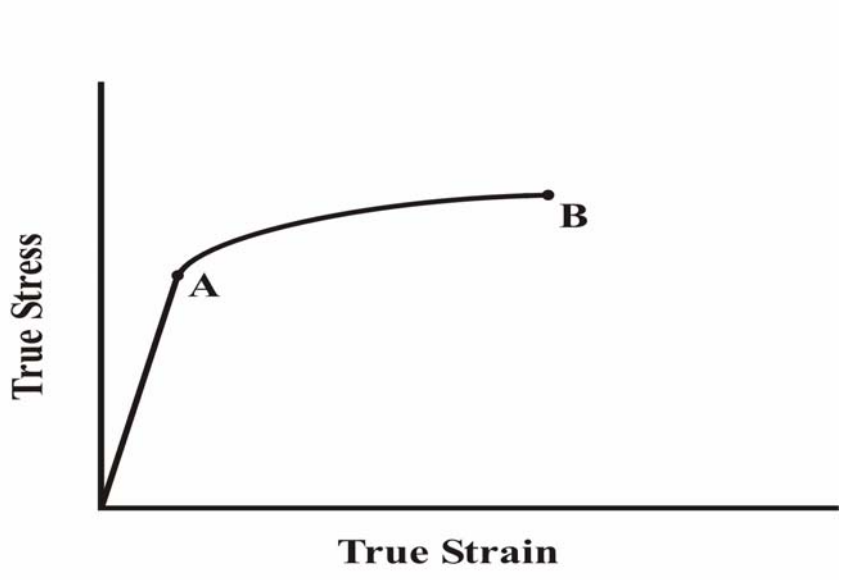

Figure 2.8. Typical shape of the stress-strain relationship for a metal under the action of a tensile stress.

The high values of strain and strain-rate mentioned in 1 and 2 mean that the material properties in cutting are considerably different from the properties of the same material when deformed in other ways, such as by metal forming processes. Consider Figure 2.8; the high strain-rate modifies the plastic flow process so that the whole curve between A and B in Figure 2.8 is raised up along the true stress axis. In addition, high temperatures, attained especially at the deformation zones, soften the material. These changes in material behavior have led to some of the major difficulties in relating metal cutting mechanics to conventional plastic deformation theory.

Salomon [10] and later Vaughn [11] have discussed an interesting, in fact somewhat unusual, machining situation, which is known as ultrahigh speed machining. This is a metal cutting operation at cutting speeds in excess of 100 meters per min (Vaughn has tested up to speeds of 6096 meters per revolution). After a certain critical speed, which depends on the material being cut, the nature of the deformation is altered, giving a decrease in forces and temperatures, with further increase in speed. Vaughn has attributed this to a modified shear process, called adiabatic shear. At the very high speeds, it is suggested that limited time for heat flow, restricts the thermal energy generated by plastic flow to a preferred zone, causing weakening of this zone and additional shearing at low values of shear stress.

2.3 Shear Zone Models

In the last thirty years many papers on the basic mechanics of metal cutting have been written. Several models to describe the process have been developed; some have been fairly successful in describing the process, but none can be fully substantiated and definitely stated to be the correct solution. Thus, while none of the analyses can precisely predict conditions in practical cutting situations, the analyses are worth examining because they can qualitatively explain phenomena observed and indicate the direction in which conditions should be changed to improve cutting performance.

There is conflicting evidence about the nature of the deformation zone in metal cutting. This has led to two basic approaches in the analysis. Many workers, such as Piispannen [5], Merchant [7], Kobayashi and Thomsen [12], have favored the thin-plane (or thin zone) model, as shown in Figure 2.9(a). Others such as Palmer and Oxley [8], and Okushima and Hitomi [9], have based analyses on a thick-deformation region as in Figure 2.9(b).

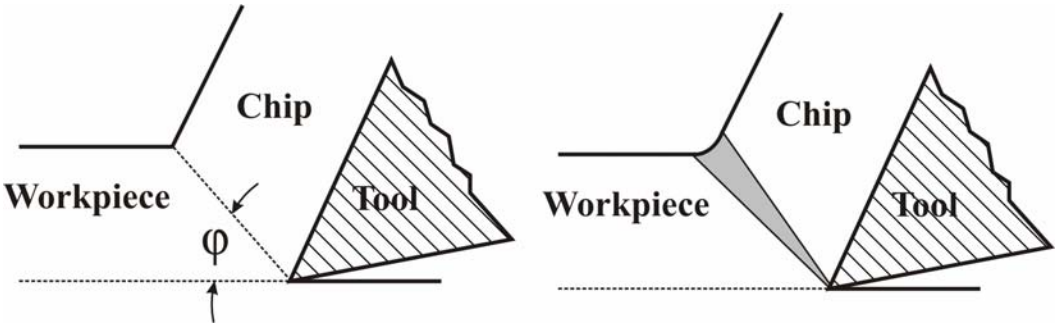

(a) (b)

Figure 2.9: Shear zone types.
(a) thin shear plane (b) thick shear zone

Available experimental evidence indicates that the thick-zone model may describe the cutting process at very low speeds, but at higher speeds most evidence indicates that a thin shear plane is approached. Thus it seems that thin-zone model is likely the most realistic for practical cutting conditions.

In addition, it leads to far simpler mathematical treatment than does the thick-zone model. For these two reasons the analysis of the thin zone has received far more attention and is more complete than that of the thick zone.

2.4 The Shear-Angle Relationships

The shear angle is of particular importance in metal cutting. In fact, the shear angle is a measure of the plastic deformation in cutting and is an essential quantity for predicting the forces in cutting. Because of this, a considerable amount of work has been done by many investigators to establish a shear-angle relationship. An examination of research publications in the metal cutting field reveals a big array of relationships. A review of these shows that many can be reduced to the form

$$\varphi = C_1 - C_2 \cdot (\beta - \gamma) \tag{2.1}$$

where C_1 and C_2 are constants, φ is the shear angle, β is the friction angle (Figure 2.10) and γ is the rake angle.

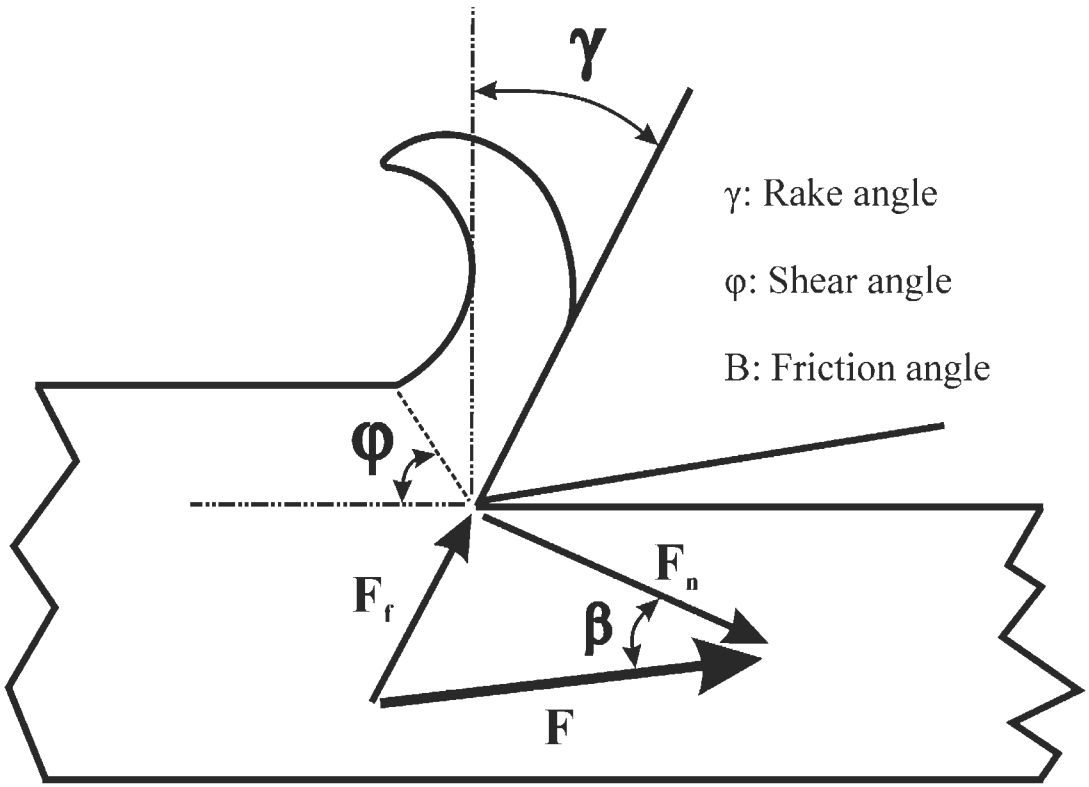

Figure 2.10: Variables used in shear angle relationships.

2.4.1 Merchant's Relationship

This is one of the earliest and possibly the best known shear-angle relationship, which suggests that material will choose to shear at angle that minimizes the required energy [7]. The relationship is given in Equation (2.2) as:

$$\varphi = \frac{\pi}{4} - \frac{1}{2} \cdot (\beta - \gamma) \tag{2.2}$$

2.4.2 Lee and Shaffer's Relationship

Lee and Shaffer [13] applied the theory of plasticity for ideal rigid-plastic material, and assumed that deformation occurred on a thin-shear plane. They considered that there must be a stress field within the chip to transmit the cutting forces from the shear plane to the tool face. They represented this by a slip-line field in which no deformation occurs although it was stressed up to yield point. Resulting equation is given as:

$$\varphi = \frac{\pi}{4} - (\beta - \gamma) \tag{2.3}$$

2.4.3 Oxley's Relationship

Oxley [14] presented an analysis which led to an implicit shear-angle relationship given by the following equations:

$$\theta = \varphi + \beta - \gamma \tag{2.4}$$

and

$$\theta = \arctan\left[\frac{1}{2} + \frac{\pi}{4} - \varphi \cdot \frac{\cos 2(\varphi - \gamma)}{2 \cdot \tan \lambda} - \frac{\sin 2(\varphi - \gamma)}{2}\right] \tag{2.5}$$

2.4.4 Other Relationships

It is interesting to note that all of the above well known shear angle relationships are independent of the material.

Coding [15] and Sata and Yoshikawa [16], have attempted to take account of material properties, but most have assumed that the material will have no

effect on the shear angle. Coding's relationship is interesting in that it points out the importance of preferred orientation. Clearly, this is likely to be an important factor since formed metal parts are all anisotropic.

Hill [17] suggested that the large number of unknown factors in metal cutting, such as anisotropy, work-hardening, variation in the coefficient of friction and thermal effects mean that a unique value of the shear angle may not exists. Thus, Hill suggests that any analysis should not be directed at establishing a single relationship, but instead should locate the possible bounds, using relations suggested by Kudo [18], Dewhurst [19] and Lee and Shaffer [13], within which the shear angle must lie. This is a reasonable approach, but suffers from the disadvantage that the boundary limits established by Hill are too far apart for the shear angle values to be of much practical use.

2.5 Friction on the Rake Face of a Cutting Tool

The laws of friction have been shown to be invalid for conditions where plastic deformation is occurring close to the sliding interface, i.e. under the conditions of very high normal load. In this situation the real area of contact approaches to the apparent area (in the extreme case the real area of contact become equal to the apparent area). Hence the proportionality between the real area of contact and the applied normal load is constant and equal to the apparent area. Under these conditions the friction force is independent of normal load [20] as shown on Figure 2.11.

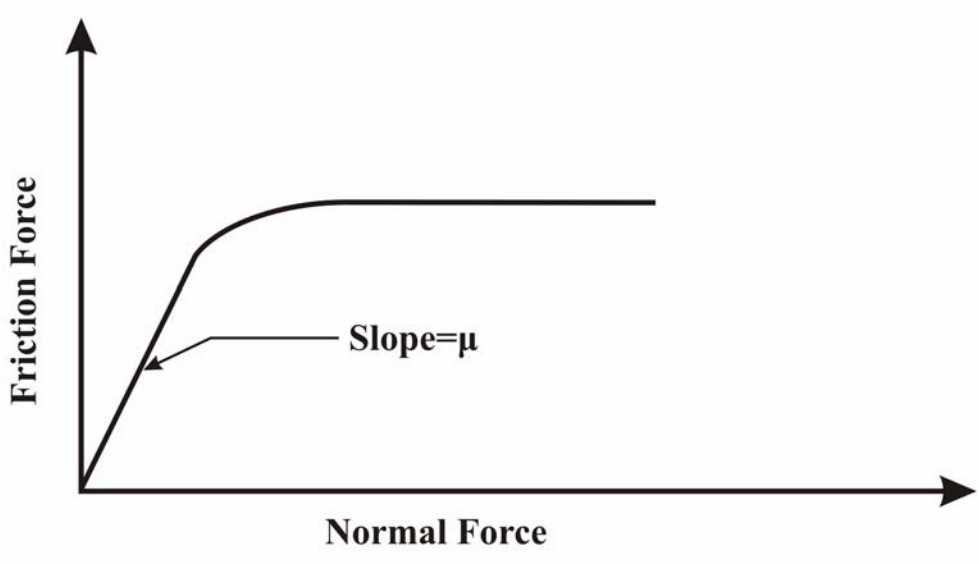

Figure 2.11: Dependence of friction force to the normal force.

In metal cutting we have a sliding situation under the conditions of exceptionally high normal force, which can explain some of the departures from the usual laws of friction depended on normal force.

An important factor to consider in discussing the friction in metal cutting is that the measured forces include a ploughing component; some account should be taken of this before calculating the value of friction on the rake face. One way of deducting this rubbing component is to plot the measured cutting forces against depth of cut and extrapolating back to zero depth [21]. The force intercept is then taken as the rubbing or edge force. When this intercept is removed, the friction parameter is still high and may vary with the cutting conditions. The dependence of friction parameter on the cutting conditions can be explained by considering the distribution of stress on the rake face of the tool.

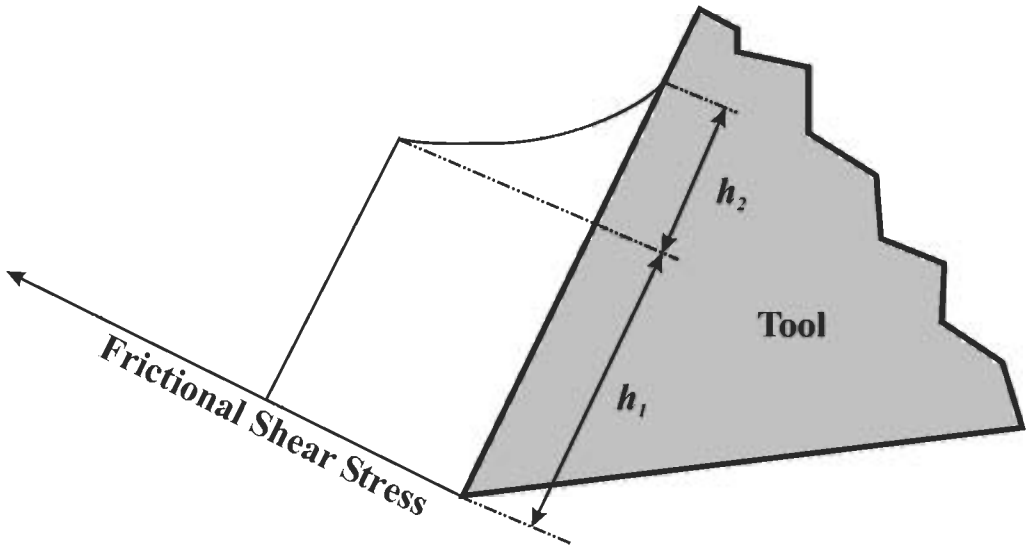

Figure 2.12: Frictional shear stress distribution on rake face of the tool.

Takeyama and Usui [22], Sata and Yoshikawa [16], Zorev [23] and Wallace and Boothroyd [24] have shown that the stress distribution on the rake face is of the form shown in Figure 2.12. Over the length h_1, the normal stress is very high and the metal adheres to the rake face; plastic flow occurs in the work material. In this region the shearing stress (or friction stress) is independent of the normal load and generally equal to the shear yield stress of the material. This is known as the sticking region of friction. On the length h_2, smaller normal stresses exist and the usual condition of sliding friction applies.

It is to be expected that any changes in the cutting conditions which change the relative length of h_1 and h_2 will alter the measured value of the friction. For example, an increase in the rake angle reduces the overall normal load on the rake face causing a decrease in ratio of h_1 and h_2.

2.6 The Shear Stress in Shear Zone During Metal Cutting

The shear stress in the shear zone is found to be higher than the yield stress determined from tensile tests on the work material. One immediate explanation

for the high yield-stress value is that two extraneous effects have been included in the calculation. These are, first the effect of rubbing on the clearance face of the tool. This introduces a force which is measured, but does not contribute to the shearing process in the shear zone. Secondly there exists a pre-flow region (Figure 2.13) for many cutting conditions which has the effect of extending the length of the shear plane or shear zone beyond that assumed in the analysis

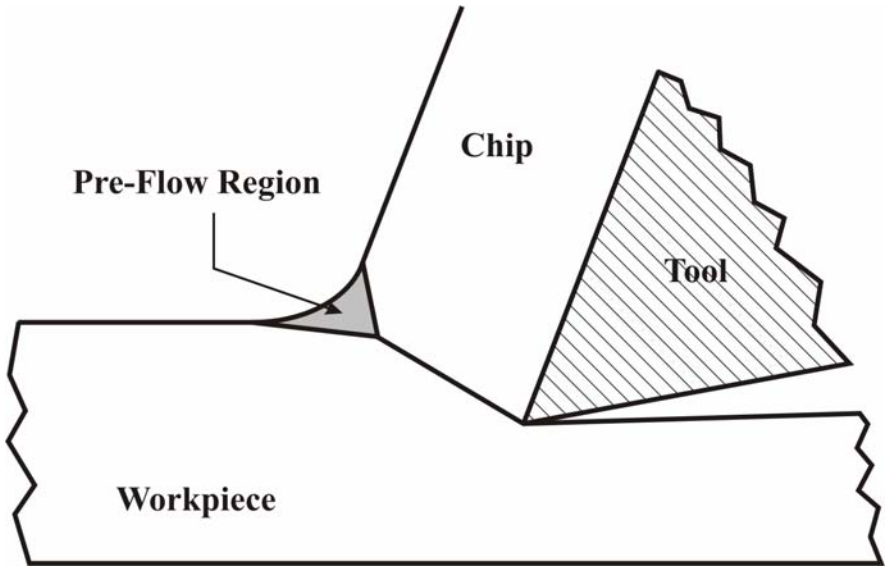

Figure 2.13: Pre-Flow region.

.

The effect of rubbing and the pre-flow region can be taken into account approximately. When this is done the value of the shear stress is still found to be higher compared with the yield stress for the material being cut. A number of explanations have been presented to explain the high stress values, even though some do not now seem likely to be fully justified.

1. It was proposed by Merchant [7], following early work by Bridgman [25], [26], that the yield shear stress on the shear plane was increased due to high values of the normal stress on this plane. However, Bridgman was concerned principally with rupture stress. Later work by Crossland [27] and

the others has shown that hydrostatic stress has very little effect on shear yield stress, although it does affect rupture stress.

2. It has been suggested by Backer, Marshall and Shaw [28] that the size of the deformation region may influence the shear-stress value. This follows from the theory of size effect for single crystals which is based on the concept that at small sizes the probability of finding dislocation sources is reduced and hence the yield stress of a material rises. The existence of the latter effect has been demonstrated by the growth of very fine single crystal whiskers [29], [30].
3. It has been claimed by Shaw and Finnie [31] and Oxley [14] that work hardening plays a part in determining the shear stress in metal cutting. However, evidence by Cotrell [32] and Kobayashi and Thomsen [12], indicates that this is probably not the case, except possibly at very low cutting speeds.
4. Strain rate and temperature are normally considered to have opposing effects on the value of yield stress for a material. Because the temperature in the shear zone and the strain rate are both high in metal cutting, it has been argued that the two effects cancel each other [32].

On the other hand, Cotrell [32] has described a mechanism of yield at high rates of strain, which suggests that above a certain critical strain rate the yield stress is independent both of the strain rate and of temperature. He considers that the obstacles preventing slip of dislocations (other dislocations, alloy precipitates, and grain boundaries) may be represented by an undulating internal stress field. When the applied stress is less than the internal stress, the dislocations cannot pass the obstacles unless thermal vibrations of the lattice provide sufficient additional energy. Since the probability of obtaining sufficient thermal energy is dependent on both time and temperature, the yield stress will depend both on strain rate and temperature. If, however, the applied stress is greater than the internal stress, rapid slip

will occur and the yield stress will be independent of strain rate. By this theory, the yield stress at high rates of strain will be higher than the static yield, but above a certain rate it will be independent of the rate of strain. The straining will be sudden and catastrophic at any applied stress level, hence work-hardening effects will not be observed.

2.7 Numerical Approach

In the two past decades, the finite element method based on Eulerian and updated Lagrangian formulation has been developed to analyze the metal cutting processes. Several special finite element techniques, such as element separation, [33], [34], [35], [36], [37], [38], modeling worn cutting tool geometry [33], [34], [35], [37], [38], mesh rezoning [36], friction modeling [33], [34], [35], [36], [37], [38] etc. have been implemented to improve the accuracy and efficiency of the finite element modeling. Detailed workpiece material modeling with the coupling of temperature, strain rate and strain hardening effects, has been applied to model the material deformation.

The literature for the numerical approach is classified so that the steady state solutions, in which separation is not included, will first be mentioned. Later, the models, which are including separation, will be explained. The latter one is also divided into two sections according to whether they simulate the chip formation from incipient to continuous stage or they simulate the chip formation at the continuous stage only.

2.7.1 Steady -State Solutions

In steady-state solutions the metal cutting problem is modeled at the steady-state conditions. These are generally one increment solutions. The chip form and the needed data are obtained from experimental and theoretical results for the definition of the model and for the boundary conditions.

Strenkowski and Kyoung-Jin Moon [40] presented an Eulerian finite element model that simulates orthogonal metal cutting and predicts chip geometry and temperature distribution in the workpiece, chip and tool without the need for empirical cutting data. They showed that the characteristics of the flow field in the vicinity of the tool can be determined such as the material velocity and the stress and strain rate distributions. They found out that the shearing occurs over a finite region in front of the tool, rather than a single shear plane. Figure 2.14 shows his initial model and the effective plastic strain rate distribution after solution.

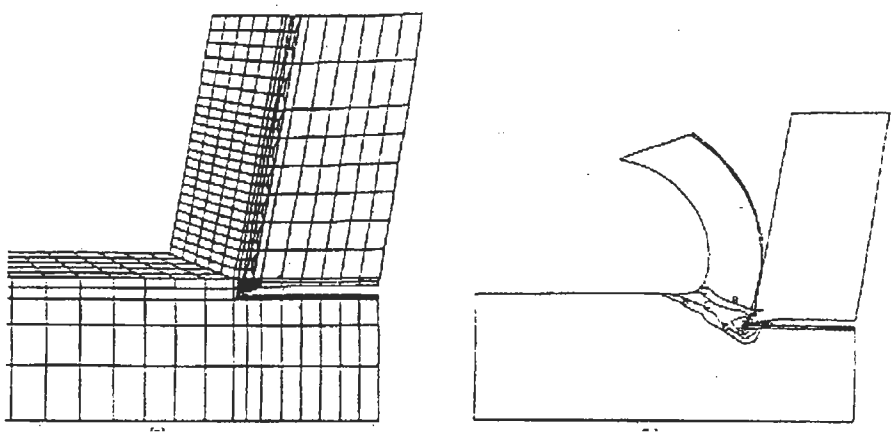

(a) (b)

Figure 2.14: Model by Strenkowski and Kyoung-Jin Moon.
(a) initial chip form (b) strain-rate distribution after solution.

Tyan and Yang [41] simulated the orthogonal metal cutting process for a controlled contact tool using a limit analysis theorem. The basic principles are in the form of a primal optimization problem with an objective function subjected to constraints of equilibrium equation, its static boundary conditions and a constitutive inequality. An Eulerian reference coordinate is used to describe the steady state motion of the workpiece relative to the tool. The results are obtained for a wide range of control parameters including cutting depth, rake angle, rake length and friction. The converged solution provides information on cutting force, chip thickness, chip flow angle and shear angle.

The temperature distributions in the workpiece and chip during orthogonal machining are obtained numerically using the Galerkin approach of finite element method for various cutting conditions by Muraka, Barrow and Hindua [42]. The effect of a number of process variables such as speed, feed, coolant, rake angle, tool flank wear and tool material on the temperatures has been investigated. The finite element solution of the problem takes into account the actual geometries of the chip and the tool, experimentally obtained velocity and heat source distribution within the primary and secondary deformation zones and the variation of density, thermal conductivity specific heat with temperature. It also takes into consideration the variation of the flow stress with strain, strain rate and temperature and heat generation due to boundary friction on the rake face and along the flank face of the tool.

Stevenson, Wrigt and Chow [43] developed the finite element program for calculating the temperature distribution in the chip and tool in metal cutting. They compared the temperatures estimated with the temperatures obtained with previously described metallographic method. Stevenson has assumed the form of the chip and cutting tool initially and then obtained the required parameters from the simulation without simulating the separation of the chip for this current cutting condition, Figure 2.15(a). The needed data for simulation were obtained from experimental and theoretical results such as chip form. The obtained temperature distribution is shown in Figure 2.15(b).

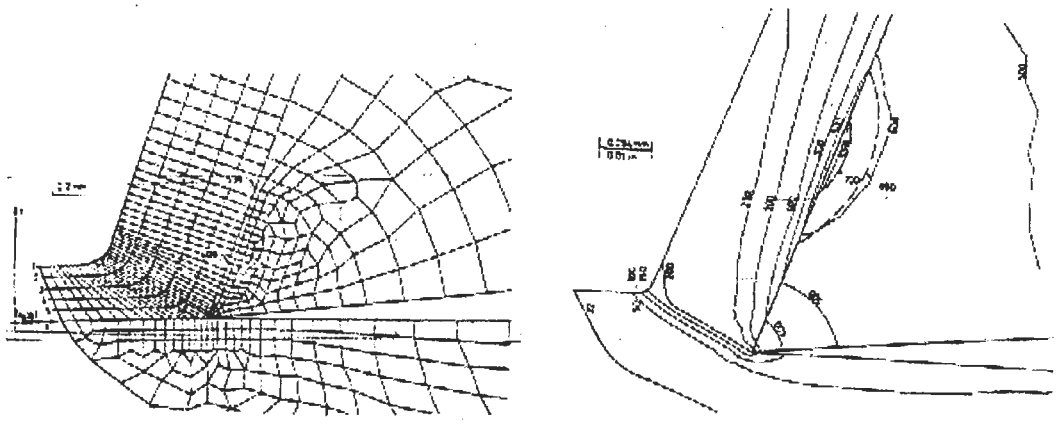

(a) (b)

Figure 2.15: Model by Stevenson, Wright and Chow
(a) initial form of chip and tool (b) obtained temperature distribution

Toshimichi, Nobuhiro and Sheng [44] presented a model with rigid plastic material law to simulate the orthogonal micro cutting process of copper taking into consideration of the roundness of the tool edge. Orthogonal micro cutting experiments of oxygen free copper are used. They analyzed the flow of generated heat and temperature distribution within both the workpiece and the tool.

Maekawa and Shirakashi [45] analyzed the prediction of chip flow and tool damage in metal cutting and included elastic-plastic material characteristic in the analysis. The temperature distribution in the tool and workpiece was also incorporated in the simulation. They compared the various simulation results with experiments.

Maekawa and Shirakashi have developed a repetition strategy named "iterative convergence method" that uses flow lines which consists of the trajectories of particles or a series of finite elements. An initial guess is required for the chip shape. The chip is supposed to be on the surface of the work material and to be stress free. Calculation proceeds by incrementally moving the workpiece towards the cutting tool. A plastic state develops in the chip deformation zone and it is

checked whether or not the consequent plastic flow is consistent with the assumed chip shape. If not, the assumed shape is systematically and automatically altered and calculation is repeated.

Iwata, Osakada and Terasaka [46] developed a rigid-plastic finite element model for orthogonal cutting in a steady state condition. The methods for determining the material and frictional properties to be used in the model are discussed. The shape of chip and distributions of stress and strain are calculated. Fracture of chip is predicted by combining the present model with the criteria of ductile fracture. In this work, an initial model is generated by giving the cutting condition and the shape of the cutting tool, and then the model is modified by using the result of the plane strain finite element analysis. The modification is repeated until the obtained shape of the chip and distribution of strain (flow stress) coincide with the assumed one. The boundary conditions are given according to the assumption of moving workpiece with a constant velocity to unmoving tool. The shear force F_s acting on the chip surface due to frictional stress is a function of normal force F_n.

Liu and Lin [47] used the finite element method to investigate the effect of shear boundary conditions on the stress field in workpiece during machining. The length of the shear plane is found to be a major parameter governing the stress field in the workpiece in machining, confirming a previous experimental study. In this work, separation of chip from the workpiece is not simulated. Force boundary conditions were used and the model is solved for one increment at the assumed cutting conditions.

Howerton, Strenkowski and Bailey [39] developed a model that predicts the onset of built-up edge. It is based on Eulerian finite element model of orthogonal cutting that treats the workpiece as a rigid-viscoplastic material. The effects of temperature and strain-rate on the flow stress are combined with the

Zener-Hollman parameter. It is found that built-up edge will occur when this parameter exhibits a negative gradient in a direction away from the cutting edge. Experimental cutting tests are conducted for aluminum 6061-T6 under orthogonal conditions.

2.7.2 Solutions for Continuous Chip Formation

In this type of simulations, incipient stage of chip formation is not included and the model is generated for continuous chip formation stage. Generally, a separation criterion is needed for the formation of chip.

Komvopoulos and Erpenbeck [35] modeled orthogonal chip formation process by using finite element method. They analyzed the effect of important factors, such as plastic flow of the workpiece material, friction at the tool-workpiece interface and wear of the tool on the cutting process. To simulate separation of chip from the workpiece, distance tolerance criterion was used by super positioning two nodes at each nodal location of a parting line of the initial mesh. Elastic - perfectly plastic and elastic plastic with isotropic strain hardening and strain rate sensitivity constitutive laws was used in the analysis. For simplicity, the tool material and the built-up edge were modeled as perfectly rigid. The dimension of the crater, assumed in the finite element simulations involving a created tool, was also determined from the experiments. Steady state magnitudes of the cutting force, shear plane angle, chip thickness and chip-tool contact length are estimated. The initial mesh configuration was based on the preliminary estimates of the shear angle and chip thickness.

2.7.3 Solutions for Transient Chip Formation

Lin and Lin [48] constructed an orthogonal cutting coupled model of thermo-elastic-plastic material under large deformation. A chip separation criterion based on the critical value of the strain energy density is introduced into the

numerical model. The flow stress is taken as a function of strain, strain rate and temperature in order to reflect realistic behavior in metal cutting. The cutting tool is incrementally advanced forward from an incipient stage of tool-workpiece engagement to a steady-state chip formation. The chip geometry, residual stresses in the machined surface, temperature distributions within the chip and tool, and tool forces are obtained. It has also been verified that the chip separation criterion value based on the strain energy density is a material constant and is independent of uncut chip thickness.

Arola and Ramulu [49] analyzed orthogonal cutting of unidirectional fiber-reinforced polymer composites using finite element method. A dual fracture process was used to simulate chip formation incorporating both maximum stress and Tsa-Hill criteria. All aspects of the cutting tool geometry are considered including the tool rake and clearance angles, nose radius and wear land, as well as the friction between the tool and the work material. Predictions of the cutting forces from numerical simulations are compared with the experimental measurements for orthogonal trimming of unidirectional graphite/epoxy. Figure 2.16 shows the initial and deformed chip and workpiece mesh configuration.

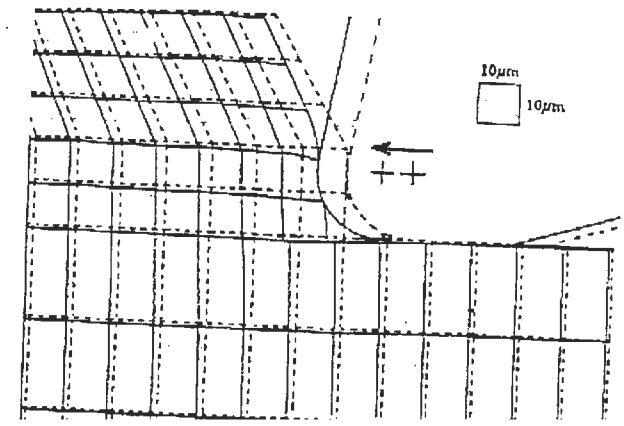

Figure 2.16: Initial and deformed of the model by Arola and Ramulu.

2.7.4 Solutions for Transient and Continuous Chip Formation

Caroll and Strenkowski [50] reviewed two finite element models of orthogonal metal cutting. From the models, the detailed stress and strain fields in the chip and workpiece, chip geometry and cutting forces can be estimated. The first model is based on a specially modified version of large deformation updated Lagrangian code developed at Lawrence Livermode National Laboratory called NIKE2D, which employs an elastic-plastic material model. The second model treats the region in vicinity of the cutting tool as an Eulerian flow field. Material passing through this field is modeled as viscoplastic. Figure 2.17 shows the model.

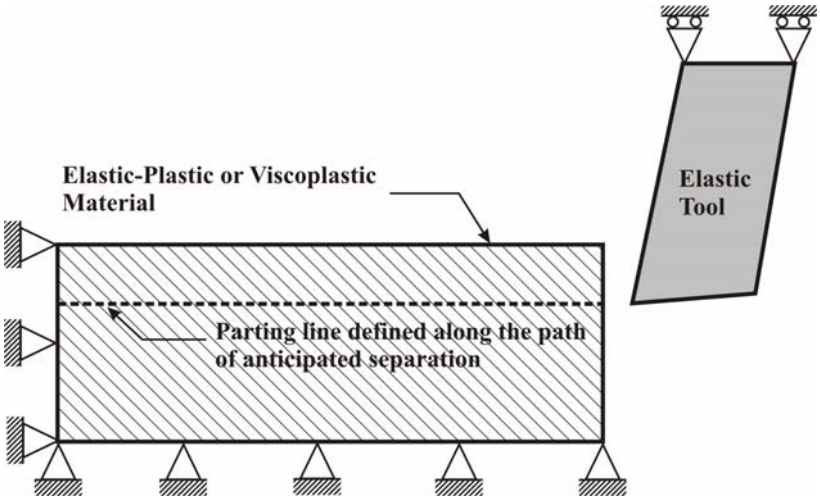

Figure 2.17: Model developed Carroll and Strenkowski.

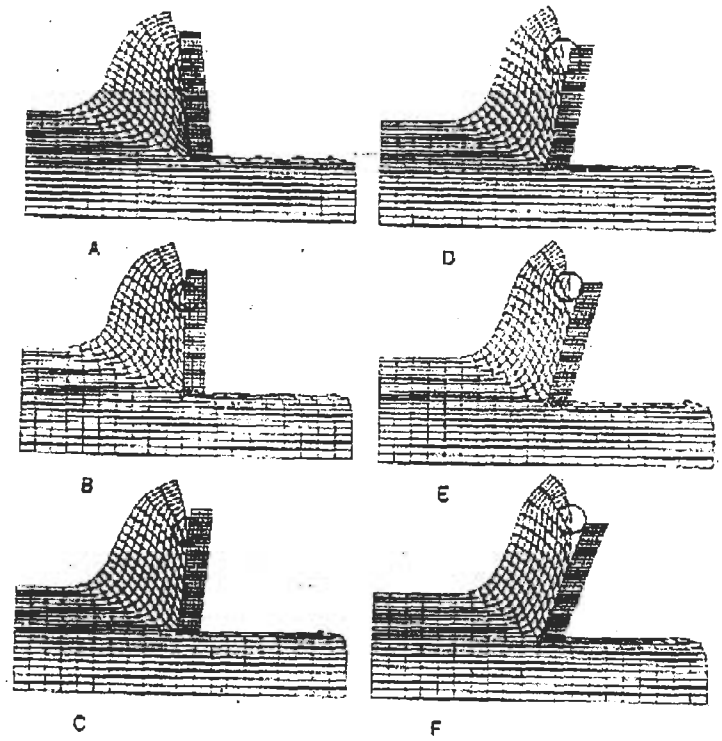

Figure 2.18: Estimated chips at different rake angles by Carroll and Strenkowski.

To allow for separation of the chip formation from workpiece, the model employs a material parting (or separation) criterion based on the effective plastic strain at the tool tip region of the workpiece

Shih and Yang [36] developed and implemented a finite element model for the simulation of plane strain orthogonal metal cutting processes with continuous chip formation, which is based on the Updated Lagrangian formulation. It includes the effects of elasticity, viscoplasticity, temperature, strain rate and large strain on the stress-strain relationship. Effect of frictional force on the tool/chip interface was also studied. An element separation criterion, which is based on the distance between the tool tip and the nodal point connecting the four elements ahead of the cutting tool implemented. They also modeled the friction as a constant friction coefficient in the sticking region and linearly decaying to zero friction coefficient in the sliding region.

Zang and Bagchi [51] presented a finite element model of orthogonal machining by using a two node link element to simulate chip separation. The chip and workpiece are connected by these link elements along an assumed separation line. The chip separation will be initiated when the distance between the leading node and the tool tip is equal to or smaller than the given value. The chip-tool interaction is modeled as sliding/sticking. In the sliding region a constant coefficient of friction is employed and in the sticking region the shear strength of the workpiece is used.

Shih and Yang [36] and Shih [37, 52] developed a mesh rezoning technique for the separation of chip from the workpiece, while the tool penetrates into the material. The finite element model is based on the plain-strain assumption. Detailed work material modeling, which includes the coupling of large-strain, high strain-rate and temperature effects, was implemented.

The chip formation was achieved by a sequence of separations between the elements in front of the tool tip. The element separation criterion was based on the distance in the cutting direction between the tool tip and the node immediately in the front. During the cutting process, finite element mesh was adaptively modified for every 70 μm movement of the cutting tool.

Figure 2.19 shows the initial finite element mesh, configuration of the cutting tool and dimensions of the elements developed by Shih [52].

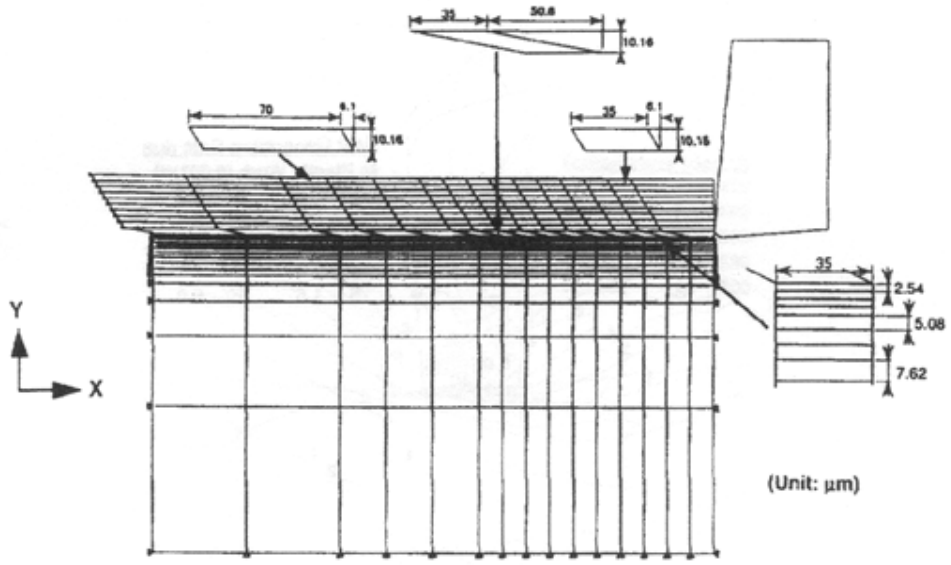

Figure 2.19: The initial finite element mesh, configuration of the cutting tool and dimensions of the elements developed by Shih [52].

Ceretti et al. [53] developed a cutting model by deleting elements having reached a critical value of accumulated damage. In this work, Deform2D was applied to simulate a plane strain cutting process. Damage criteria was used for predicting when the material starts to separate at the initiation of cutting for simulating segmented chip formation. For this purpose, special subroutines was implemented and tested.

Ceretti, Lucchi and Altan [54] used ductile fracture criteria to simulate orthogonal cutting with serrated chip formation. For this purpose, user subroutines, which has the potential of simulation material breakage by deleting the mesh elements of the workpiece material when their damage is greater than a defined critical value, were written and used together with the commercial code Deform2D. The Cockroft-Latham damage criterion was used to calculate the cumulative damage in elements.

In this work, the workpiece was also remeshed when the elements are too distorted or at a regular limiting range of steps defined by the user. Figure 2.20 shows the algorithm of the remeshing module of this work.

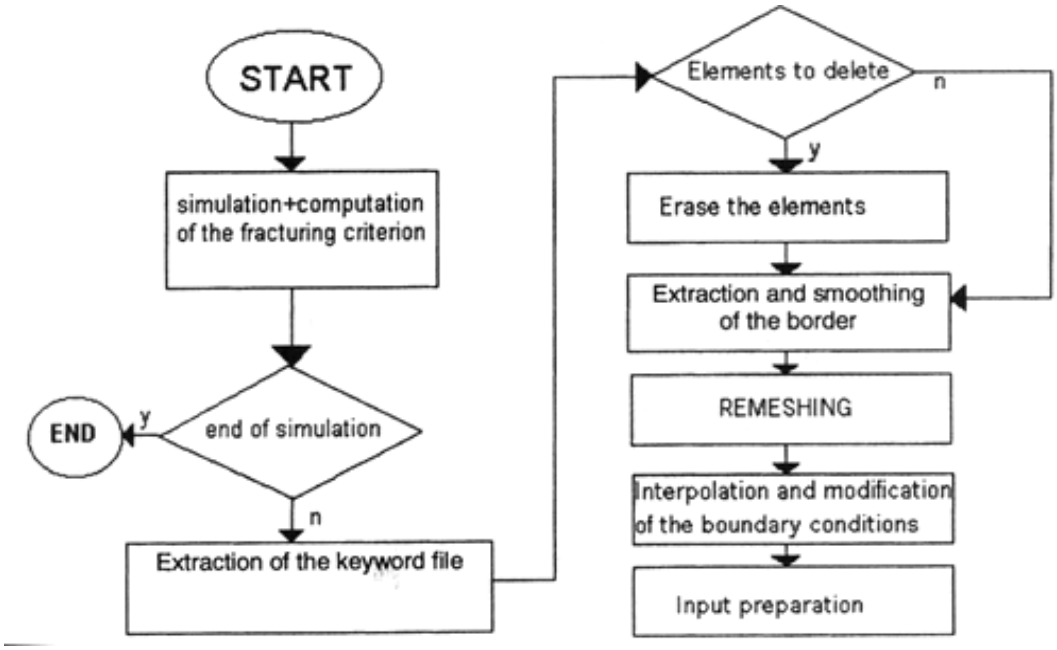

Figure 2.20: Remeshing module used by Ceretti, Lucchi and Altan [54]

Shatla, Kerk and Altan [55] was suggested a method for flow curve determination from machining experiments, which is introduced first by Oxley [56].

Figure 2.21 show the flow Chart by Oxley. On this graph, C is constant that relates the shear strain-rate at the shear zone to the Vs/L, where Vs is the velocity of the workpiece material at the shear zone and L is the length of the shear zone. The other constant, δ, is the ratio of the plastic zone thickness to the cut chip thickness at the tool-chip interface.

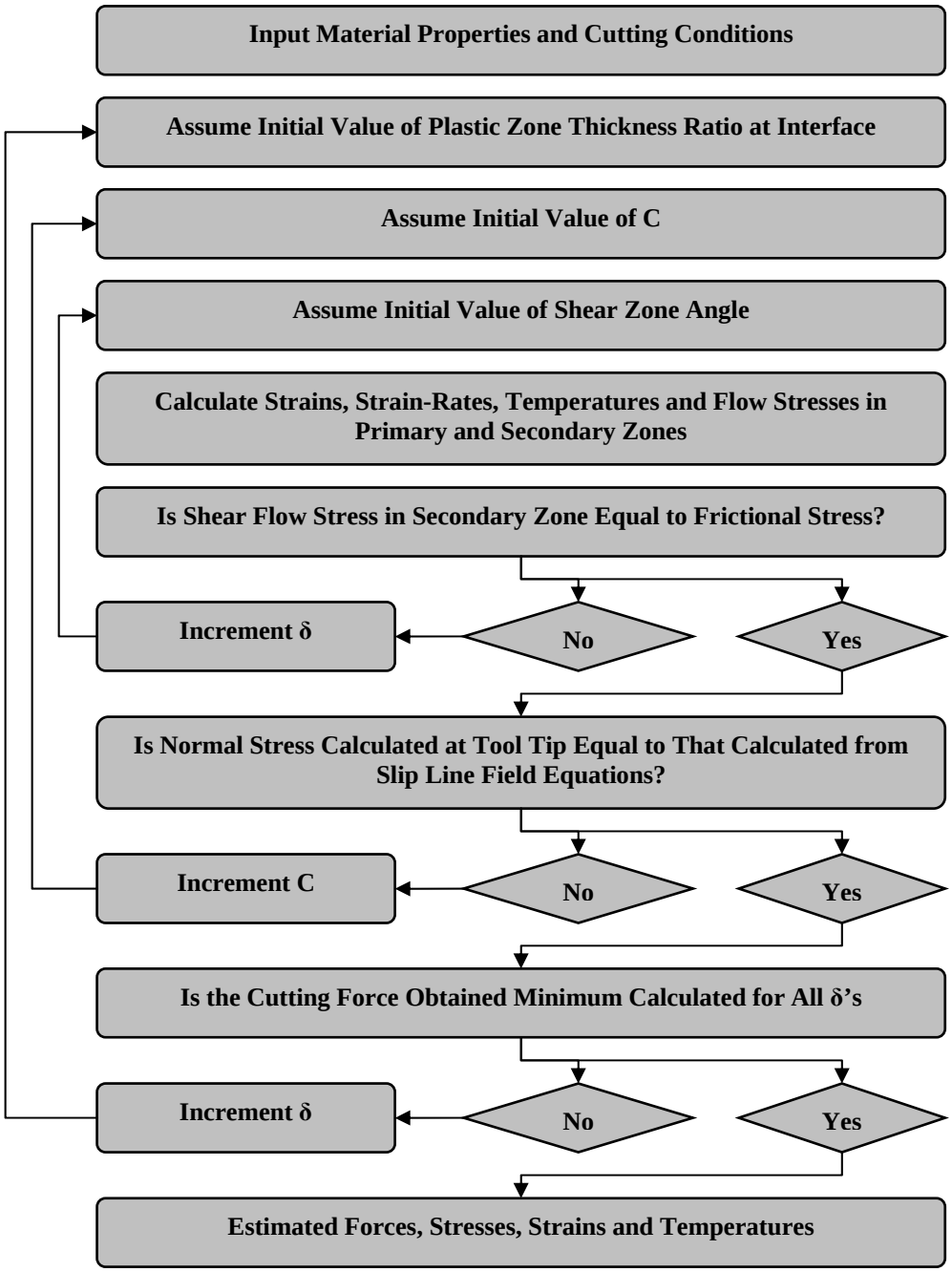

Figure 2.21: Oxley's theory and its simplified flow chart.

In the work by Shatla, Kerk and Altan [55], two dimensional orthogonal slot milling experiments in conjunction with an analytical-based computer code were used to determine flow stress data as a function of high strains, strain-rates and temperatures encountered in metal cutting.

Maekawa and Maeda [57] took into account of elasticity, plasticity, temperature, strain rate friction and tool flank wear to predict the effect of tool front edge and side edge on the workpiece during a 3D cutting process simulation.

Borouchaki, Cherouat, Laug and Saanouni [58] introduced the concept of using adaptive remeshing for ductile fracture prediction. In this work, remeshing is applied after each deformation increment by defining the new geometry after deformation, geometric error estimation, physical error estimation and adaptation of mesh element size with respect to damage. Figure 2.22 shows simulation results of this work.

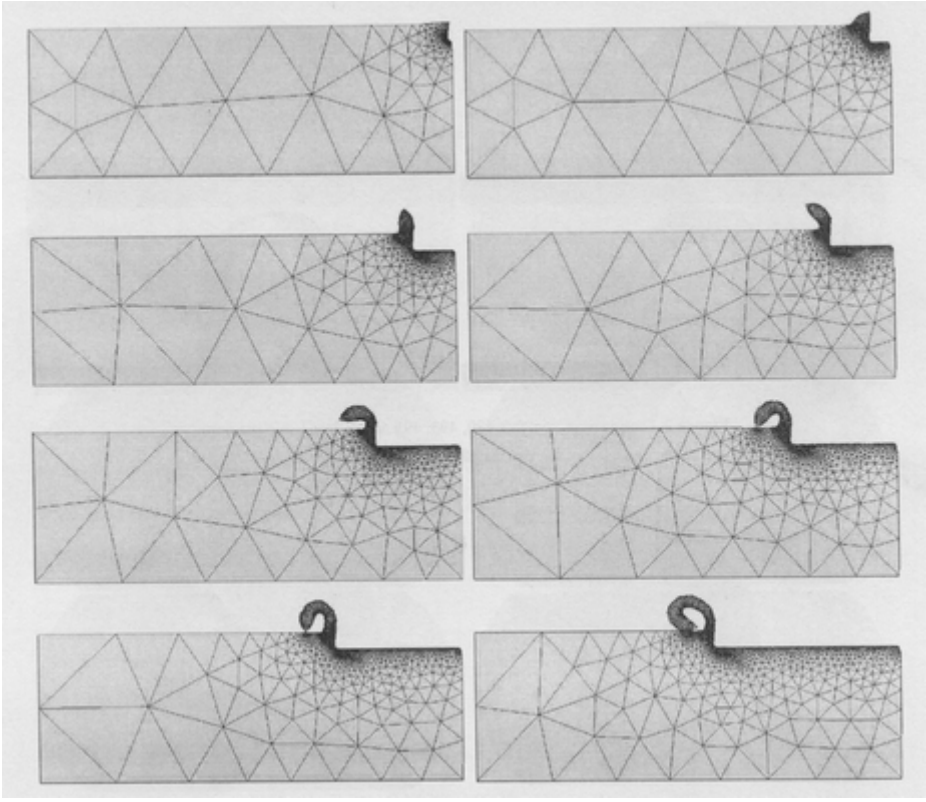

Figure 2.22: Results of the work done by Borouchaki, Cherouat, Laug and Saanouni

In the recent years, several models [59], [60], [61], [62] have been developed by several researchers to analyze the effect of different process parameters by using

the above mentioned numerical techniques regarding the material modeling, separation criterion and etc.

2.8 Conclusion

Simulation of orthogonal metal cutting operations is very popular nowadays and there are a lot of researchers studying on this subject. As described in this Chapter, since the second half this century, a lot work has been carried out for developing successful models of orthogonal metal cutting operations.

During this period, a lot of different aspects of the models have been studied. For example, there are a lot of separation criteria to separate chip from the workpiece. The same is also true for friction condition and material modeling used in these works. In addition, most of the researchers have verified their results with only one or two process variable, such as cutting or thrust forces.

However, there is almost no work on comparing these different aspects in the literature. In addition, the verification of all process variables is very difficult to find in the literature of the subject of metal cutting simulation.

Therefore, this work is intended to compare various models of orthogonal metal cutting operations with each other as well as with experiments. The results will be assessed with all process variables, which is a more realistic way since good agreement can be obtained in individual results by tuning the process parameters. At the end, the effects of various process parameters, such as friction or separation criteria, will be clear.

CHAPTER 3

EXPERIMENTAL WORK

3.1 Introduction

The purpose of the experiments performed in this work is to verify the results of numerical solution obtained by the finite element method. During experiments, following items were measured:

- Cutting force,
- Thrust force,
- Contact length between the chip and rake face of the tool,
- Chip thickness.

In addition, for every experiment, sample chips were collected and their thicknesses were measured on a microscope. Therefore, chip thicknesses as well as the calculated shear angles from the measurements were compared with the numerical solutions by finite element method.

Simulation results are also compared with experimental results found in literature, as well as with those obtained in this experimental work.

3.2 Orthogonal Cutting

Orthogonal cutting, Figure 3.1, is defined as a cutting operation where, cutting edge of the tool is perpendicular to the relative motion between the tool and workpiece. A cutting operation on a shaping or a planing machine with single point cutting tool is an example of simple orthogonal metal cutting.

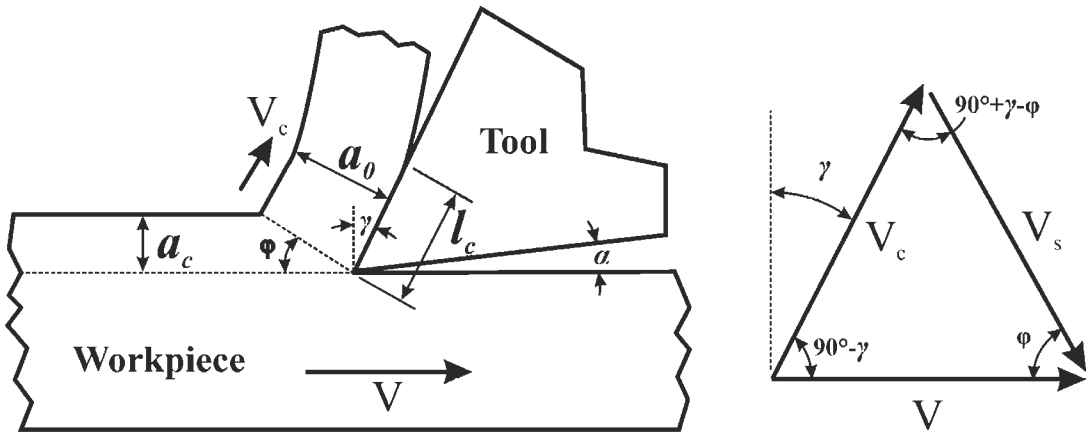

Figure 3.1: (a) Schematic representation of orthogonal cutting (b) velocity diagram associated with orthogonal cutting.

There are other methods to do experiments where orthogonal metal cutting is studied. For example, machining a hollow cylinder, which has a large diameter and small wall thickness, on a lathe from the end is also an example of practical orthogonal metal cutting operation (Figure 3.2).

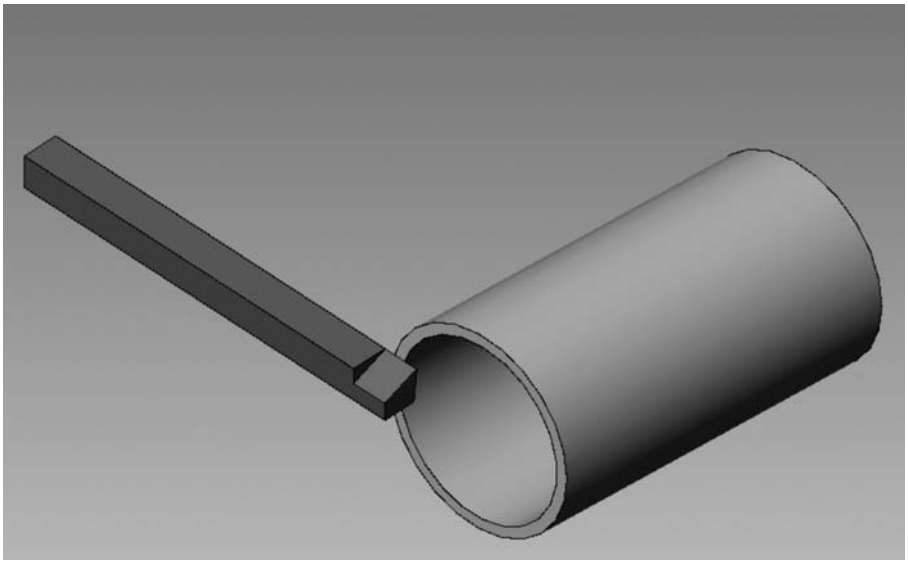

Figure 3.2: Orthogonal turning operation on a lathe.

In this work, the latter one is used. The important thing here is that, wall thickness, which is depth of cut in this case, must be significantly larger than the feed rate (undeformed chip thickness when side cutting edge angle is 0°) to satisfy the plane-strain assumption of finite element model.

3.3 Workpiece Material

Workpiece is a hollow cylinder made of C15 steel. This is a low carbon steel whose corresponding AISI standard designation is 1015. The outer and inner diameters of the workpiece are 56 and 53.1 millimeters respectively. Therefore, the depth of cut is 1.45 millimeters.

Table 3.1 and Table 3.2 show chemical composition and mechanical properties of the workpiece material.

Table 3.1: Chemical composition of C15 steel in weight percent.

C	Si	Mn
0.15	0.20	0.45

Table 3.2: Mechanical and thermal properties of the workpiece material, C15 steel.

Poisson's Ratio	Density (g/cm^3)	Modulus of Elasticity (GPa)	Thermal Conductivity (W/m.K)	Specific Heat (J/g.K)	Coefficient of Thermal Expansion (m/m.K)
0.3	7.85	210	58.6	0.46	$14.9x10^{-6}$

3.4 Test Setup

All cutting experiments were done on a universal lathe (Figure 3.3) with the cutting speed and feed rate being selected from the available options, which can be supplied automatically by the machine.

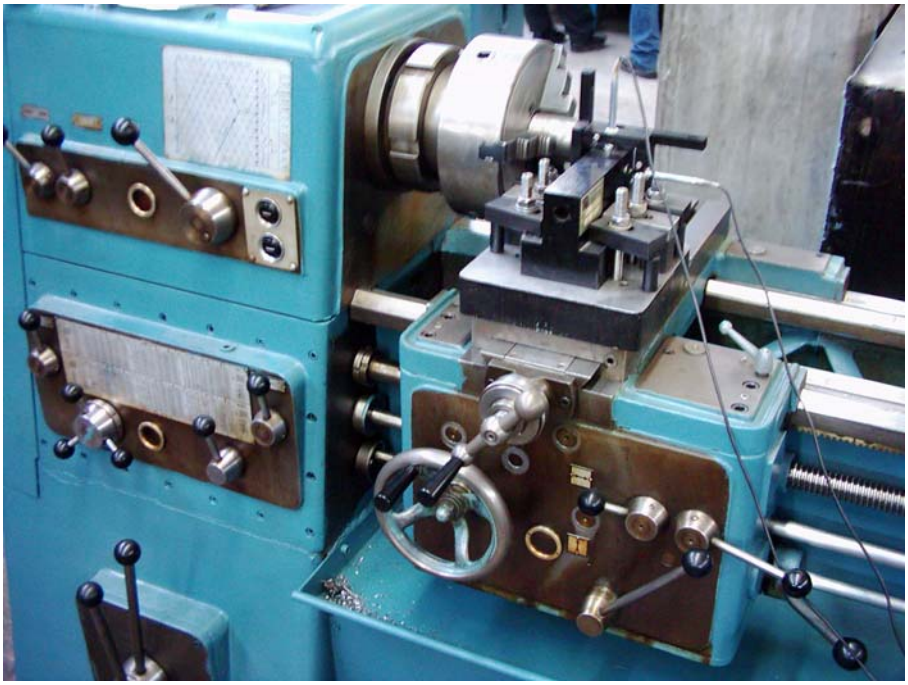

Figure 3.3: Test Setup

Force measurements are taken by means of a dynamometer which can be seen on Figure 3.4. It is composed of a cutting tool mounted on a horizontal column whose deflections in both of the horizontal and vertical directions are measured

by means of two mercer probes. The dynamometer itself is made of cast iron and able measure tangential forces up to 2500 N.

Figure 3.4: Lathe tool dynamometer setup.

Mercer probes have a maximum total tip travel of 4.5 mm. Their linearity over the measuring range is 0.1%. In addition, the repeatability value of these probes is given as 0.1 μm.

Measured deflections are sent to the analog display, where they can be seen in micrometers. This display can be scaled to different ranges, making it easier to read the data. Available ranges are 1500, 500, 150, 50, 15 and 5 μm. The photograph of the analog display can be seen on Figure 3.5.

Figure 3.5: Analog display of the dynamometer.

Since the forces are not measured directly and they are found via the deflection of the horizontal column, a careful calibration of the dynamometer is needed.

The calibration is done by applying known weights and collecting the measured deflection data, which can be seen on Figure 3.6. The load was varied from 0 to 135 N and the calibration curves were drawn for both loading and unloading conditions. Therefore if there is any hysterisis in the measurement, it can be seen. This procedure is applied for both cutting and thrust force measurements.

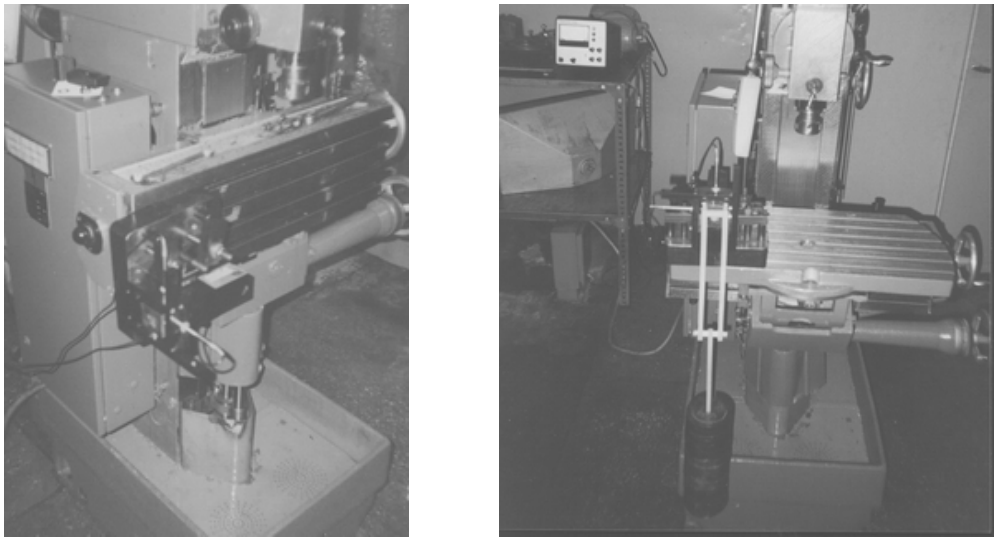

(a) (b)

Figure 3.6: Calibration of the device. (a) thrust force (b) cutting force

At the end, the gathered calibration curves are as shown on Figure 3.7.

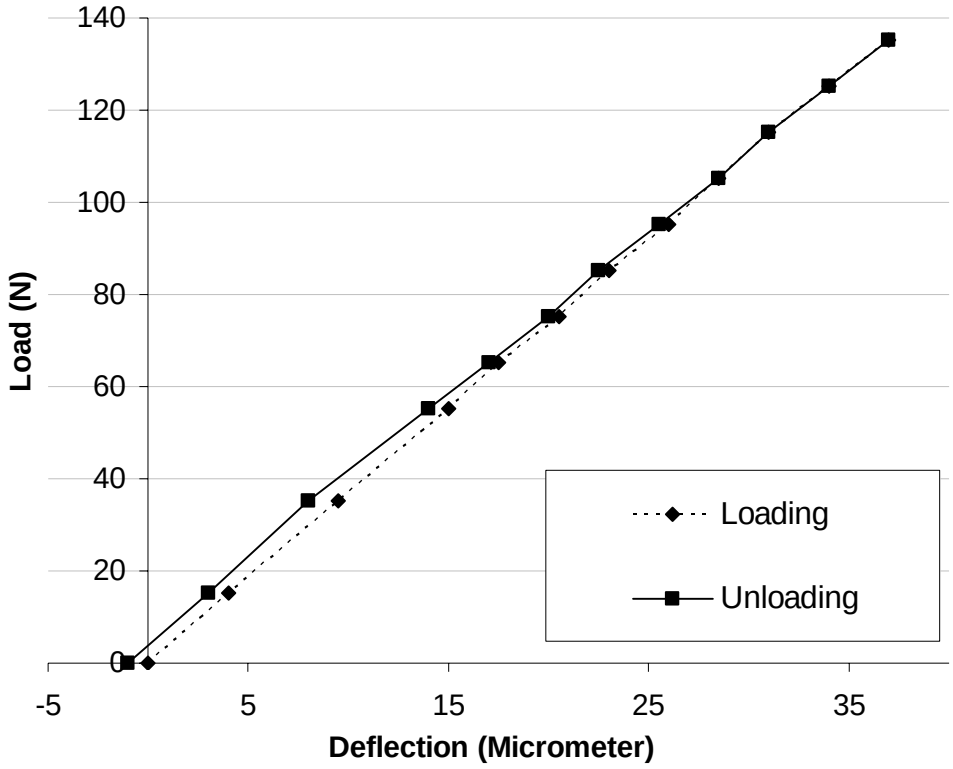

Figure 3.7: Calibration curve for cutting force.

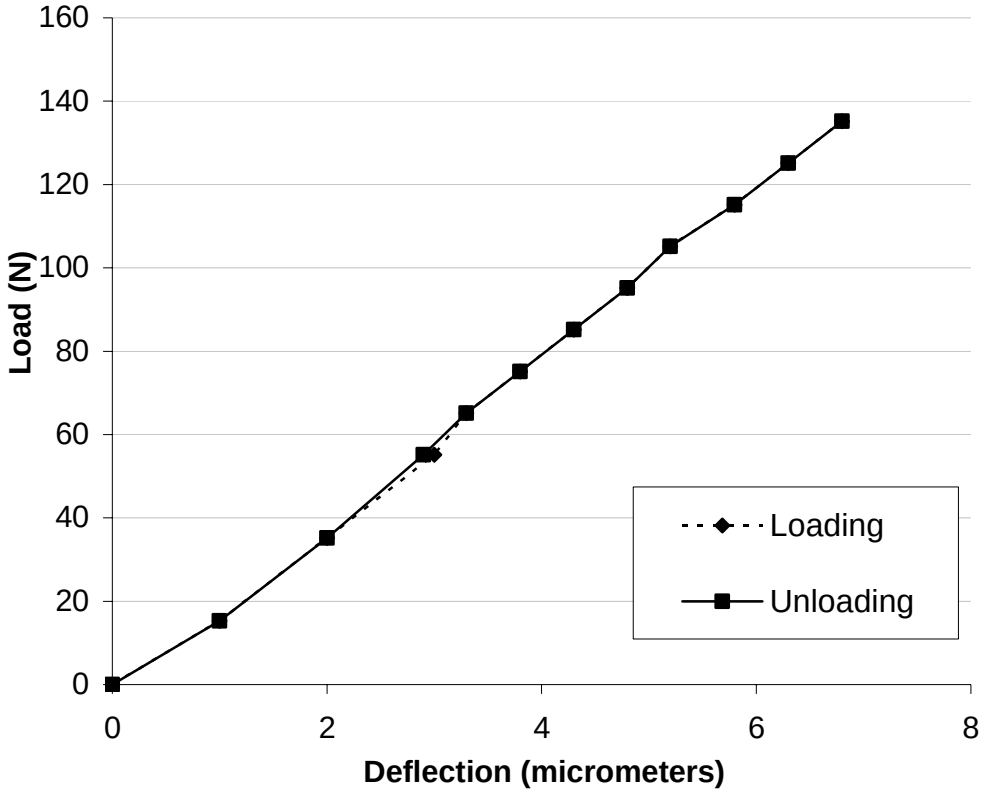

Figure 3.8: Calibration curve for thrust force.

It can be seen that, although the thrust force calibration curve is good, there is a very small hysterisis for the tangential force calibration curve. However, hysterisis is active, where the cutting forces are quite small. In the experiments, usually the forces are larger, thus they are not affected from this hysterisis. It is also important that, the lines are very close to a straight line. Therefore, linear extrapolation may be used for the loads, which are above the range of calibration curves.

Contact length and chip thickness measurement were done by means of a Topcon tool maker's microscope, which is able measure as small as 1 micron. Specifications of this device can be found in Table 3.3.

Table 3.3: Specifications of the Topcon Universal Measuring Microscope.

	Measuring Ranges	**Minimum Divisions**	**Overall Accuracies**
Longitudinally	200 mm	0.001 mm	(2+0.01 L) μ
Transversely	75 mm	0.001 mm	(2+0.01 L) μ
Height	60 mm	0.01 mm	10'
Goniometric Head	360°	1'	30'
Rotary Table	360°	10"	15'
Dividing Head	360°	5'	

Before cutting experiments, rake face of the tool was painted and after the experiment completed, length of the erased part was measured by mentioned microscope. Figure 3.9, Figure 3.10 and Figure 3.11 shows contact length on the tools rake face, the device and a sample chip thickness.

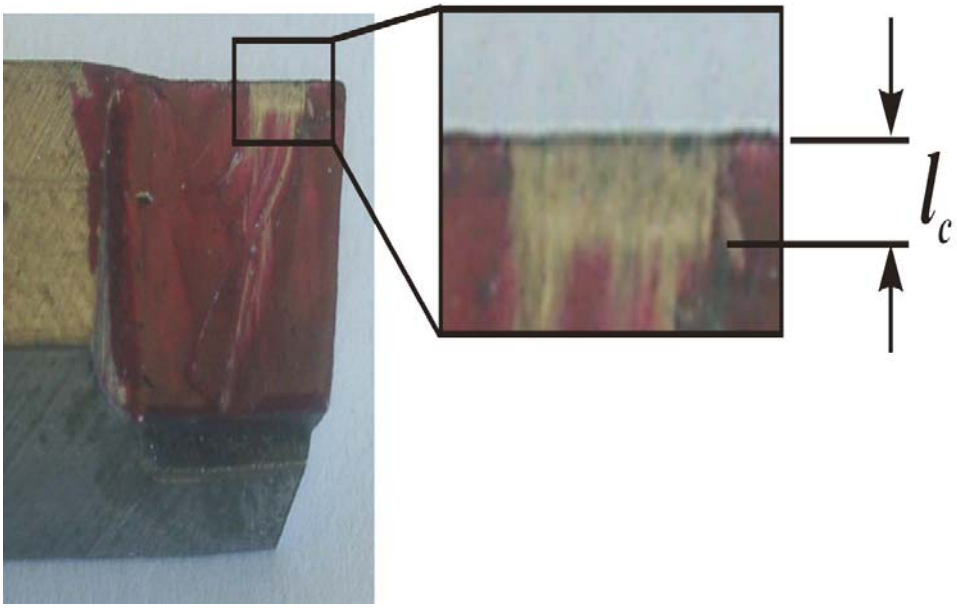

Figure 3.9: Contact length on the rake face of the tool.

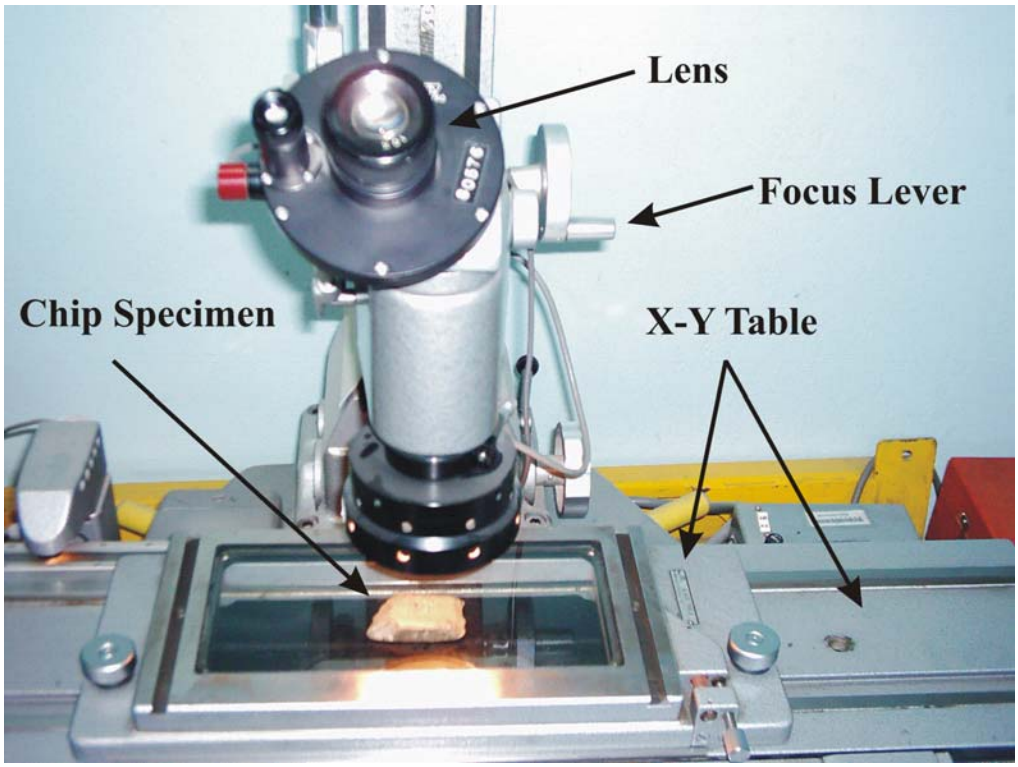

Figure 3.10: Topcon microscope by which the thicknesses of chips were measured.

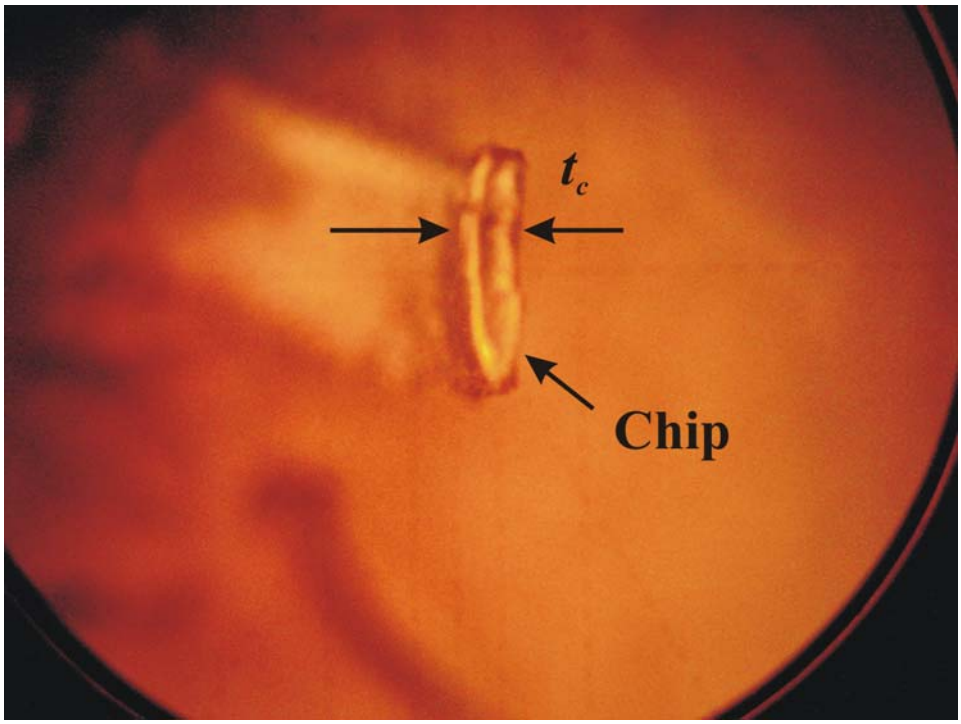

Figure 3.11: A sample microscope view while measuring thickness.

3.5 Cutting Experiments Performed in This Work

As it is mentioned before, orthogonal cutting tests were conducted at the end of hollow work parts on a lathe. Following variables were measured.

- Cutting force
- Thrust force
- Contact length on the rake face of the tool
- Chip thickness

Experiments were performed for four different cutting conditions depending on two different rake angles and 2 different feed rates. Table 3.4 shows the cutting conditions of the experiments. Cutting tools have 5° clearance angle, 0° side cutting edge angle, 0° back rake angle. In addition, tool inclination is 0°.

Table 3.4: Cutting conditions at which experiments were performed.

		Feed rates (mm/rev)	
		0.05	**0.1**
Rake angles	**20°**	Exp. 1	Exp.2
	25°	Exp. 3	Exp. 4

In addition to the cutting experiments compression test were also performed on the workpiece material to verify the flow curves used during the simulations.

3.6 Compression Test

As it is mentioned before, cutting experiments were performed with the workpiece material being C15 (AISI 1015) steel. In the simulations, flow curves are used from the database of the commercial codes. For the MSC.Marc and Deform2D they are given in tabular format, whereas Thirdwave AdvantEdge uses analytical formulation for material flow curve. Therefore, these flow curves need to be verified for the good representation of material behavior, which is used in the cutting experiments.

For this purpose, ring compression test were performed on the workpiece material. The resulted punch displacement – punch force curve were compared with the simulation of the same process.

At this point it should be noted that, many of the parameters used in analytical formulation implemented in Thirdwave AdvantEdge are hidden to the user. Therefore, the comparison of flow curve is not available for Thirdwave AdvantEdge. Figure-3.12 show the experimentally compressed specimen and the results of simulations obtained by MSC.Marc and Deform2D.

(a) (b) (c)

Figure 3.12: Comparison of experimental and simulated compressed specimens.
(a) Simulation by Deform2D (b) Compressed specimen (c) Simulation by MSC.Marc

On Figure 3.12, it can be seen that the geometry of the compressed specimen is estimated very well.

Comparison of punch displacement – punch force diagram can be seen on Figure-3.13.

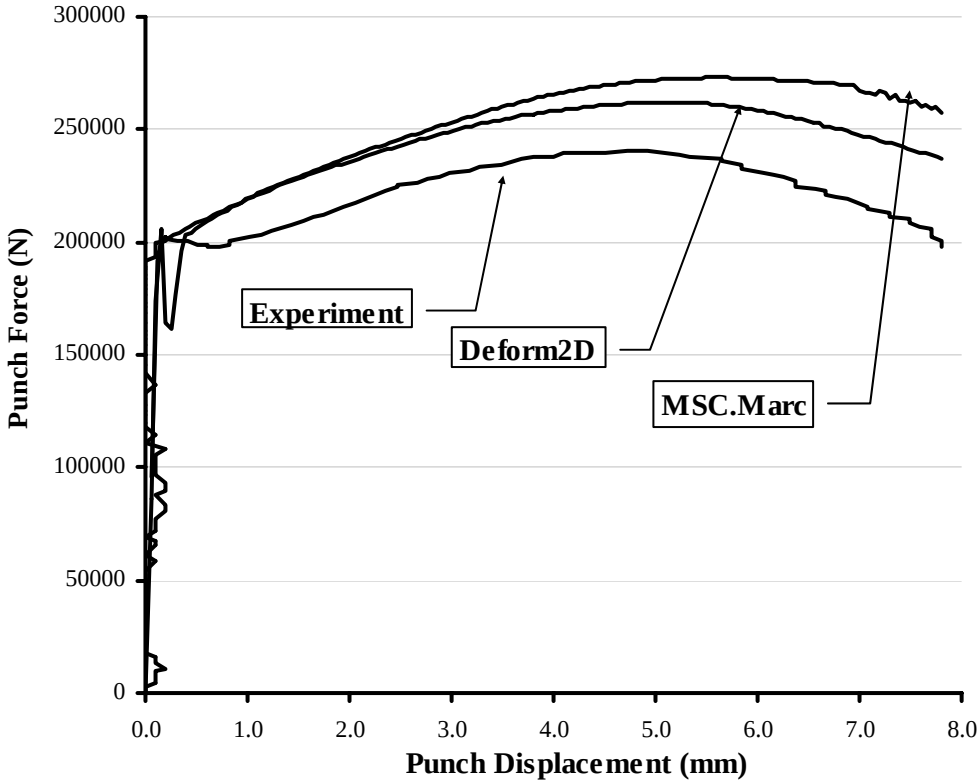

Figure 3.13: Comparison of punch displacement – punch force diagram.

It is seen that the yield point is estimated very well, although there are small differences in the plastic region. However this difference might be explained by the different strain-rates faced during the experiments and available in the flow curves of commercial codes. Experiments were performed at very small strain-rates, which are about $4x10^{-4}$ s^{-1}. Flow curves, on the other hand does not include data for such small strain-rates, which leads to about 10 % error in the punch displacement-punch force curve.

CHAPTER 4

NUMERICAL MODEL OF ORTHOGONAL METAL CUTTING

4.1 Introduction

In recent years, finite element method became the main tool for the analysis of metal cutting. Because it has important advantages, which can be counted as follows.

- Material properties can be handled as a function of strain, strain-rate, and temperature
- Nonlinear geometric boundaries, such as free surfaces, can be modeled.
- Other than global variables like cutting force, thrust force; local variables like strains, strain-rates, stresses, etc. can be obtained
- Interaction of chip and tool can be modeled in different forms.

In this work three different commercial finite element codes were used to model two dimensional plain-strain orthogonal metal cutting operations. These are MSC.Marc, Deform2D and Thirdwave AdvantEdge. MSC.Marc and Deform2D are static implicit codes, whereas Thirdwave AdvantEdge is a dynamic explicit code.

4.2 Finite Element Models

On the following pages, finite element models of all codes will be explained in different sections. Since three commercial codes have been used, the sections are as the following:

1. Finite element model of MSC.Marc.
2. Finite element model of Deform2D.
3. Finite element model of Thirdwave AdvantEdge.

At the very end of this chapter, a comparison of all codes will be made in the sense of finite element formulation, boundary conditions, separation criterion and etc.

4.2.1 Finite Element Model with MSC.Marc

The model is plane-strain thermo-mechanically coupled and material behavior is elastic-plastic. The assumption of plane-strain condition is valid if the width of the cut is significantly larger than the uncut chip thickness. In the model, width of cut is ten times larger than the uncut chip thickness; therefore the assumption of plane-strain condition is satisfied.

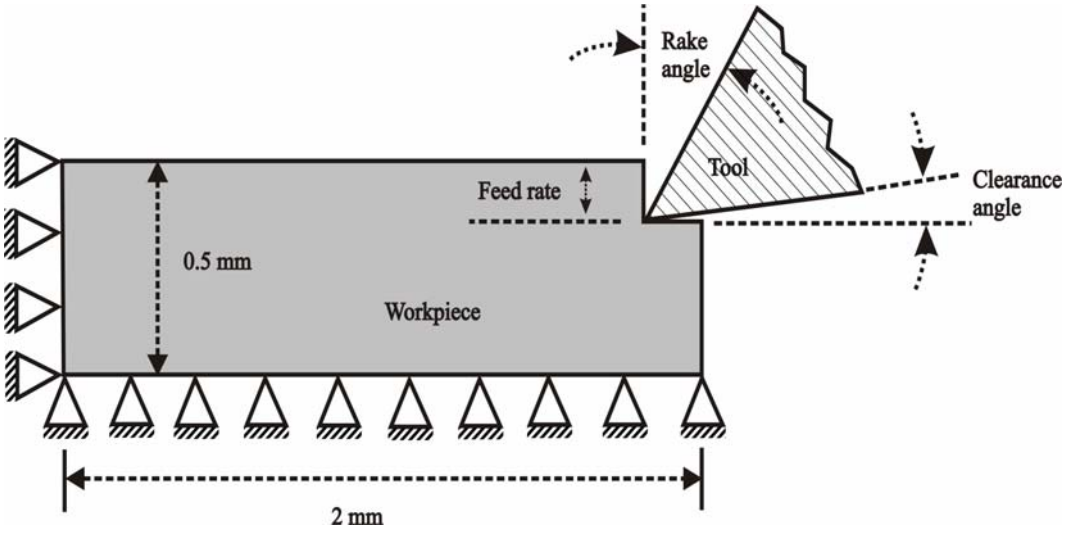

Figure 4.1: Finite element model of MSC.Marc

Figure 4.1 shows the finite element model for MSC.Marc. The workpiece dimensions are 2 mm in width and 0.5 mm in height. The left and bottom boundary nodes of the workpiece is restricted so that they can not move in both of the x and y directions. This is achieved by gluing a stationary rigid curve to those nodes. This could also be done by defining boundary conditions; however MSC.Marc can not handle this, when global remeshing is enabled. Hence, rigid curves have been used to satisfy the necessary boundary conditions. The top and right boundaries were left as free surfaces.

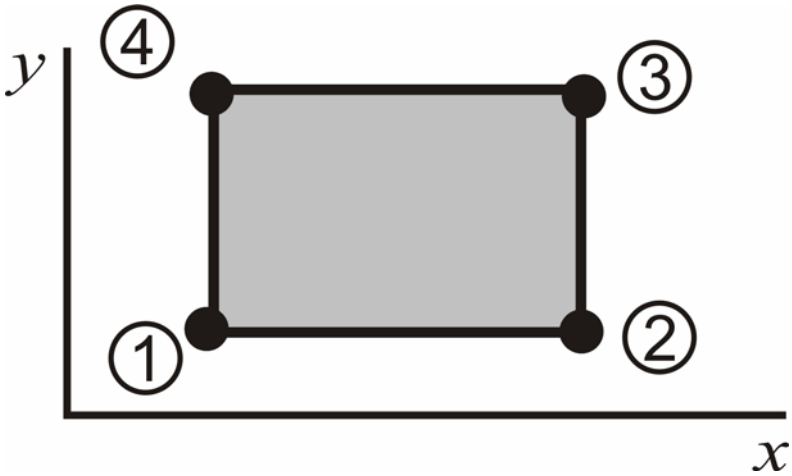

Figure 4.2: Quadrilateral element

Workpiece was discritized by bilinear quadrilateral elements, which can be seen on Figure 4.2. Element type is 11, which is written for plane-strain applications, from MSC.Marc Element Library.

In this work, it is assumed that the tool is not plastifying. Hence it is considered as rigid and modeled as a curve. Its parameters are rake angle, clearance angle and cutting edge roundness. Although the rake angle is changing in different simulations according to the cutting conditions for which it is done, the clearance angle and nose radius is constant in all of the simulations carried out in this work. The value of clearance angle is 5° and the value of edge roundness is 0.002 mm.

Since this is a thermo-mechanically coupled model, there are also thermal boundary conditions defined. First of all, the workpiece is loosing heat to the environment, which is assumed to be at 20 °C, at a rate of 0.4 N/mm.°C. Workpiece loses heat to the environment due to convection according to the following formula.

$$q = h \cdot (T_w - T_0) \tag{4.1}$$

where, h is the convection heat transfer coefficient of the workpiece (0.4 N/(mm.˚C)), T_w is the workpiece surface temperature, and T_o is the ambient temperature (20 C˚).

On the other hand, the heat is generated due to two reasons.

- Due to the heavy plastic work done at the shear zone. It is assumed that, 90% of all plastic work is converted into heat.
- Due to friction at the interface of tool and chip.

The half of the generated heat due to friction at the tool chip interface is given to each of the two contacting bodies, which are chip and tool in this case (Figure 4.3).

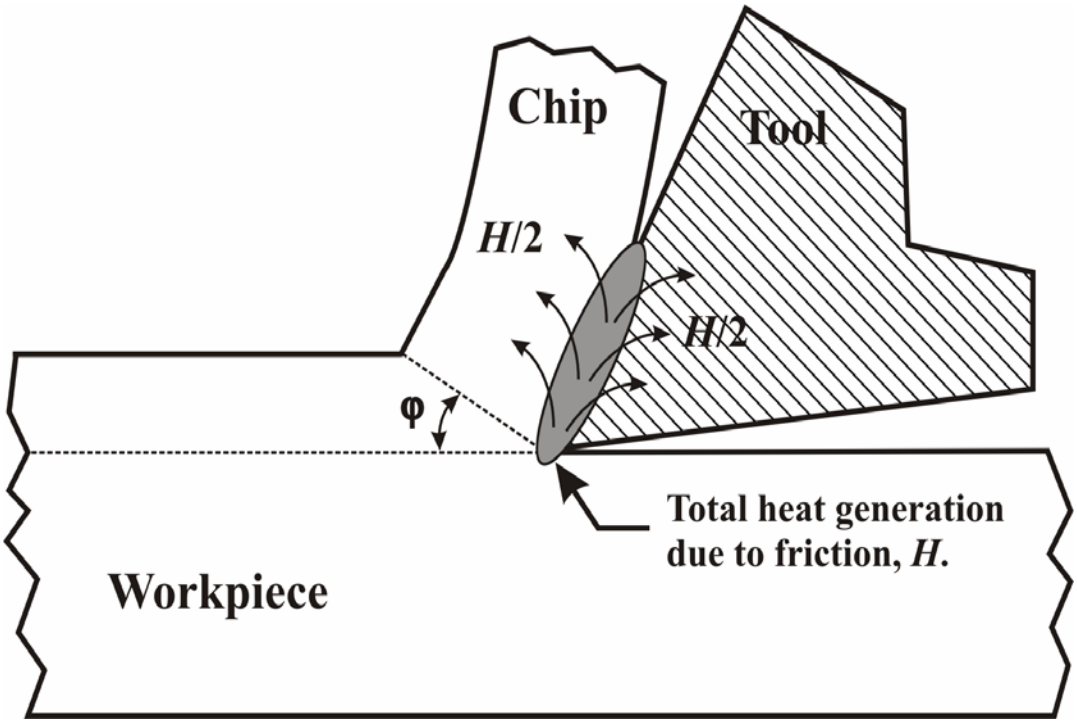

Figure 4.3: Distribution of generated heat due to friction.

Heat generated due to friction is given by the following formula:

$$q = F_{fr} \cdot v_r \cdot M \tag{4.2}$$

where, F_{fr} is the friction force, v_r is the relative sliding velocity between tool and chip, and M is the mechanical equivalent of heat (M=1.0).

The rate of specific volumetric flux due to plastic work is given by the following formula:

$$R = \frac{M \cdot f \cdot W^{p}}{\rho} \tag{4.3}$$

where, W^p is the rate of plastic work, f is the fraction of plastic work converted into heat which is assumed to be 0.9, M is the mechanical equivalent of heat (taken as 1.0 by default) and ρ is the density of workpiece material (7.85 g/cm^3).

The workpiece material used for this plane-strain orthogonal metal cutting simulation is C15 steel. Its flow curve is represented by several tabulated data (MSC.Marc database) which depends on strain, strain-rate and temperature.

The material data is represented by several flow curves at 3 different strain-rates (1.6, 8 and 40 s^{-1}) and at 13 different temperatures (20, 100, 200, 300, 400, 500, 600, 700, 800, 900, 1000, 1100, 1200 ˚C), while strain is changing between 0 and 1. Figure 4.4, 4.5 and 4.6 shows the flow curves of the material for different strain rates.

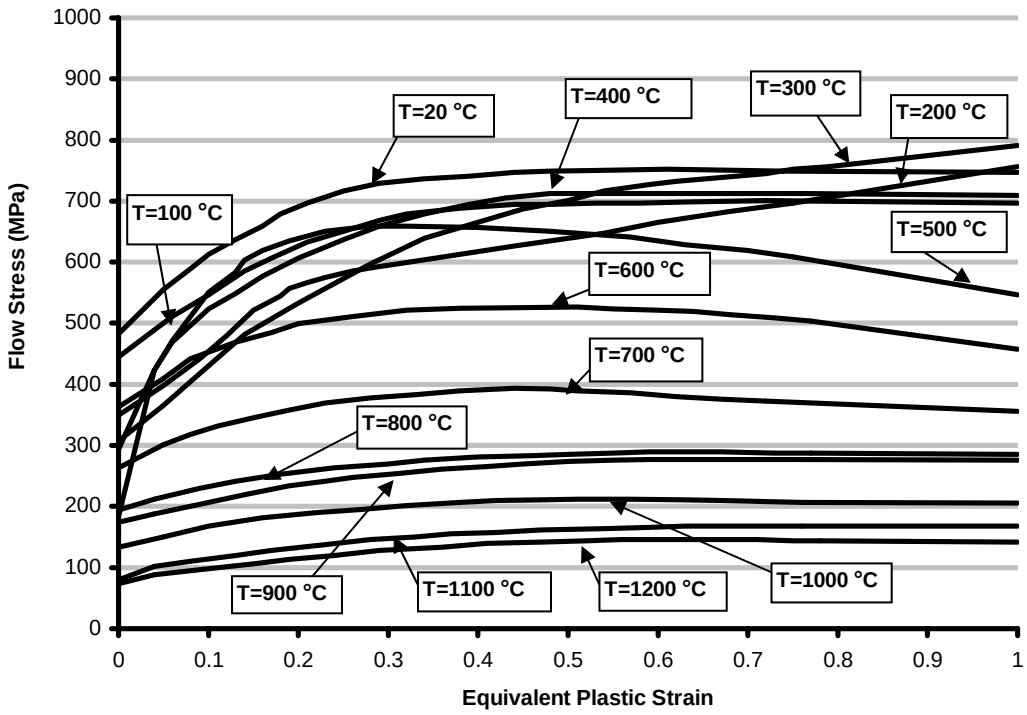

Figure 4.4: Workpiece flow curve for strain-rate of 40 (s^{-1}).

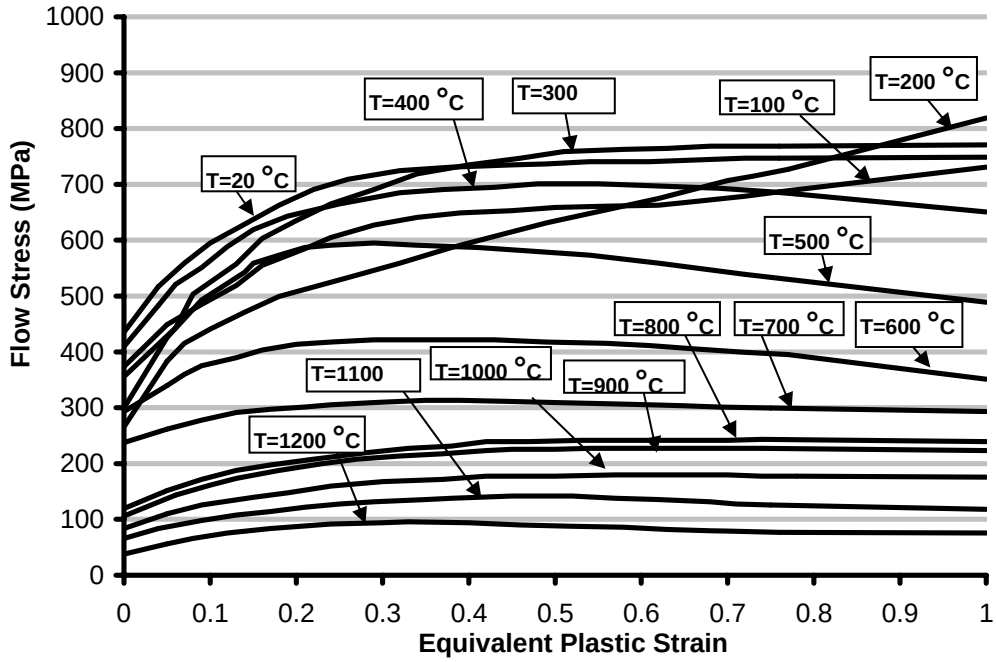

Figure 4.5: Workpiece flow curve for strain-rate of 8 (s^{-1}).

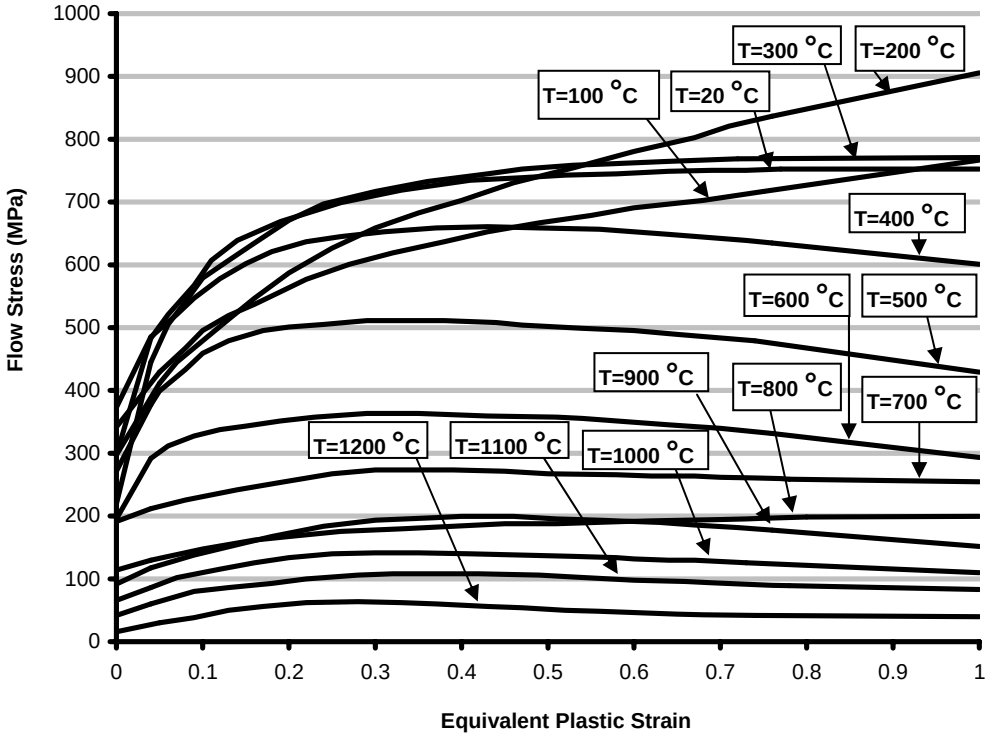

Figure 4.6: Workpiece flow curve for strain-rate of 1.6 (s^{-1}).

In the cutting process, the deformation of material at the cutting zone takes place at elevated temperatures and strain rates. However, if the given flow curves are exceeded, then required data is calculated at the border. Therefore, after exceeding the highest value of strain-rate available, calculations are always done using the same flow curve set, which, in this case, the one available for 40 s^{-1}. This is the weakest point of this finite element model. Although the strain-rates at the shear zone can be extremely high, the flow stress of the material can only be calculated at a maximum strain-rate of 40 s^{-1}.

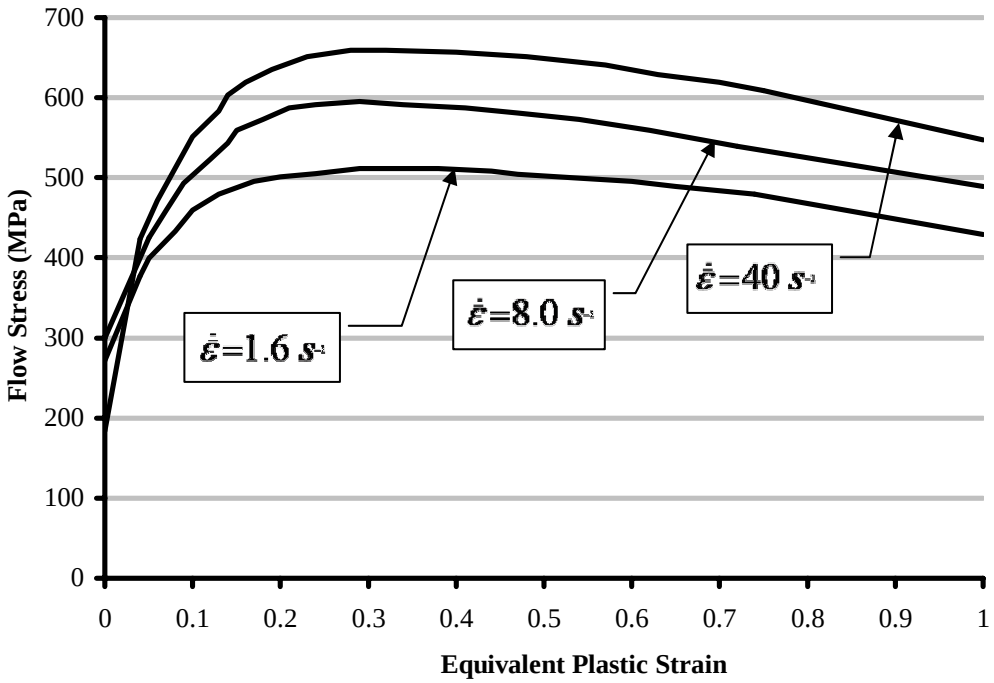

Figure 4.7: Effect of strain-rate on the flow curves.

Figure-4.7 is flow curves of the workpiece material at 500 °C and at different strain-rates. This figure can give an idea of error introduced by improper flow stress evaluation at elevated strain-rates.

In the simulations, the tool is pushed to penetrate through the workpiece at the cutting speed. The friction between the tool and the chip is modeled as constant

shear type which states that frictional stress is a fraction of the shear yield stress of the material (or the effective stress in the material):

$$\sigma_{fr} = -m \cdot k_y \cdot t = -m \cdot \sqrt{\tfrac{1}{3}} \cdot \bar{\sigma} \cdot t \tag{4.4}$$

where, m is the friction factor or coefficient of shear friction whose value being between 0 and 1, k_y is the shear yield stress of the workpiece material, t is the tangential vector in the direction of relative velocity and $\bar{\sigma}$ is the equivalent stress in the material.

Quite often in contact problems, neutral lines develop. This means that along a contact surface, the material flows in one direction in part of the surface and in the opposite direction in another part of the surface. Therefore, the friction stress has a step function behavior based upon the value of v_r or Δu.

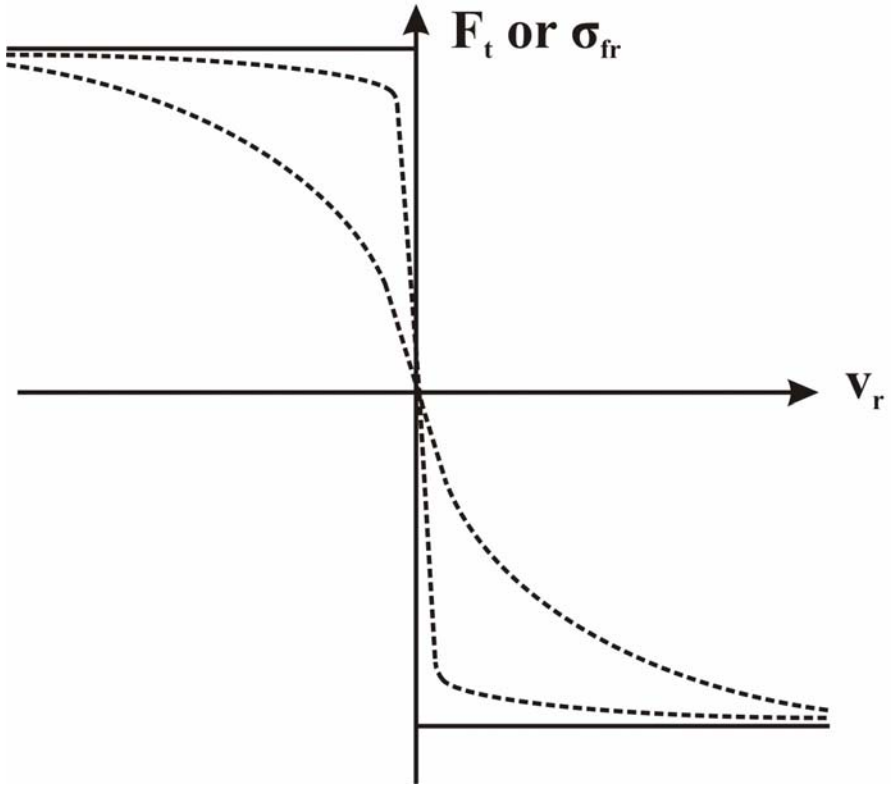

Figure 4.8: Step function frictional stress and approximation by Equation 4.5.

This discontinuity in the value of σ_{fr} can result in numerical difficulties, so a modified Constant Shear friction model is implemented in MSC.Marc whose formula is given as:

$$\sigma_{fr} = -m \cdot \frac{\bar{\sigma}}{\sqrt{3}} \cdot \frac{2}{\pi} \cdot \tan^{-1}\left(\frac{v_r}{C}\right) \cdot t \tag{4.5}$$

where, v_r is the magnitude of relative velocity between the die and the workpiece and C is a constant, named relative sliding velocity.

Figure 4.8 show the step function behavior of friction (solid line) and its approximation by Equation 4.5 (dash lines). Depending on the value of C, degree of approximation can be changed.

Physically, C has the value of the relative velocity when sliding occurs. The value of C is important in determining how closely the mathematical model represents the step function. A very large value of C results in a reduced value of the effective friction. On the other hand, a very small value results in poor convergence. It is recommended that the value of C be 1% or 10% of a typical relative sliding velocity, v_r. Because of this smoothing procedure, a node in contact always has some slipping.

In this work, the value of the coefficient of shear friction has been changed in the range of 0.2 to 0.7 to see the effects on the process results like shear angle, cutting force, thrust force, and etc. The value of C was taken as 1 % of the magnitude of the relative sliding velocity between the chip and tool.

As already discussed in the Chapter 2, (Literature survey), there are a number of methods to separate material from the workpiece to form the chip while the tool penetrates into it. In this model, the method of remeshing was applied. Therefore, the workpiece is remeshed whenever the tool penetrates into the workpiece by a

predefined threshold value. Figure 4.9 shows how a new surface is generated on the workpiece by remeshing when a penetration occurs.

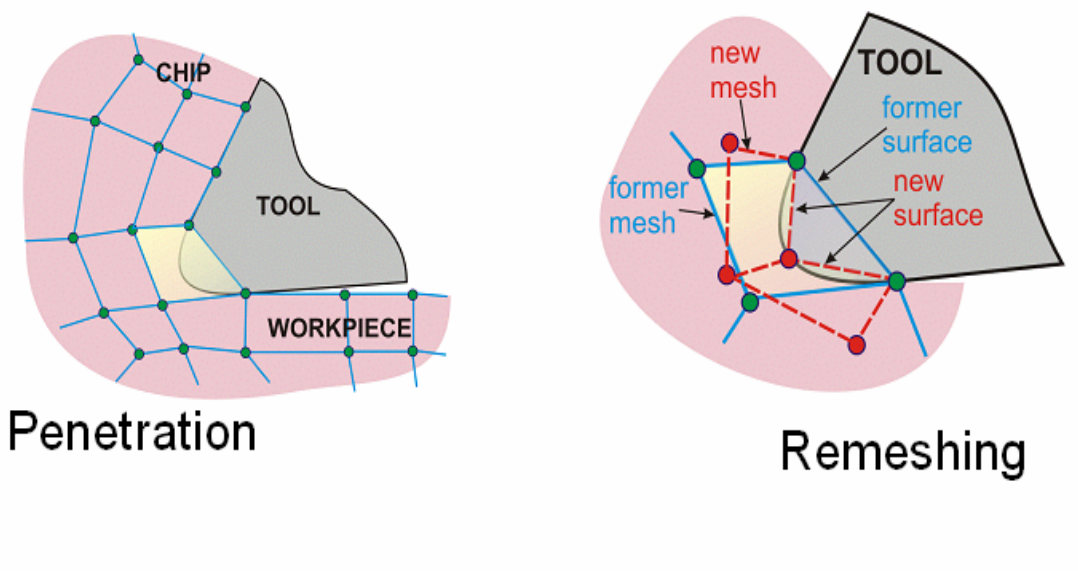

Figure 4.9: Separation of chip from the workpiece by continuous remeshing.

By default MSC.Marc takes penetration value as 0.05 of the minimum element edge length, however it is possible to change it. In addition, the time of penetration check can also be altered, being either at the end of increments, or at every iteration. Although the penetration value does not introduce a significant difference, the type penetration check leads to major changes in the results. The effects of these two variables can be seen in Chapter 5 (Results and Comparison).

4.2.2 Finite Element Model with Deform2D

The model of Deform2D is not so different than the model of MSC.Marc. This is again a thermo-mechanically coupled simulation with elastic-plastic material modeling. There are two differences between the models of MSC.Marc and Deform2D:

1. The method used to satisfy the necessary boundary conditions on the bottom and left boundary nodes of the workpiece.
2. The method used to separate the chip from the workpiece.

Figure 4.10 shows the finite element model of orthogonal cutting, which is used with Deform2D.

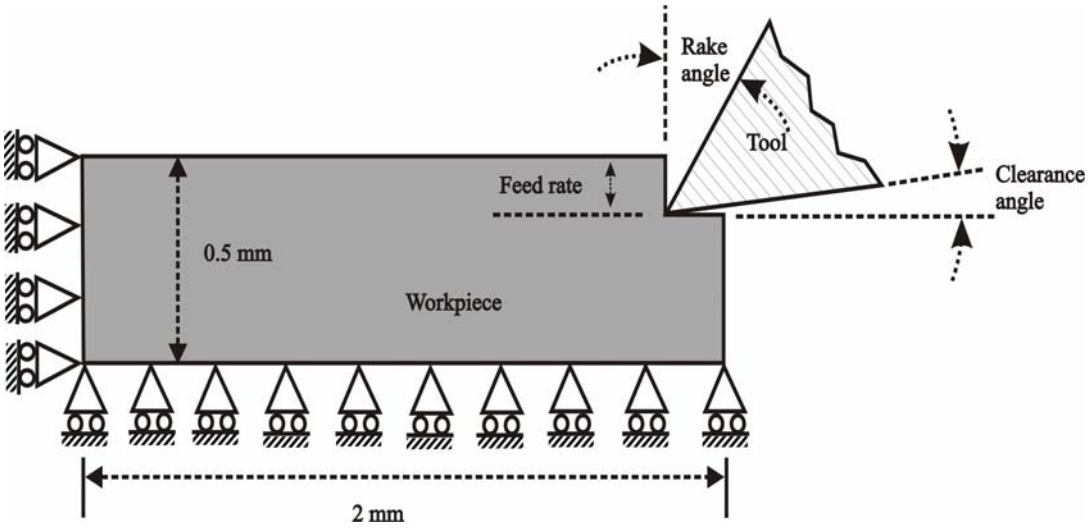

Figure 4.10: Finite element model of Deform2D.

Deform2D is able to handle global remeshing when there is displacement boundary conditions defined for the workpiece. Therefore, in the model with Deform2D, the left boundary nodes are fixed in x-direction, and the bottom boundary nodes are fixed in y-direction.

As it is the case with MSC.Marc, in the simulation with Deform2D, the tool was pushed to penetrate through the workpiece to form the chip. However, the formation of chip is different for Deform2D. The idea is that, while the tool penetrates, the elements at the tip of the tool are erased via remeshing whenever they reach a critical damage value. Figure 4.11 shows an element erase stage during the two consequent increments of simulation. It can be seen that, element is erased and the workpiece is remeshed.

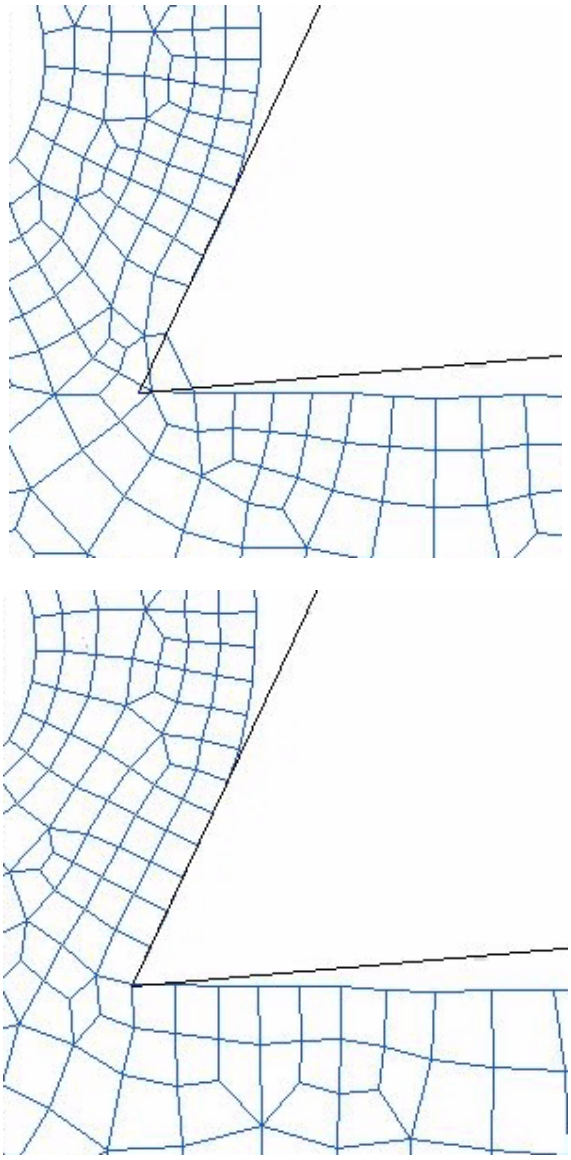

Figure 4.11: Element erase due to damage via remeshing in Deform2D

In Deform2D, different damage models can be defined and among those Normalized Cockroft-Latham damage criterion was used to initiate deletion of elements for separating the chip from the workpiece. Critical damage value, *C*, is used as 0.2, which is found from literature.

Workpiece dimensions are again 2 mm in width and 0.5 mm in height. It was discritized by bilinear quadrilateral elements (Figure 4.2).

Thermal boundary conditions were defined to enable the coupling of thermal and mechanical solutions:

1. Heat is generated due to plastic work done on the workpiece while the tool penetrates through the material (Equation 4.3). It is assumed that 90% of all plastic work is converted into heat.
2. Heat is generated due to friction between the tool and the chip (Equation 4.2).
3. The workpiece is loosing heat to the environment (Equation 4.1). The value of convection coefficient, h, is taken as 0.4 (N.mm/°C) and the ambient temperature is assumed to be at 20 °C.

Workpiece material was chosen as 0.15 % Carbon steel from the database of Deform2D. This database includes only the flow stress of the chosen material. Therefore, the other input data should be entered separately, such as elastic modulus, poison's ratio, thermal expansion coefficient, thermal conduction coefficient and heat capacity of the material. If the simulation conditions of the material exceed the bounds of the strain, strain rate or temperature defined in the tabular data, Deform2D extrapolates the tabulated data based on the last two data points to find the desired flow stress.

Friction between the tool's rake face and chip is modeled by the constant shear law, which is the same as the model of MSC.Marc. The friction factor has been changed between 0.2 and 0.7 to see the effects of friction on the process variables.

4.2.3 Finite Element Model with Thirdwave Systems Advantedge

Thirdwave Systems Advantedge is a special program written only for machining simulations. It is a dynamic explicit Lagrangian formulation. The model is built

by selecting the type of machining operation (e.g. turning, broaching, sawing or milling) and defining the necessary process parameters. Since the main subject of this work is turning operations, the process parameters that should be inputted to Advantedge are feed rate, depth of cut, length of cut, cutting speed and initial temperature of the workpiece. Other parameters are fixed automatically by the code and hidden to the user..

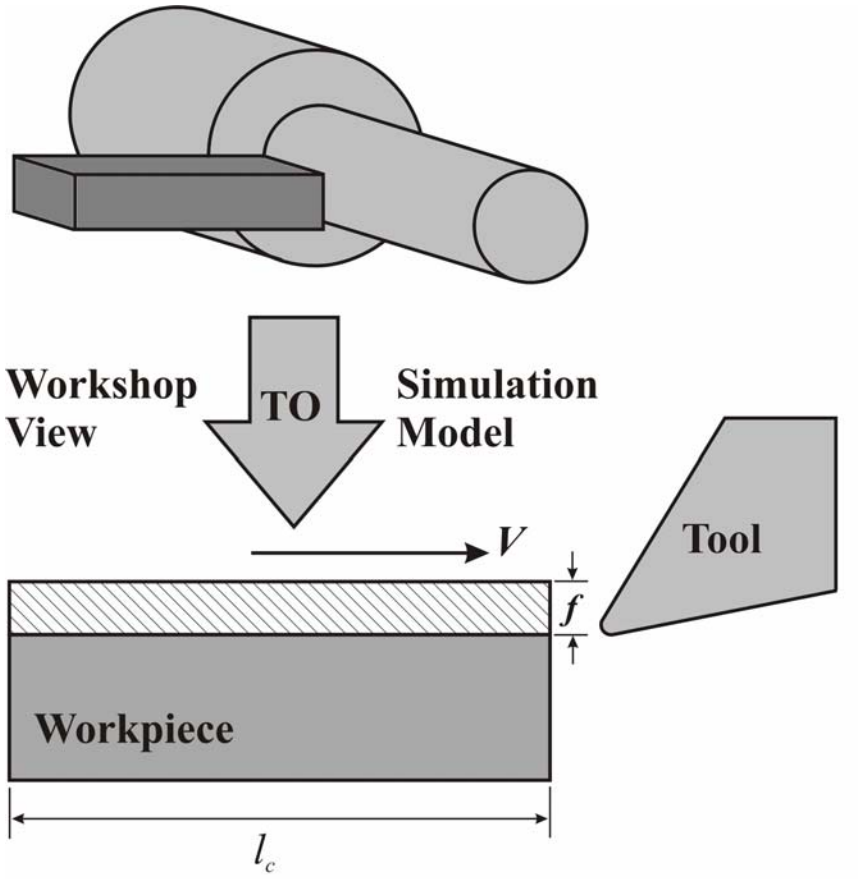

Figure 4.12: Finite element model of Third Wave Systems AdvantEdge.

Figure 4.12 shows both the turning operation itself and the two dimensional modeling in Thirdwave AdvantEdge. On this figure, l_c is the length of cut, f is the feed rate and V is the cutting speed. Depth of cut is defined as the dimension to the inside of the paper.

This model is also thermo-mechanically coupled. In Advantedge a staggered procedure is adopted for the purpose of coupling the thermal and mechanical equations. Geometrically identical meshes for the thermal and mechanical models are used. Mechanical and thermal computations are staggered assuming constant temperature during the mechanical step and constant heat generation during the thermal step. A mechanical step is taken first based on the current distribution of temperatures, and the heat generated is computed from plastic working and frictional heat generation. The heat thus computed is transferred to the thermal mesh and the temperatures are recomputed by recourse to the forward-Euler algorithm. The resulting temperatures are transferred to the mechanical mesh and are incorporated into the thermal-softening model, which completes one time-stepping cycle.

Thermal boundary conditions for Thirdwave AdvantEdge are given as:

1. The heat is generated due to heavy plastic work done on the workpiece, whose formula is given in Equation 4.3.
2. The heat is generated due to friction between the chip and the rake face of the tool according to Equation 4.2.
3. The generated frictional heat is distributed to chip and tool according to the Equation 4.6, where Q_{chip} is the heat given to the chip, Q_{tool} is the heat given to the tool, $Q_{friction}$ is the total heat generated due to friction, k is the conductivity, ρ is the density and c is the heat capacity.

$$\frac{Q_{chip}}{Q_{tool}} = \frac{\sqrt{k_{chip} \cdot \rho_{chip} \cdot c_{chip}}}{\sqrt{k_{tool} \cdot \rho_{tool} \cdot c_{tool}}} \qquad (4.6)$$

and

$$Q_{chip} + Q_{tool} = Q_{friction}$$

The finite deformation formulation in Third Wave AdvantEdge incorporates six-noded quadratic triangular elements for the spatial discretization. The element has three corner and three mid-side nodes providing quadratic interpolation of the displacements within the element.

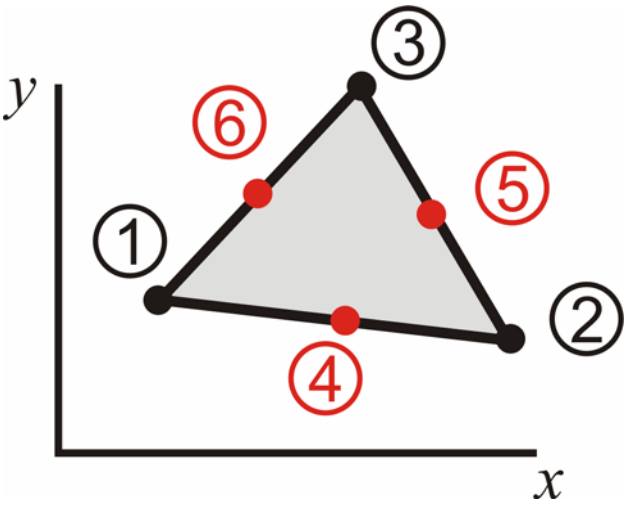

Figure 4.13: Six-noded triangular element.

The separation of nodes, thus forming the chip from the workpiece during a cutting simulation is achieved by continuous remeshing, which is also applied for the simulations with MSC.Marc. Therefore, during metal cutting the workpiece material is allowed to flow around the cutting tool edge and when the elements in this vicinity become distorted and lose accuracy, Thirdwave AdvantEdge alleviates element distortion by updating the finite element mesh periodically by refining large elements, remeshing distorted elements, and coarsening small elements.

As it is mentioned before, in a typical machining event, very high strain rates, in excess of 10^4 s^{-1} may be attained within the primary and secondary shear zones, while the remainder of the workpiece deforms at moderate or low strain rates. In order to account for a variation in the strain rate sensitivity at low and high strain rates, AdvantEdge incorporates a stepwise variation of the rate sensitivity

exponent m while maintaining continuity of stress. This leads to the following relations for low and high strain-rates.

$$\bar{\sigma} = \sigma_f\left(\varepsilon^p\right)\cdot\left(1+\frac{\dot{\varepsilon}^p}{\dot{\varepsilon}_0^p}\right)^{1/m_1}, if\ \ \dot{\varepsilon}^p \le \dot{\varepsilon}_t^p \tag{4.7}$$

$$\bar{\sigma} = \sigma_f\left(\varepsilon^p\right)\cdot\left(1+\frac{\dot{\varepsilon}^p}{\dot{\varepsilon}_0^p}\right)^{1/m_2}\cdot\left(1+\frac{\dot{\varepsilon}_t}{\dot{\varepsilon}_0^p}\right)^{1/m_1},\ if\ \ \dot{\varepsilon}^p > \dot{\varepsilon}_t^p \tag{4.8}$$

where, $\bar{\sigma}$ is the effective Von-Mises stress, σ_f is the flow stress, ε^p is the accumulated plastic strain, $\dot{\varepsilon}_0^p$ is a reference plastic strain rate, m_1 and m_2 are low and high strain-rate sensitivity exponents respectively and $\dot{\varepsilon}_t$ is the threshold strain-rate which separates the two regimes. In calculations, a local Newton-Raphson iteration is used to compute $\dot{\varepsilon}_0^p$ according to the low-rate equation, and switches to the high rate equation if the result lies above $\dot{\varepsilon}_t$.

AdvantEdge uses an adopted power hardening law with thermal softening with the governing equation being as the following.

$$\sigma_f = \sigma_0\cdot T\left(T\right)\cdot\left(1+\frac{\varepsilon^p}{\varepsilon_0^p}\right)^{1/n} \tag{4.9}$$

where, n is the hardening exponent, T is the current temperature, σ_0 is the initial yield stress at the reference temperature T_0, ε_0^p is the reference plastic strain, $T(T)$ is a thermal softening factor ranging from 0 to 1 and has a general representation depending on the workpiece material of interest.

4.3 Comparison of Finite Element Models.

Table 4.1 shows the differences of models developed by different commercial codes.

Main differences are the formulation, the separation criterion, friction law, material modeling and initiation of remeshing.

Table 4.1: Comparison of three commercial codes.

	MSC.Marc	Deform2D	Thirdwave AdvantEdge
Formulation	Static Implicit	Static Implicit	Dynamic Explicit
Chip Separation	Remeshing	Element Erase due to Damage	Remeshing
Friction Modeling	Constant Shear	Constant Shear	Coulomb
Boundary Conditions	Both edges are fixed in 2 directions	Bottom is fixed in Y direction Left is fixed in X direction	Automatic
Material Modeling	Tabulated data No extrapolation	Tabulated Data Extrapolation	Analytical Formula
Geometry	2D Plane strain	2D Plane strain	2D Plane strain
Element Type	4-Noded Bilinear Quadrilateral	4-Noded Bilinear Quadrilateral	6-noded Quadratic Triangular
Remeshing Initiation	Tool Penetration	Element Distortion	Periodic

CHAPTER 5

RESULTS AND COMPARISON

5.1 Introduction

Finite element simulations were carried out for 4 cases of experiments composing of 2 different rake angles and 2 different feed rates with MSC.Marc, DEFORM2D and Thirdwave AdvantEdge separately. Table 5.1 shows the different cutting conditions under which simulations were carried out. It should be noted that, due to a repeated software crash, simulation 3 of Deform2D could not be completed. Hence, the results of this simulation will not be available on the charts related with Deform2D.

Table 5.1: Simulations were done under four different cutting conditions.

		Feed Rates (rev/min)	
		0.05	**0.1**
Rake Angles	**20°**	Sim-1	Sim-2
	25°	Sim-3	Sim-4

In all simulations, it is made sure that steady state has reached and some more data is collected after that time. Figure 5.1 shows a typical cutting force versus increment number graph, where it can be seen that after some point steady-state is

reached. Therefore all the results presented in this work were gathered under steady state conditions.

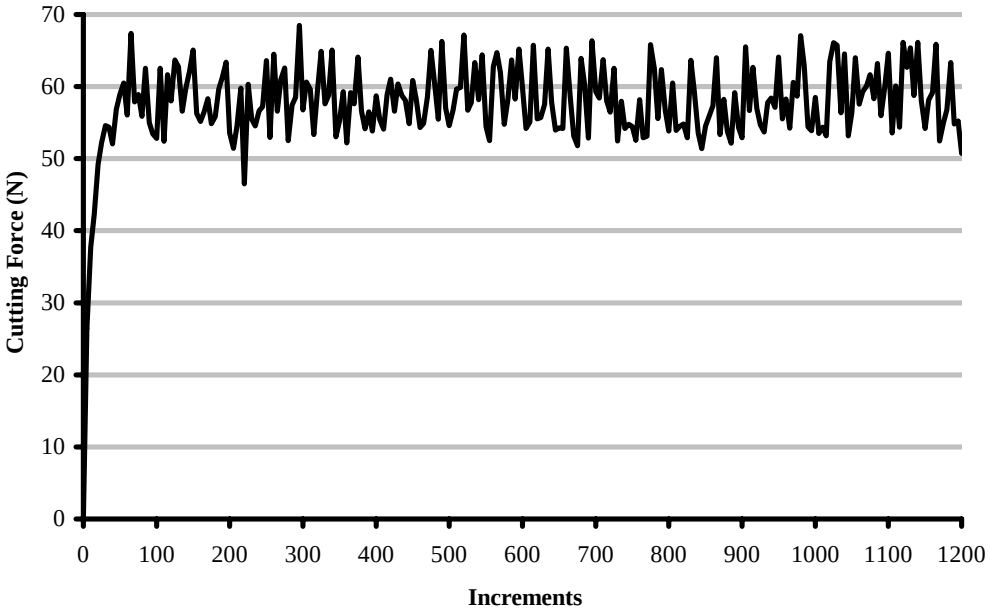

Figure 5.1: A typical diagram of cutting force versus increment number.

An analysis on the effect of friction factor to the results was also done for all of the simulations, results of which will be given on forthcoming pages of this chapter.

In addition, since in the simulations with MSC.Marc chip separation was achieved by continuous remeshing which is triggered by tool penetration, the effect of its parameters were studied. First, penetration value was altered and the effects were examined. Secondly, the time of penetration check, which can be at every iteration or at the end of increments, was changed and the results were presented. Although the effect of penetration value is not changing the results significantly (Figure 5.2), the method of penetration check leads to major changes in the results.

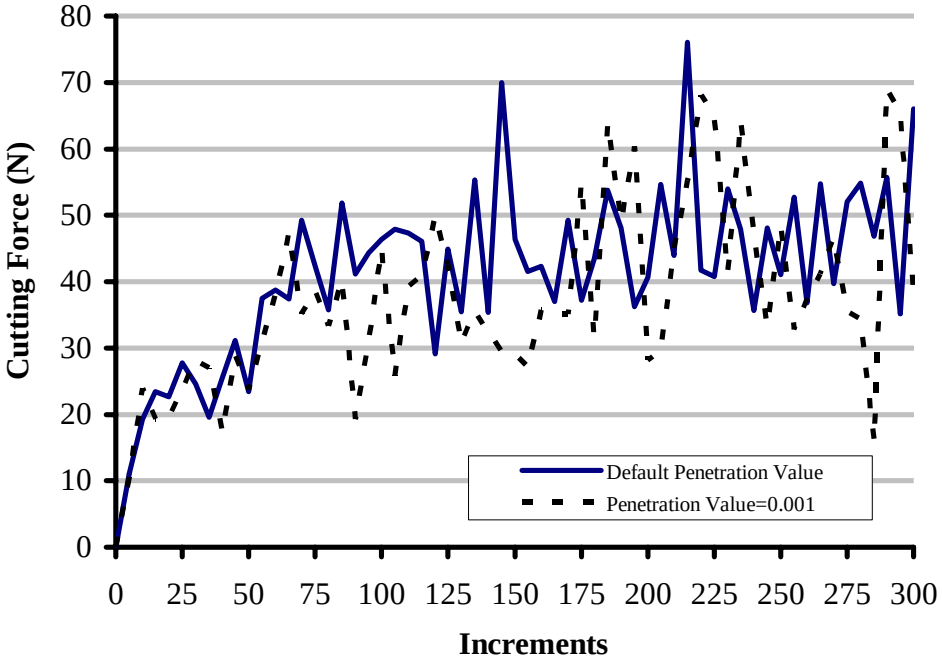

Figure 5.2: Effect of contact penetration value.

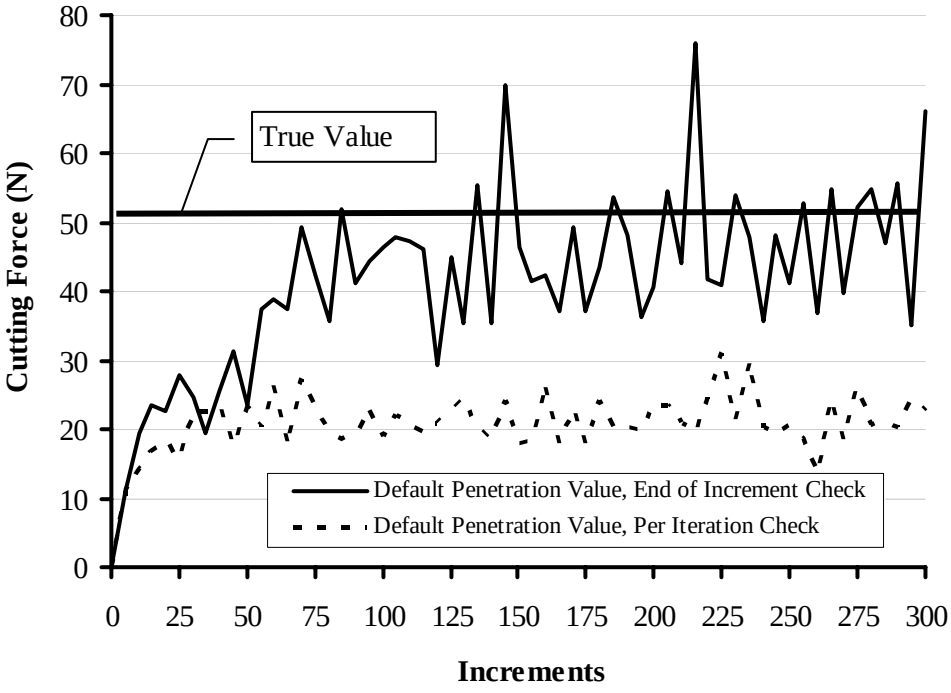

Figure 5.3: Effect of penetration check method on the results.

Figure 5.3 shows the cutting force results with two different penetration check methods for the same simulation. The simulation, in which the penetration is checked at every iteration gives results, which are almost half of the results obtained by the other method..

From the simulations, variables like stresses, strains, strain rates and temperature distribution can be obtained. However, these are all very difficult to measure experimentally. On the other hand, cutting force and thrust force can be measured relatively easily. In addition to this, contact length of chip on the rake face and the thickness of the chips, from which the shear angle can be found, can be measured.

Therefore, in this chapter, cutting force, thrust force, chip thickness, contact length and shear angle found from own experiments are compared with the simulations of three commercial codes. Also experimental results from literature are compared with the simulations. In addition, the results of simulations are verified with analytical solutions available.

5.2 Comparison with Analytical Solutions

Slip-line models by Lee & Shaffer [13], Kudo [18] and Dewhurst [19] gives an allowable range for the possible solutions of the relation between φ, γ, β. where φ, γ, β denotes shear plane angle, rake angle of the tool and chip-tool friction angle respectively. The diagrammatic view of these angles can be seen on Figure 5.4. In this study, diagrams have been drawn ($\varphi - \gamma$) against β according to Hill's [17] overstressing criterion as suggested by Childs [63]. Figure 5.5 and Figure 5.6 show allowable ranges for the rake angles of 20° and 25° respectively.

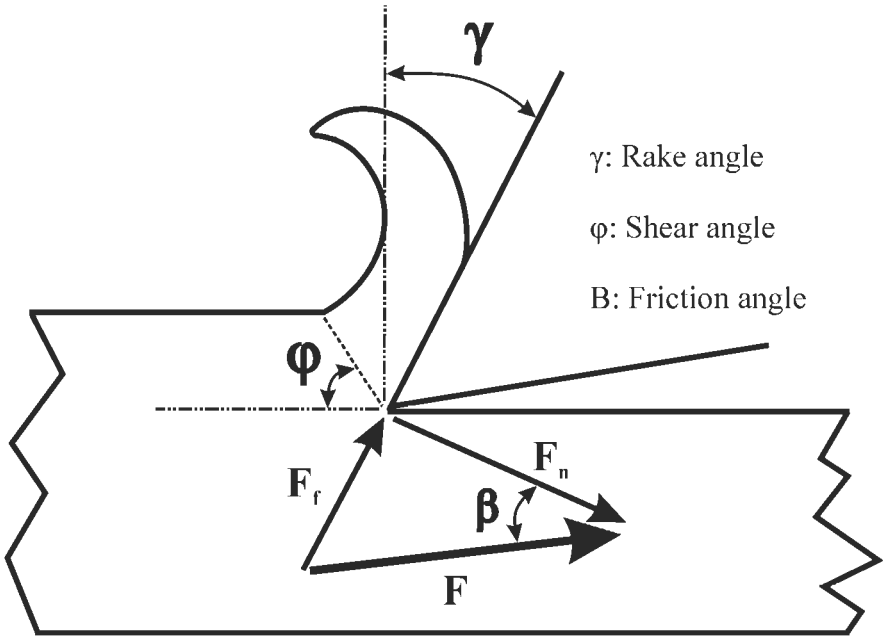

Figure 5.4: Rake, Shear and Friction angle for an orthogonal cut.

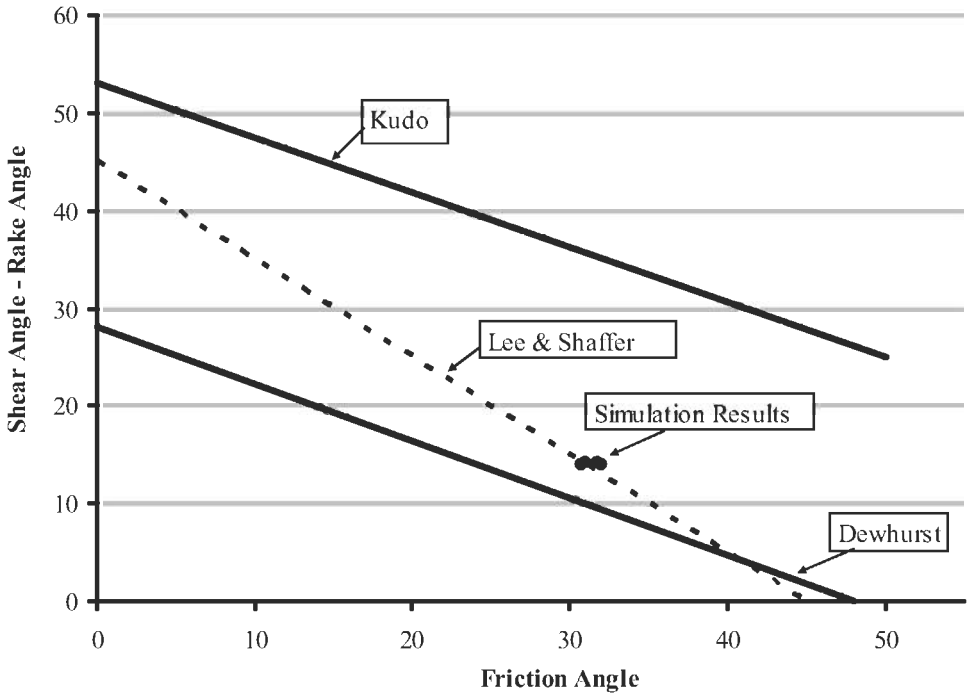

Figure 5.5: Allowable slip-line model solutions for rake angle of 20°

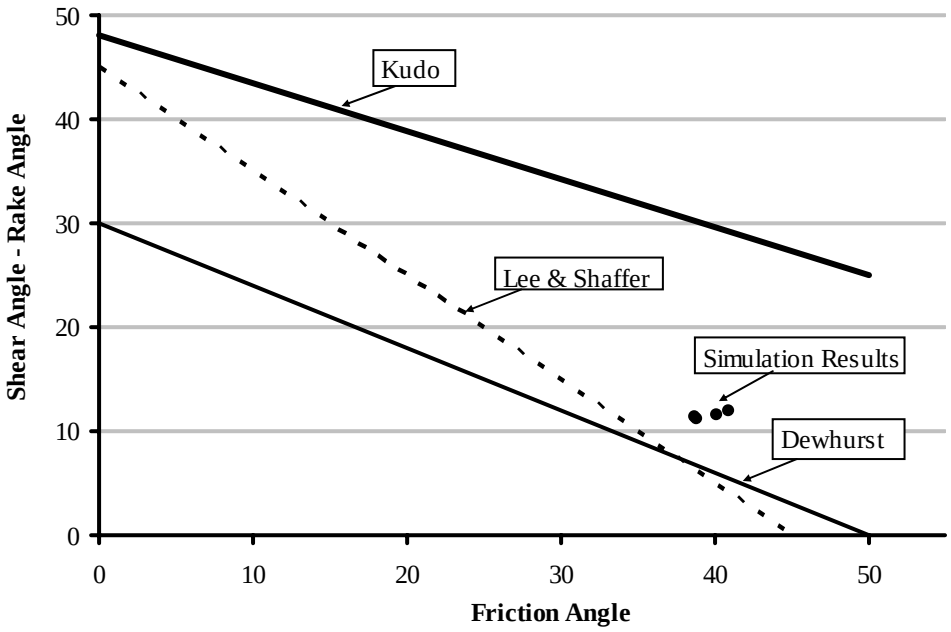

Figure 5.6: Allowable slip-line model solutions for rake angle of 25°.

The graphs also contain the simulation results of MSC.Marc. All the results are between the upper and lower bounds suggested by Kudo and Dewhurst respectively. The graph also shows that, Lee and Shaffer model, which is relatively simple than the others, gives good predictions. Especially for the rake angle of 20°, simulated results are almost coincident with the suggested solution of Lee and Shaffer.

5.3 Comparison of Chip Geometry

As it is mentioned before, thickness of the cut chips and contact lengths between the chip and rake face of the tool were measured by means of a microscope. Table 5.2 shows the experimental results, where γ is the rake angle, f is the feed rate (uncut chip thickness for 0° side cutting edge angle), a_0 is the chip thickness, φ is the shear angle and l_c is the contact length between the chip and the rake face of the tool.

Table 5.2: Experimental results of chip geometry parameters

γ	f (mm/rev)	a_0 (mm)	φ	l_c
20°	0.05	0.10	29.54	0.85
	0.1	0.27	21.73	1.10
25°	0.05	0.12	24.62	1.00
	0.1	0.21	28.24	0.90

Simulations of these experiments were carried out with the three codes for different friction factors by MSC.Marc and Deform2D and for different friction coefficients by Thirdwave AdvantEdge.

Table 5.3: Chip geometry results with MSC.Marc.

γ	f (mm)	a_0 (mm)			φ° (estimated from Strain-Rate)		
		m=0.2	m=0.4	m=0.7	m=0.2	m=0.4	m=0.7
20°	0.05	0.08	0.09	0.09	31.62	28.01	28.45
	0.1	0.16	0.18	0.22	30.77	30.97	25.61
25°	0.05	0.07	0.08	0.11	34.83	32.39	27.73
	0.1	0.15	0.18	0.22	33.63	29.01	27.39
γ	f (mm)	φ° (estimated from Chip Thickness)			l_c		
		m=0.2	m=0.4	m=0.7	m=0.2	m=0.4	m=0.7
20°	0.05	37.65	32.66	32.45	0.06	0.08	0.12
	0.1	37.20	32.45	26.83	0.09	0.11	0.22
25°	0.05	40.60	36.22	28.38	0.05	0.05	0.30
	0.1	40.07	34.32	27.68	0.10	0.15	0.22

Table-5.3 shows the results of MSC.Marc. It can be seen that chip thickness is best estimated when the friction factor is taken as 0.7. In the simulations, shear angle has been found by two ways. First, since strain-rate is significantly larger in the shear zone than the remaining parts of the workpiece, plotting the equivalent strain-rate distribution shows the place of shear zone clearly. Therefore, shear angle can be found (Figure 5.7).

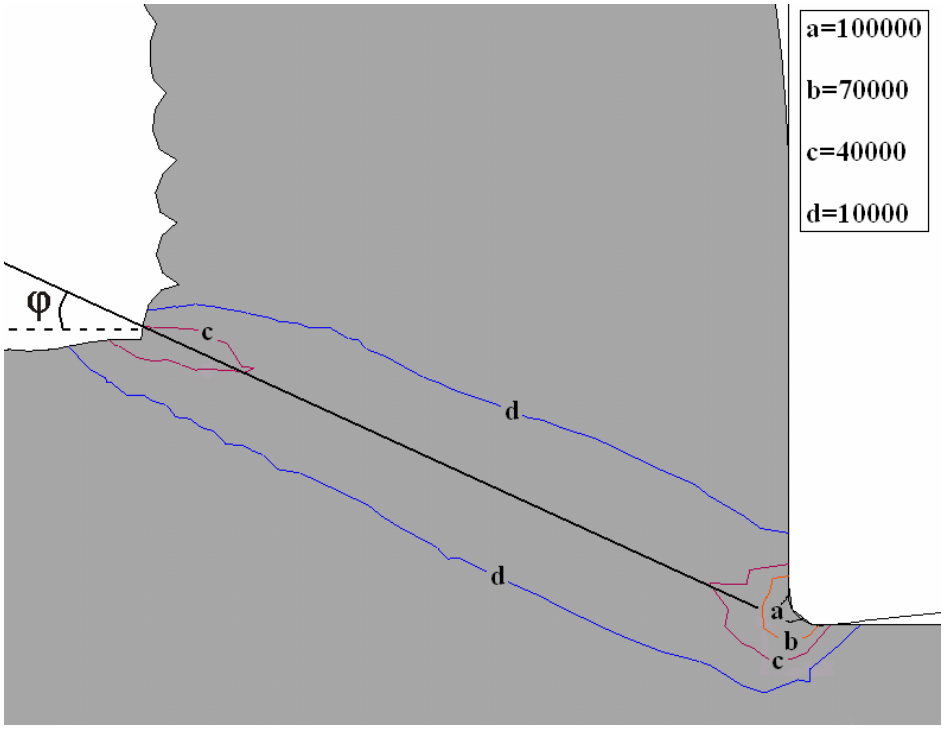

Figure 5.7: Shear angle can be found from strain-rate distribution.

Second method is that, it can be calculated from the computed chip thicknesses. Equation 1 gives shear angle as depended on rake angle and chip thickness ratio.

$$\tan(\varphi) = \frac{r_c \cdot \cos(\gamma)}{1 - r_c \cdot \sin(\gamma)} \tag{1}$$

where, φ is the shear angle, γ is the rake angle, and r_c is the chip thickness ratio, which is defined as the ratio of uncut chip thickness to cut chip thickness.

Results show that, although both are in good agreement, strain-rate distribution gives a better estimation of the shear angle. Contact lengths, on the other hand, are very poorly estimated.

Figure 5.8, Figure 5.9 and Figure 5.10 show the chip thickness, shear angle calculated from chip thickness results and contact length estimations of MSC.Marc in comparison with experiments, respectively. It can be seen that

there is a gradual convergence to the experimental results with increasing friction factor.

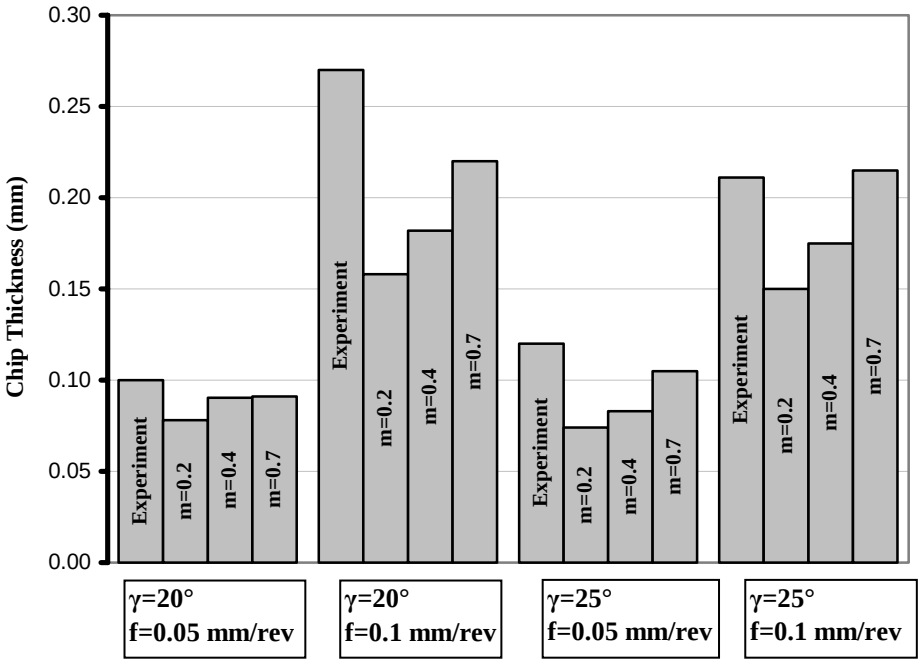

Figure 5.8: Effect of friction factor on the chip thickness results obtained by MSC.Marc.

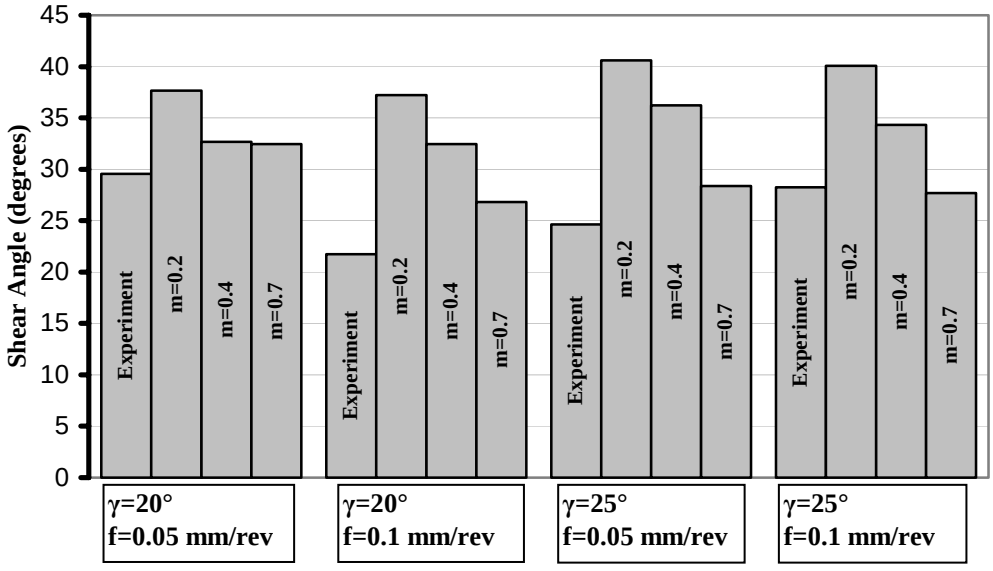

Figure 5.9: Effect of friction factor on the shear angles obtained by MSC.Marc calculated from chip thickness results.

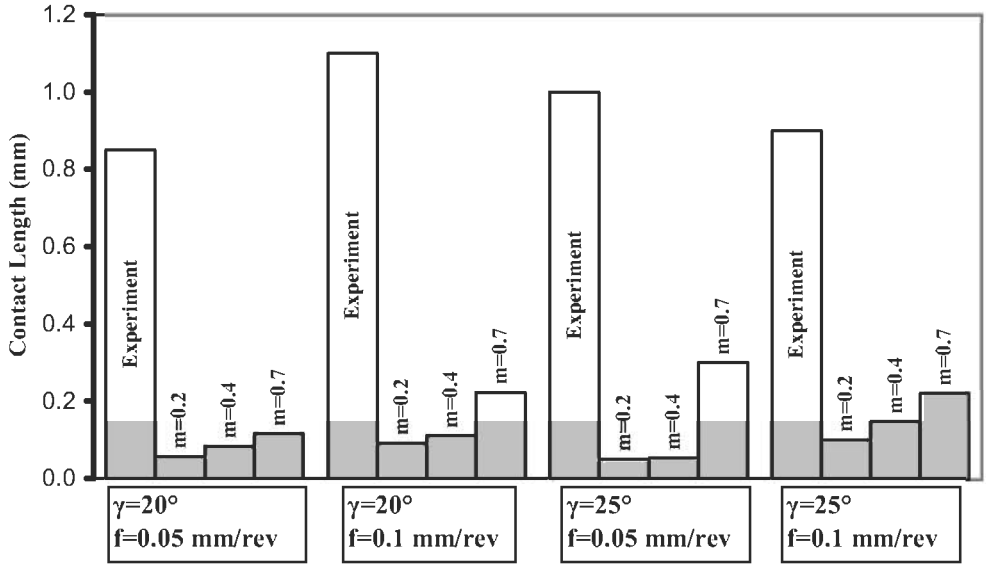

Figure 5.10: Effect of friction factor on the contact length results with MSC.Marc.

Table 5.4: Chip geometry results from Deform2D.

γ	f (mm)	a_0 (mm)			$\varphi°$ (estimated from strain-rate)		
		m=0.2	m=0.4	m=0.7	m=0.2	m=0.4	m=0.7
20°	0.05	0.07	0.08	0.09	32.74	29.60	33.69
	0.1	0.12	0.13	0.14	38.74	37.41	33.69
25°	0.05	-	0.07	0.08	-	29.93	26.57
	0.1	0.12	0.12	0.13	33.42	31.36	29.28
γ	f (mm)	$\varphi°$ (estimated from chip thickness)			l_c		
		m=0.2	m=0.4	m=0.7	m=0.2	m=0.4	m=0.7
20°	0.05	44.45	39.06	34.68	0.06	0.07	0.08
	0.1	48.27	43.28	42.99	0.11	0.13	0.14
25°	0.05	-	44.65	37.59	-	0.06	0.09
	0.1	51.25	49.38	46.26	0.12	0.11	0.12

Table 5.4 shows the results of Deform2D. Chip thicknesses are not very good estimated but again the results are best when the friction factor is 0.7. Since chip thicknesses are poorly estimated, the shear angles, which are calculated from

them, are not also in agreement with the experiments. On the other hand, strain-rate distribution gives better results. Contact lengths are again very poorly estimated.

Figure 5.11, Figure 5.12 and Figure 5.13 show the chip thickness, shear angle calculated from chip thickness estimation and contact length computations in comparison with experimental results, respectively.

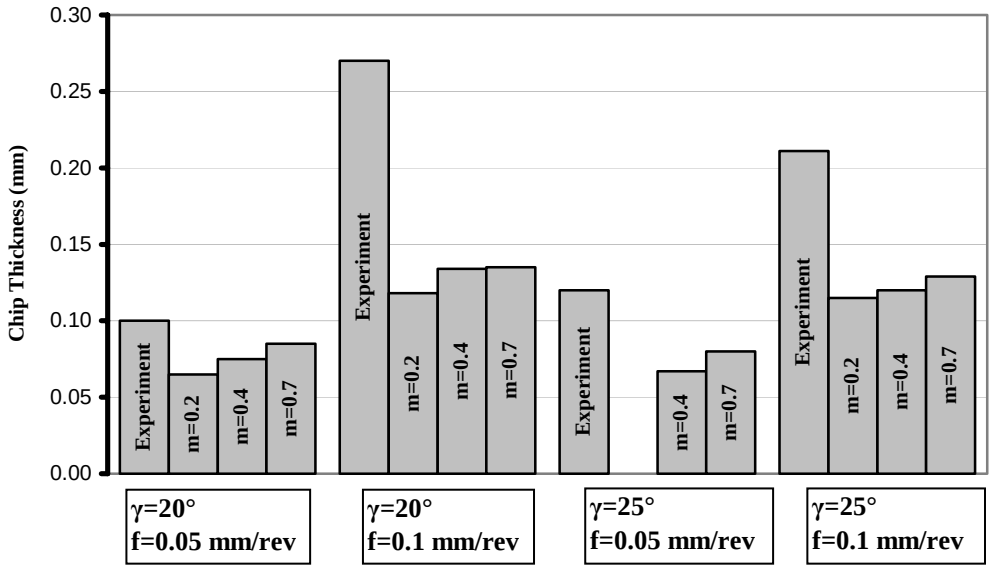

Figure 5.11: Effect of friction factor on the chip thickness results with Deform2D.

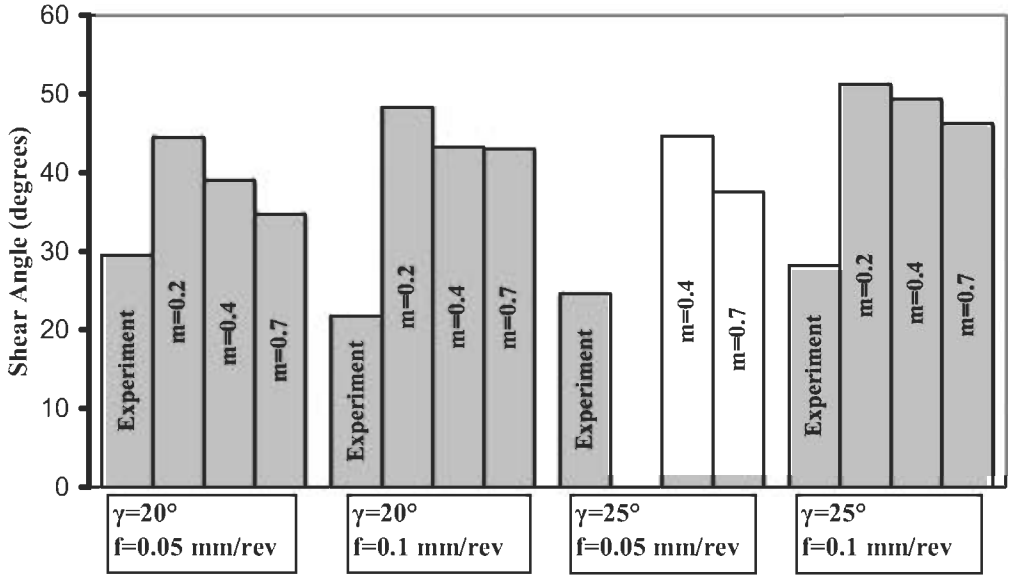

Figure 5.12: Effect of friction factor on the shear angles obtained by Deform2D calculated from chip thickness results

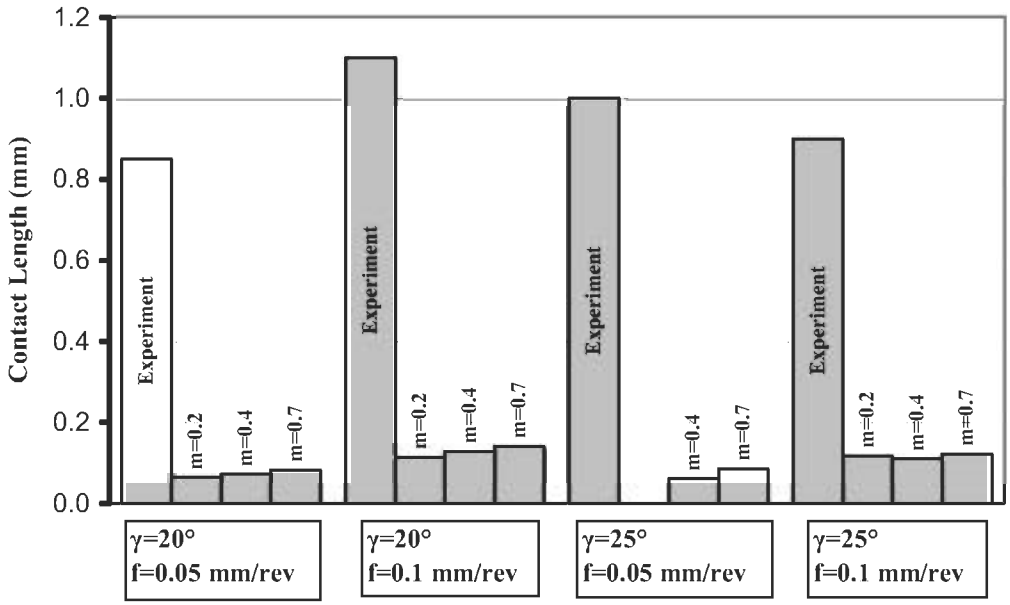

Figure 5.13: Effect of friction factor on the contact length results with Deform2D.

The former three graphs show visually that Deform2D better estimates the chip thickness and shear angle when the feed rate is smaller. However, for the bigger feed rates, there are significant errors. On the other hand, contact length is again underestimated which is also the case for the other codes.

It is also important to note that there are some inconsistencies between the simulations. For example, shear angle for the simulation, where rake angle is 20 and feed rate is 0.05 mm/rev, is estimated best at the friction factor of 0.4. However, for the other cutting conditions it is generally estimated best at the friction factor of 0.7.

Table 5.5 shows the results of Thirdwave AdvantEdge and Figures 5.14, 5.15 and 5.16 show the results in comparison with experiments on charts.

Table 5.5: Chip geometry results from Thirdwave AdvantEdge.

γ	f (mm)	a_0 (mm)			$\varphi°$ (estimated from strain-rate)		
		μ=0.2	μ=0.4	μ=0.5	μ=0.2	μ=0.4	μ=0.5
20°	0.05	0.09	0.103	0.11	27.73	27.39	27.78
	0.1	0.18	0.211	0.23	31.04	26.39	26.15
25°	0.05	0.09	0.10	0.10	32.21	31.18	26.50
	0.1	0.18	0.20	0.21	32.86	29.22	30.25
γ	f (mm)	$\varphi°$ (estimated from chip thickness)			l_c		
		μ=0.2	μ=0.4	μ=0.5	μ=0.2	μ=0.4	μ=0.5
20°	0.05	32.92	28.59	26.82	0.07	0.08	0.13
	0.1	32.02	27.97	25.89	0.13	0.17	0.24
25°	0.05	34.72	30.71	29.53	0.06	0.06	0.12
	0.1	33.93	30.24	28.35	0.13	0.15	0.17

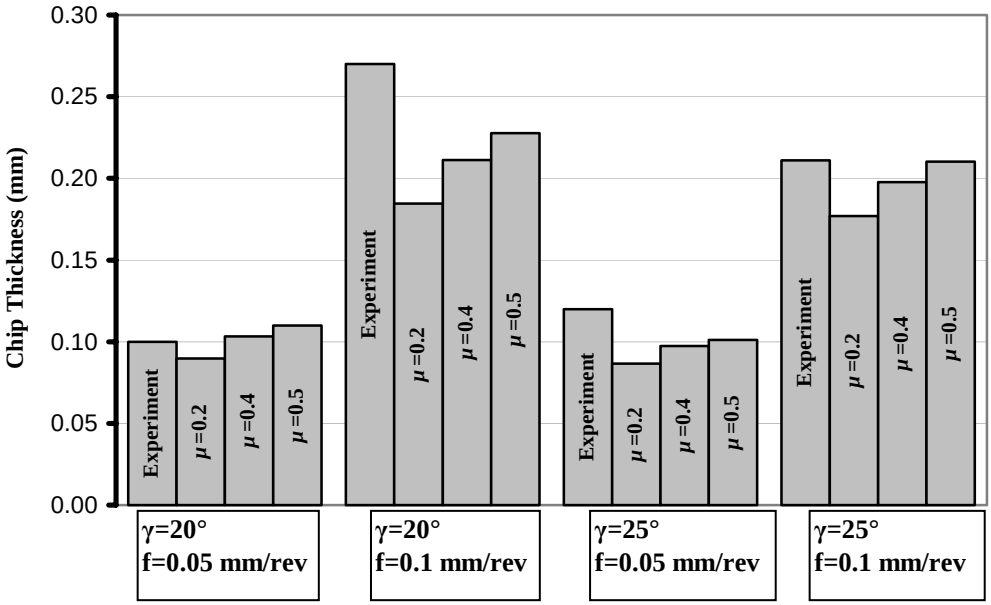

Figure 5.14: Effect of friction factor on the chip thickness results with Thirdwave AdvantEdge.

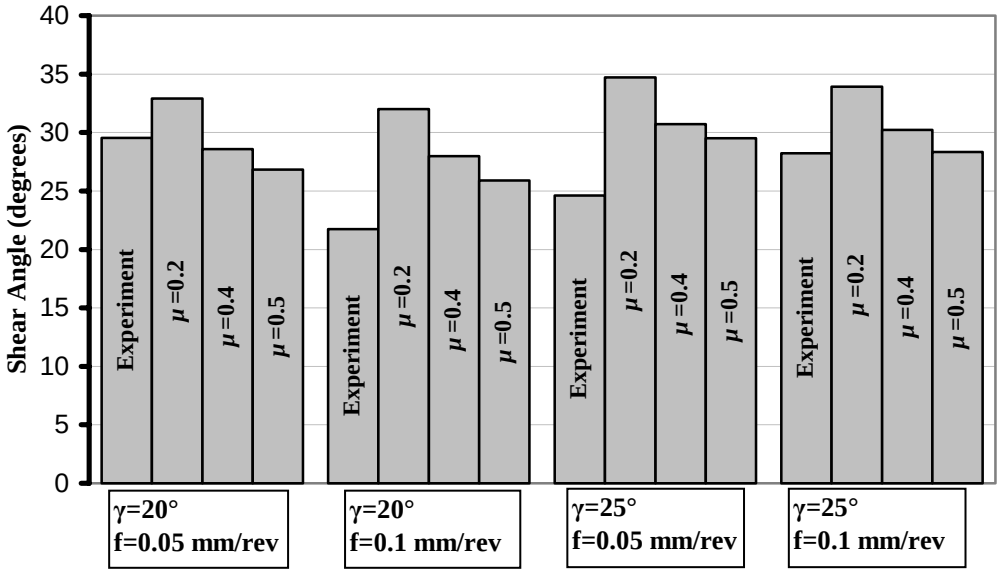

Figure 5.15: Effect of friction factor on the shear angles obtained by Thirdwave AdvantEdge calculated from chip thickness results

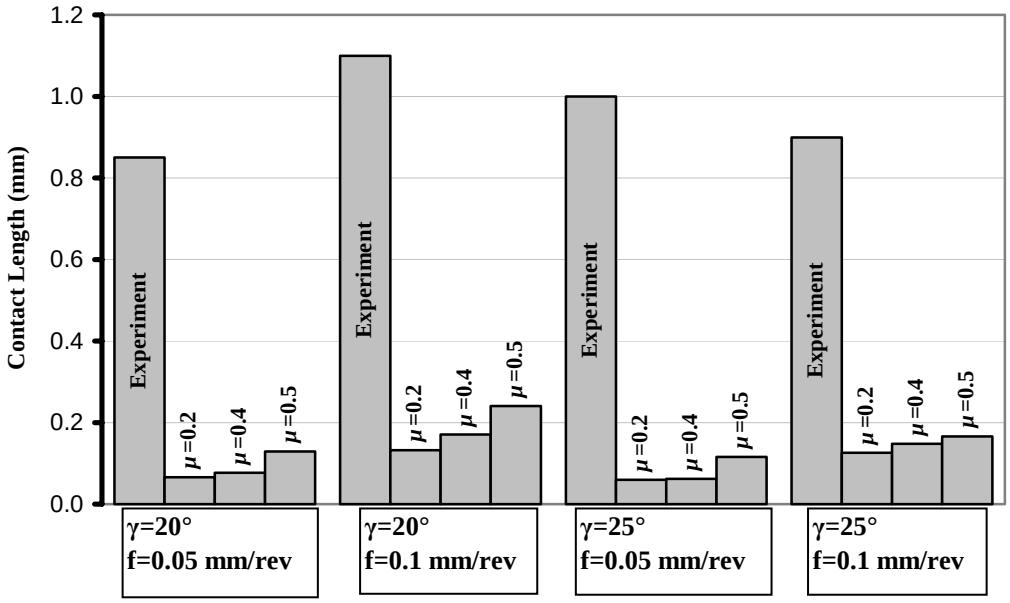

Figure 5.16: Effect of friction factor on the contact length by Thirdwave AdvantEdge

The results of both chip thickness and shear angle are in very good agreement with the experiments. As it is mentioned before, this program uses Coulomb friction model and the chip geometry results are best estimated when the friction coefficient is taken as 0.5. On the other hand, contact lengths are significantly different from the results of experiments, which was also the case with MSC.Marc and Deform2D. In addition, some inconsistencies also exist in the results of Thirdwave AdvantEdge. For example, although the chip thickness is generally underestimated by the code, for the cutting condition, where rake angle is 20° and feed rate is 0.05 mm/rev, it is overestimated after a friction coefficient of 0.4.

Figure 5.17, Figure 5.18 and Figure 5.19 show the results of chip thickness, shear angle calculated from chip thickness estimation and contact length respectively from all of the three codes with their best estimations in comparison with experimental results.

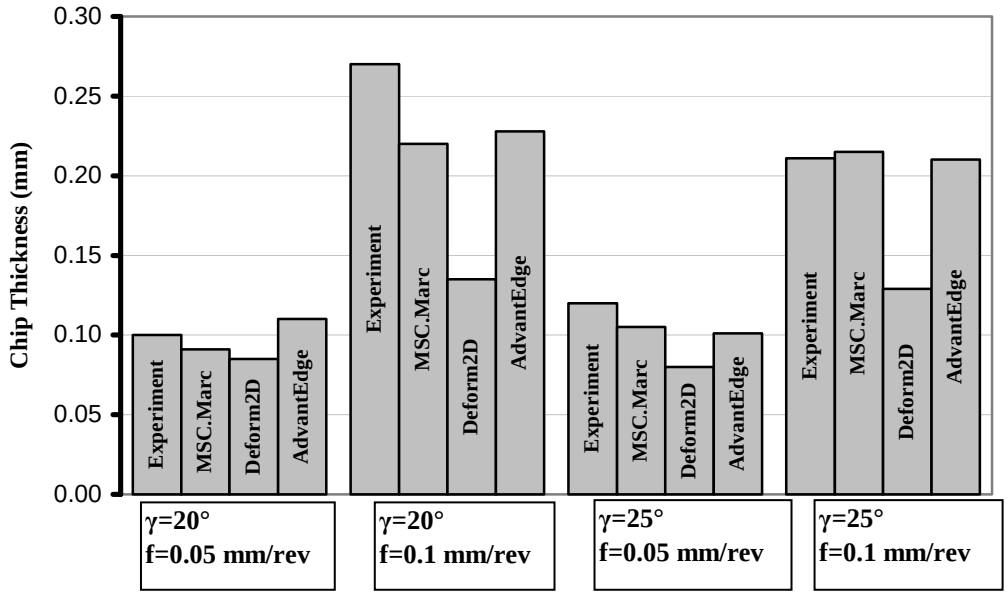

Figure 5.17: Comparison of chip thickness results from three codes with experiments. m=0.7 for MSC.Marc and Deform2D and μ=0.5 Thirdwave AdvantEdge

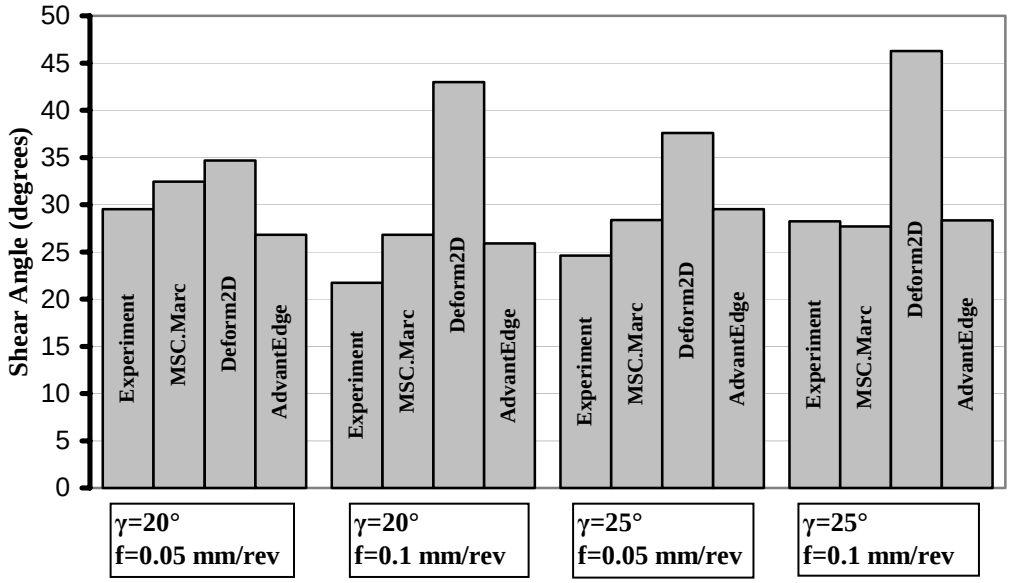

Figure 5.18: Shear angles obtained by three codes by calculating from chip thickness estimation.
m=0.7 for MSC.Marc and Deform2D and μ=0.5 Thirdwave AdvantEdge

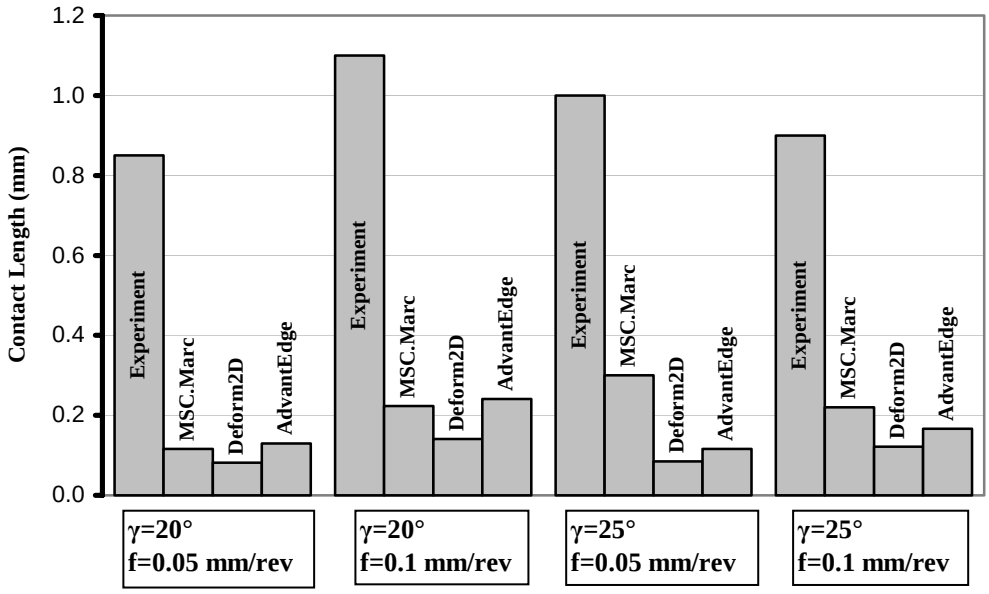

Figure 5.19: Comparison of contact length results of codes with experiments. m=0.7 for MSC.Marc and Deform2D and μ=0.5 Thirdwave AdvantEdge

In the view of above results, it can be concluded that, the three commercial codes estimate the chip thickness, and shear angle quite well. However, the estimation of contact length between the chip and rake face of the tool is not in agreement with the experiments for all of the codes.

In addition, although the results of MSC.Marc and Thirdwave AdvantEdge are similar to each other, Deform2D generally predicts different values than the other two commercial codes. The reason behind this fact might be the use of a different chip separation criterion. Because, as it is already explained in Numerical Modeling of Orthogonal Metal Cutting Chapter, MSC.Marc and Thirdwave AdvantEdge separates the chip from the workpiece by continuous remeshing, whereas, Deform2D uses Cockroft-Latham damage criterion to erase the elements at the tool tip which exceed a predefined damage value.

Table 5.6: Cutting conditions for the chip geometry verification.

	$\gamma°$	$\alpha°$	f (mm/rev)	d_c (mm)	V_c (rev/min)	m	μ
1	20°	5°	0.1	1.45	125	0.7	0.5
2	25°						

Figure 5.20 (a), (b) and (c) show simulated chip geometries as computed by MSC.Marc (m=0.7), Deform2D (m=0.7) and Thirdwave AdvantEdge (μ=0.5)respectively. All the pictures were drawn for the same tool stroke, so that, they are comparable with each other. Cutting conditions are as given in the first row of Table 5.6, where γ is the rake angle, β is the clearance angle, f is the feed rate, d_c is the depth of cut and V_c is the cutting speed. Figure 5.21, on the other hand, shows simulated chip geometries from three codes when the rake angle has been changed to 25°, while the other cutting conditions were kept constant.

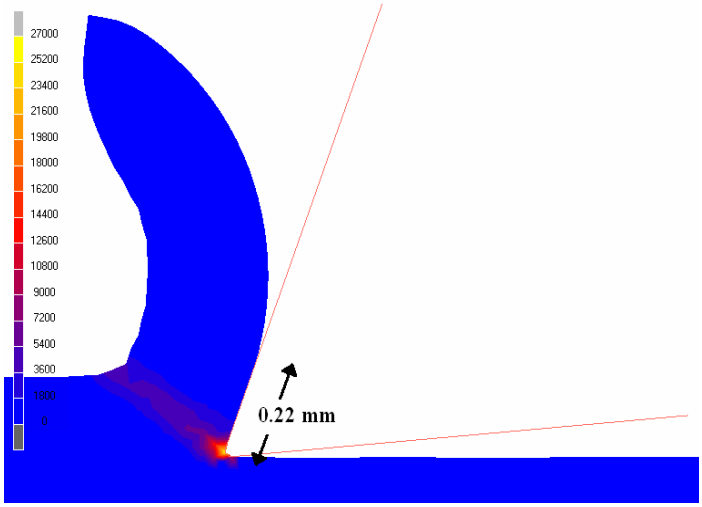

(a)

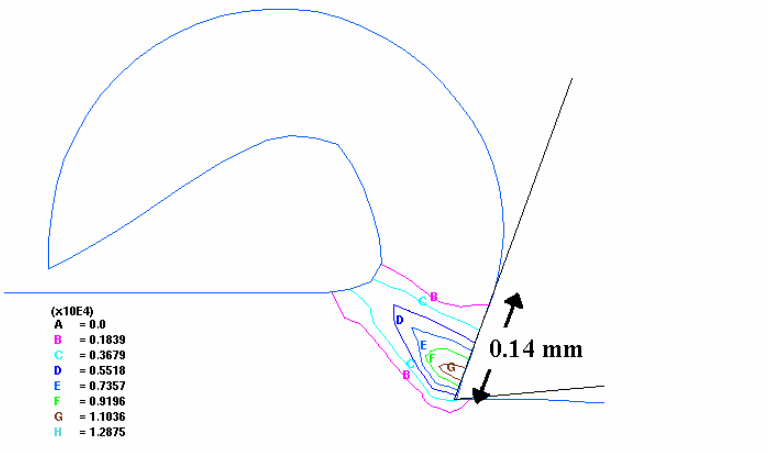

(b)

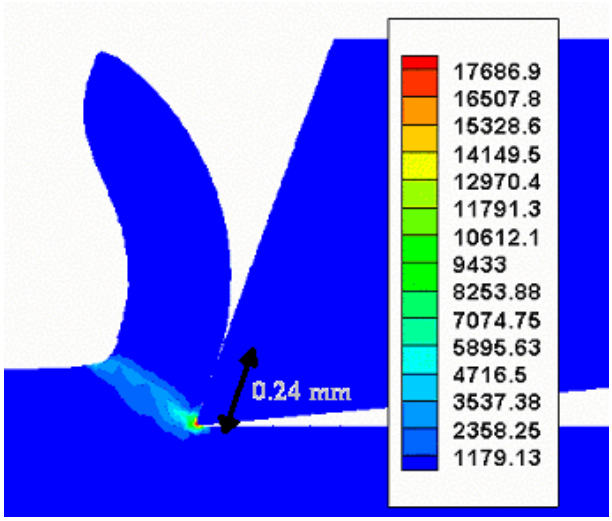

(c)

Figure 5.20: Simulated chip geometries from three commercial codes at 20° rake angle.
(a) MSC.Marc (m=0.7), (b) Deform2D (m=0.7), (c) Thirdwave AdvantEdge (μ=0.5).

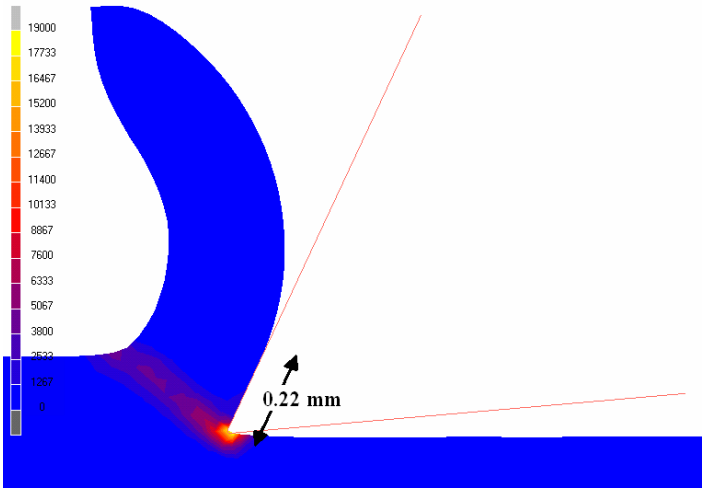

(a)

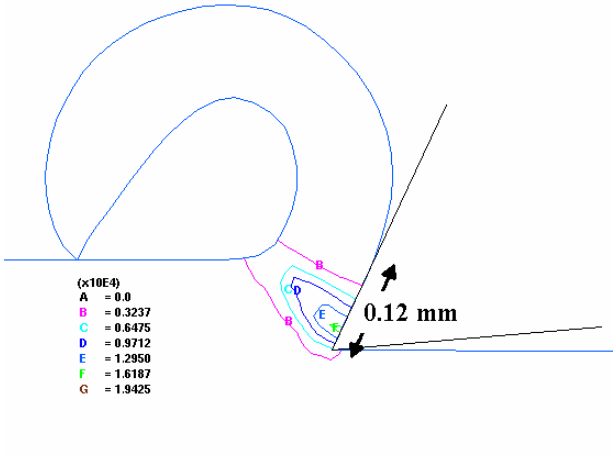

(b)

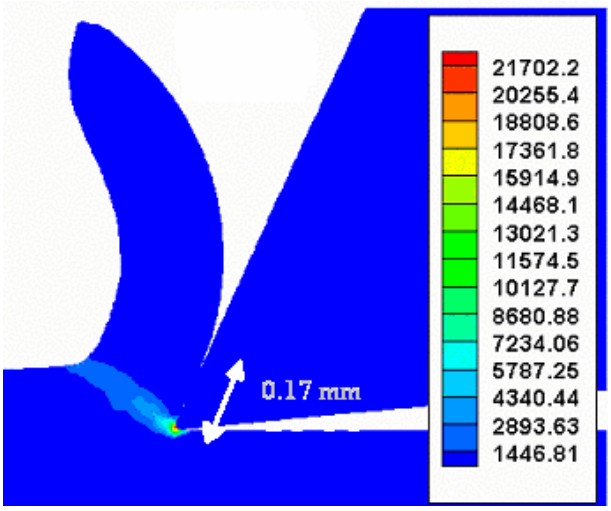

(c)

Figure 5.21: Simulated chip geometries with three commercial codes at 25° rake angle
(a) MSC.Marc (m=0.7), (b) Deform2D (m=0.7), (c) Thirdwave AdvantEdge (μ=0.5).

Above figures show that, MSC.Marc and Thirdwave AdvantEdge gives almost the same chips. On the other hand, Deform2D simulates a more curled chip. From contact length measurements, it can be seen that Deform2D simulates smaller values than the other two commercial codes, which is the reason of more curled chip. On the figures, equivalent plastic strain rate distribution, from which shear angle can be estimated, was plotted, so it can also be compared. It is seen that, MSC.Marc and Thirdwave AdvantEdge again gives very similar results, whereas Deform2D simulates a larger shear angle although the difference is small.

5.4 Comparison of Cutting Forces

Table 5.7: Experimentally measured cutting force results.

			Feed Rate (mm/rev)	
			0.05	**0.1**
Rake Angle		**20°**	62 N	132 N
		25°	59 N	128 N

Effect of friction factor on the cutting and thrust force results were also examined in this study. Table 5.8 shows the results of MSC.Marc for cutting forces. In the view of results, it can be stated that, contrary to the chip geometry variables, cutting forces are best estimated when the friction factor is small.

Table 5.8: Predicted cutting force results from MSC.Marc.

		Feed Rate (mm/rev)							
		0.05				**0.1**			
		***m*=0.1**	***m*=0.2**	***m*=0.4**	***m*=0.7**	***m*=0.1**	***m*=0.2**	***m*=0.4**	***m*=0.7**
Rake Angle	**20°**	64	65	74	90	126	126	142	174
	25°	58	60	65	86	125	121	139	171

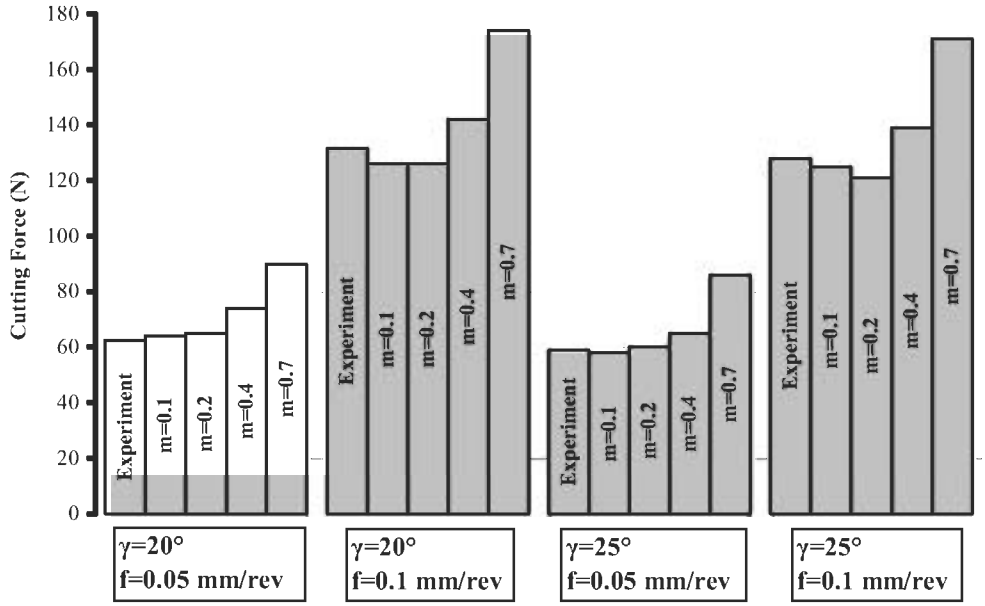

Figure 5.22: Effect of friction on the cutting force results of MSC.Marc.

Figure-5.22 shows that when the coefficient of shear friction is taken as 0.1, which is the smallest value used in the simulations, cutting forces are estimated with a maximum error of 4 %. However, it should be noted that this is not a realistic friction assumption, which might be used, for example, in a cold forming operation with a very good lubrication and a low friction coating on the die surfaces. This is not the case in metal cutting.

Table 5.9: Predicted cutting force results from DEFORM2D.

		Feed Rate (mm/rev)							
		0.05				0.1			
		m=0.1	m=0.2	m=0.4	m=0.7	m=0.1	m=0.2	m=0.4	m=0.7
Rake Angle	20°	66	63	67	76	125	110	119	136
	25°	59	-	68	72	100	100	110	125

Table 5.9 and Figure 5.23 show the estimated cutting force results with Deform2D. It can be seen that, changing friction factor does not affect the results

as much as the effects it did with the simulations of MSC.Marc. However again, cutting forces are best estimated when the friction factor is 0.1.

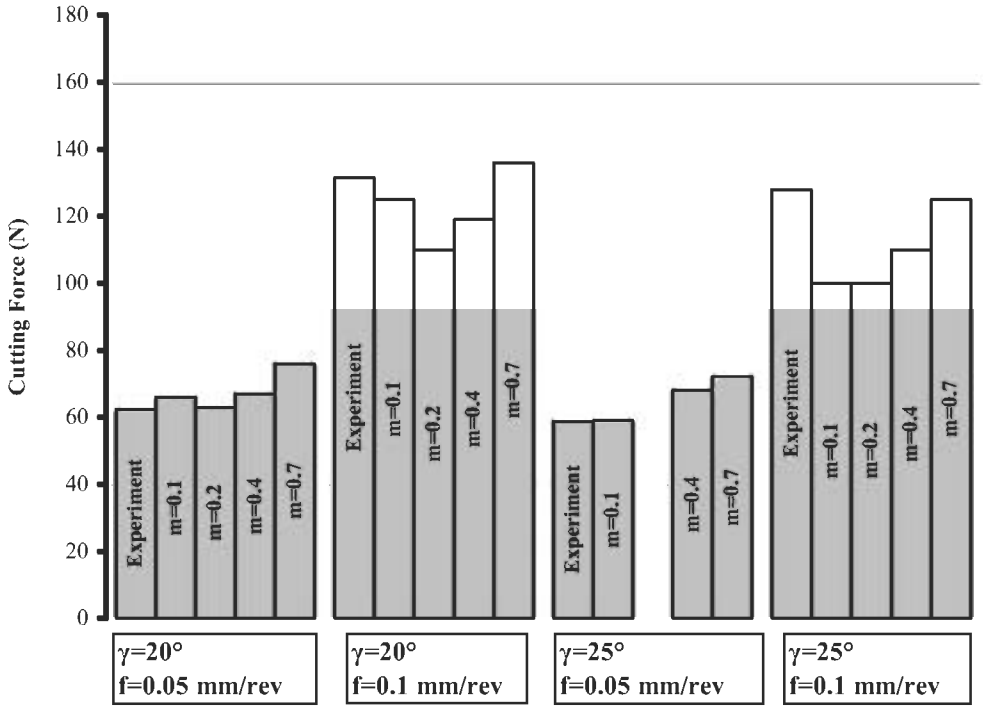

Figure 5.23: Effect of friction on the cutting force results of Deform2D.

Table 5.10 shows the cutting force results of Thirdwave AdvantEdge. The normal forces on the rake face of the tool is extremely high (generally between 350 and 500 MPa in simulations) in a cutting process. Since the coulomb friction model assumes the friction force as a fraction of normal force, it shows its effect and the forces are overestimated, which can also be seen on Figure 5.24.

Table 5.10: Predicted cutting force results from Thirdwave AdvantEdge.

		Feed Rate (mm/rev)					
		0.05			0.1		
		μ=0.2	μ=0.4	μ=0.5	μ=0.2	μ=0.4	μ=0.5
Rake Angle	20°	110	118	130	200	215	220
	25°	100	108	120	185	195	215

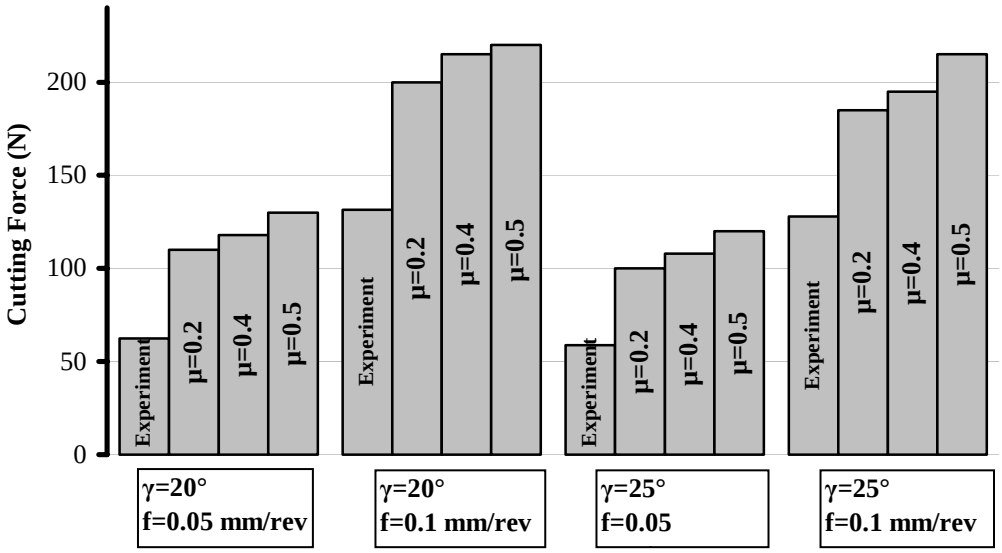

Figure 5.24: Effect of friction on the cutting force results of Thirdwave AdvantEdge.

Figure 5.25 shows the comparison of best cutting force estimations obtained by all of the three commercial codes. Therefore, m=0.7 for MSC.Marc and Deform2D and μ=0.5 for Thirdwave AdvantEdge.

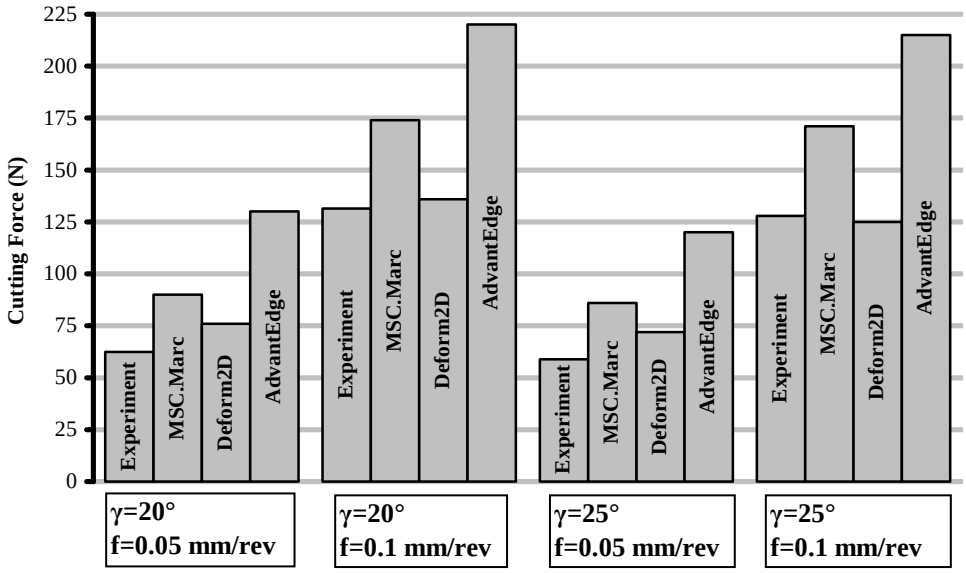

Figure 5.25: Comparison of cutting forces estimated by three codes and experiments
m=0.7 for MSC.Marc and Deform2D and μ=0.5 for Thirdwave AdvantEdge

5.5 Comparison of Thrust Forces:

Figure 5.26 shows the forces acting on the cutting tool, where F_c is the cutting force, F_t is the thrust force (or feed force), F_n is the normal force, F_f is the friction force, $(F_f)^x$, $(F_f)^y$, $(F_n)^x$ and $(F_n)^y$ are Cartesian components of friction force and normal force respectively. F, on the other hand, denotes the total force, which is the summation of either cutting force and thrust force or friction force and normal force.

In a cutting operation, thrust force is determined by the vertical components of normal and friction force. If $(F_n)^y$ is greater than $(F_f)^y$, then thrust force appears to draw the tool inside of the workpiece. Otherwise, it pushes the tool to outside of the material.

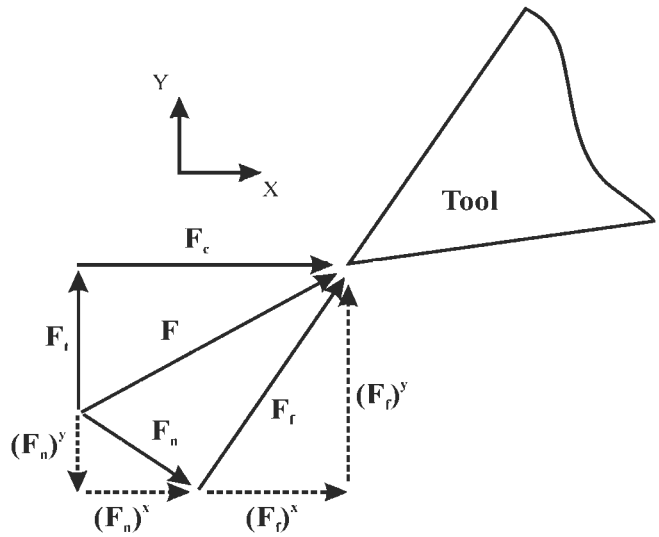

Figure 5.26: Forces acting on the tool.

Table 5.11: Experimentally measured thrust force results.

			Feed Rate (mm/rev)	
			0.05	0.1
Rake	Angle	20°	55 N	65 N
		25°	50 N	57 N

Table 5.11 is showing the experimentally measured thrust force results.

Table 5.12: Predicted thrust force results estimated by MSC.Marc.

		Feed Rate (mm/rev)							
		0.05				0.1			
		m=0.1	m=0.2	m=0.4	m=0.7	m=0.1	m=0.2	m=0.4	m=0.7
Rake Angle	20°	-13	-10	-4	12	-24	-16	-5	28
	25°	-16	-14	-9	9	-39	-26	-5	13

From the results of Table 5.12, it can be seen that, for small friction factors tool is drawn to the inside of material. The reason for this is that, for small coefficient of shear frictions, (referring to the Figure-5.26) vertical component of normal force, $(F_n)^y$, exceeds the normal component of friction force, $(F_f)^y$, hence the tool is pushed to the inside of the workpiece. When the friction factor is taken as 0.7, the results of thrust force switches to the positive values. However, there are still significant errors in the results. Figure 5.27 shows the results on a chart, where the result of friction factor can be seen easily.

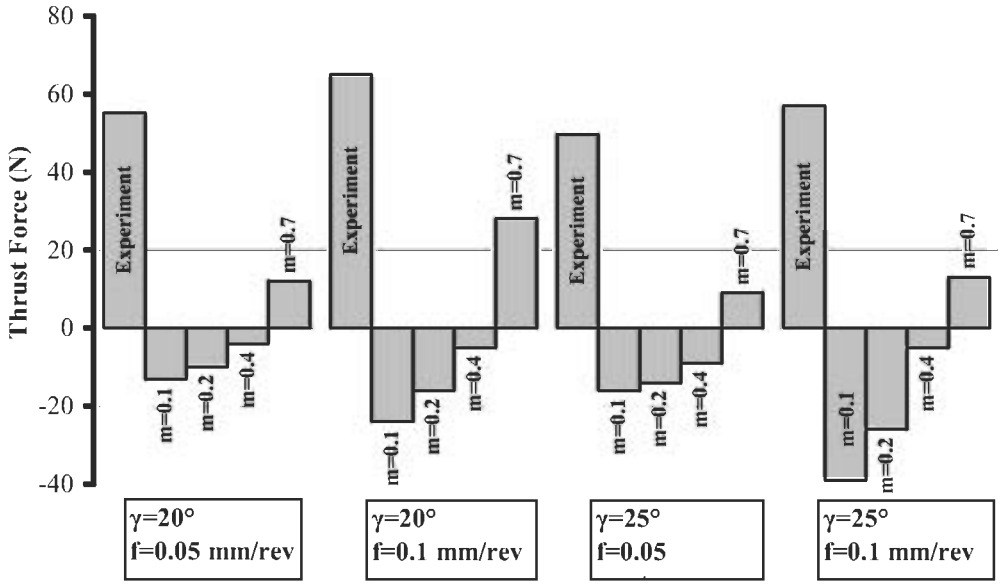

Figure 5.27: Effect of friction factor on the thrust force prediction of MSC.Marc.

Table 5.13: Predicted thrust force results from DEFORM2D.

		Feed Rate (mm/rev)							
		0.05				0.1			
		m=0.1	m=0.2	m=0.4	m=0.7	m=0.1	m=0.2	m=0.4	m=0.7
Rake Angle	20°	-23	-22	-14	-6	-42	-31	-24	-10
	25°	-25	-	-15	-8	-45	-38	-32	-21

Table 5.13 and Figure 5.28 shows the simulated thrust force results from Deform2D. It is seen that the same negative values also exists here. However, the results never switch to the positive values, even when the friction factor is increased. This means that, $(F_n)^y$ is always estimated larger than $(F_f)^y$.

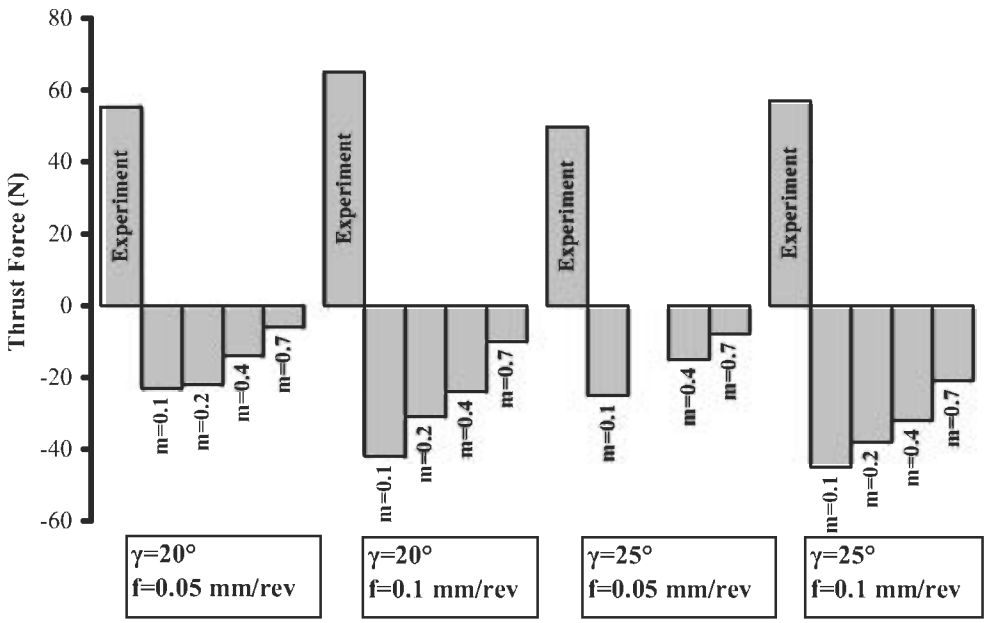

Figure 5.28: Effect of friction factor on the thrust force prediction of Deform2D.

Table 5.14: Predicted thrust force results from Thirdwave AdvantEdge.

		Feed Rate (mm/rev)					
		0.05			0.1		
		μ=0.2	μ=0.4	μ=0.5	μ=0.2	μ=0.4	μ=0.5
Rake Angle	20°	18	26	35	10	30	45
	25°	15	20	30	5	20	32

Thrust force results from Thirdwave AdvantEdge can be seen on Table-5.14. It gives the best results for the thrust forces among the three commercial codes. Since this code uses Coulomb friction model, frictional stress on the rake face is calculated from the normal stress acting on the same surface and not from the shear yield stress of the material, which results in larger friction forces. Therefore, $(F_f)^y$ becomes larger than $(F_n)^y$, which means a positive thrust force. On the above table it can also be seen that thrust forces are best estimated when the friction coefficient is taken as 0.5. Figure 5.29 shows the effect of friction coefficient on the thrust forces on a chart.

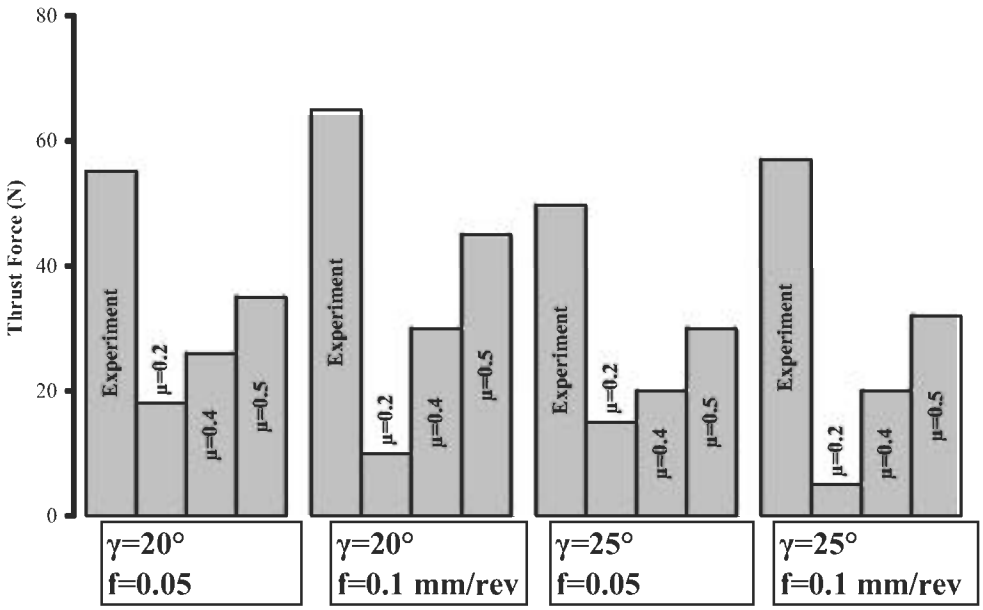

Figure 5.29: Effect of friction factor on the thrust force with Thirdwave AdvantEdge.

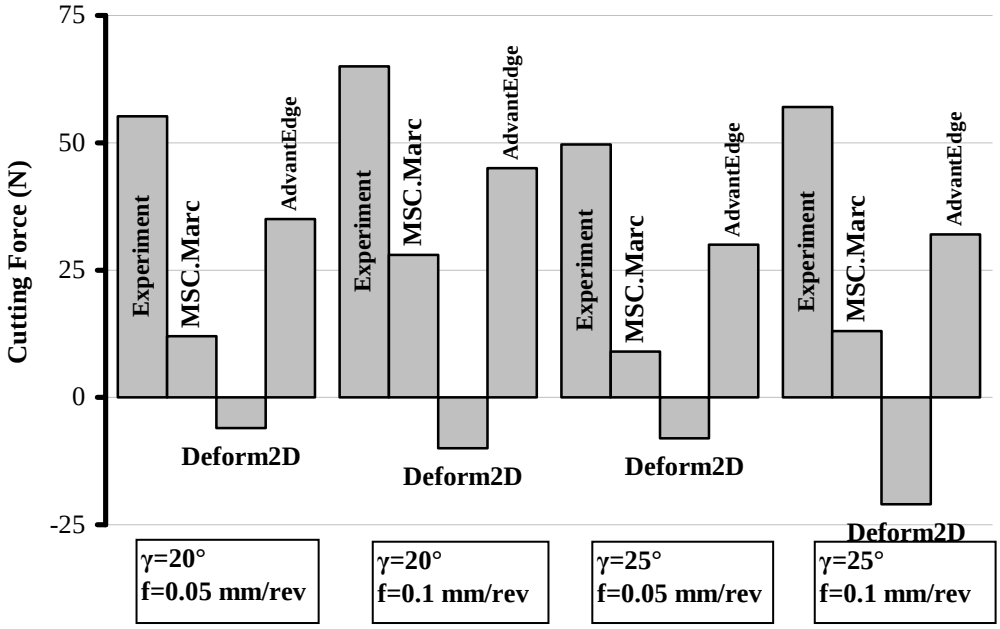

Figure 5.30: Comparison of thrust forces estimated by three codes and experiments
m=0.7 for MSC.Marc and Deform2D and μ=0.5 for Thirdwave AdvantEdge

5.6 Comparison of Simulation with the Experimental Results from Literature

Cutting and thrust forces, shear angle, contact length and temperature distribution obtained by the model of MSC.Marc in this work are compared with the results found from literature.

Movahhedy and Altintas [20] did some orthogonal metal cutting experiments with low carbon steel for the verification of their finite element model in which they have measured cutting force, thrust force, shear plane angle, contact length and maximum temperature reached.

Cutting conditions and experimental results as well as the simulation results of Movahhedy and Altintas can be found in Table 5.15.

Table 5.15: Experimental and Simulation results of Movahhedy and Altintas.

	$\gamma°$	V_c (m/min)	f (mm/rev)	d_c (mm)	F_c (N)	F_t (N)	$\varphi°$	l_c (mm)	T_{max} (°C)
Experiment	0°	150	0.1	1	174	83	18.8°	0.6	590
Simulation	0°	150	0.1	1	207	96	22°	0.55	571

Table 5.16 shows the results of this work predicted by MSC.Marc, where friction factor was taken as 0.1. It can be seen that the predicted thrust force, the shear angle and the contact length is not in agreement with the experiments. However cutting force is predicted well. Temperature prediction has an error about 9 percent which can be treated as a good estimation.

Table 5.16: Comparison with literature (m=0.1).

	$\gamma°$	V_c (m/min)	f (mm/rev)	d_c (mm)	F_c (N)	F_t (N)	$\varphi°$	l_c (mm)	T_{max} (°C)
Experiment	0°	150	0.1	1	174	83	18.8°	0.6	590
Simulation	0°	150	0.1	1	174	20	22.1°	0.168	535

Table 5.17, on the other hand, shows the results predicted by MSC.Marc with a friction factor of 0.7, which is proved to supply better results according to the comparisons with experiments performed in this work. With this simulation thrust force prediction becomes quite precise while the cutting force is overestimated. Shear angle was simulated with an error of about 5 percent. Temperature prediction becomes even better due to higher heat generation at the chip tool interface because of higher friction factor. The error is about 7 percent.

Table 5.17: Comparison with literature (m=0.7).

	$\alpha°$	V_c (m/min)	f (mm/rev)	d_c (mm)	F_c (N)	F_t (N)	$\varphi°$	l_c (mm)	T_{max} (°C)
Experiment	0°	150	0.1	1	174	83	18.8°	0.6	590
Simulation	0°	150	0.1	1	225	85	17.7°	0.45	547

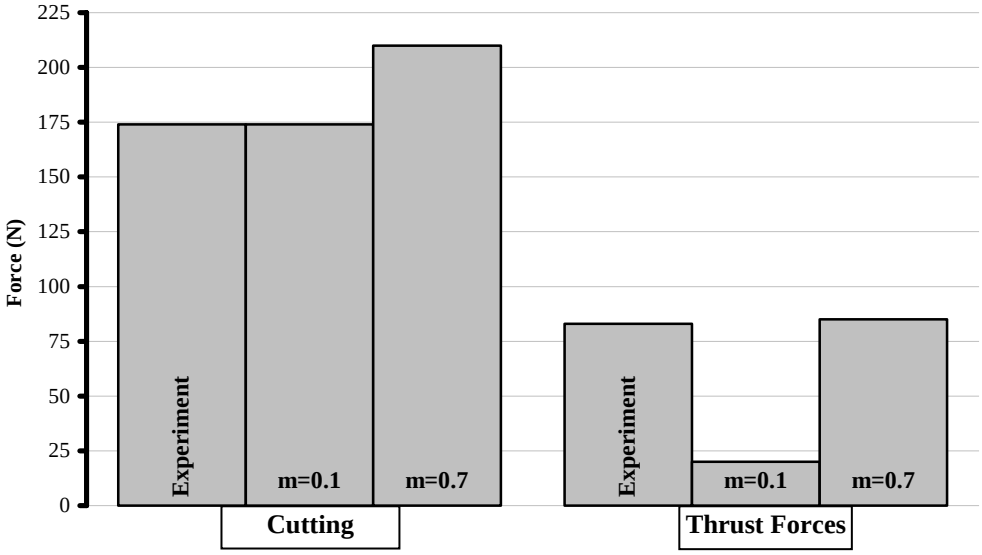

Figure 5.31: Comparison of cutting and thrust forces obtained by MSC.Marc with experiment from literature

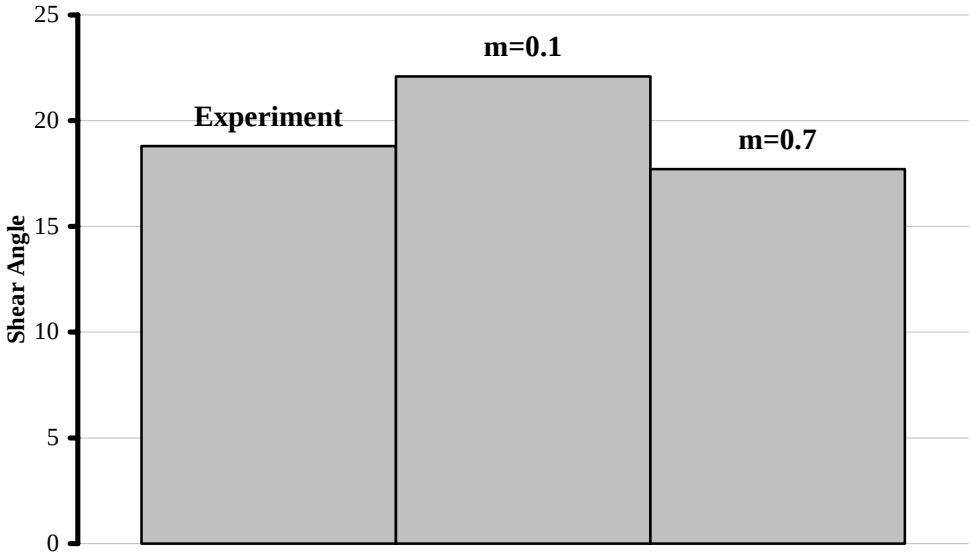

Figure 5.32: Comparison of shear angle obtained by MSC.Marc with experiment from literature

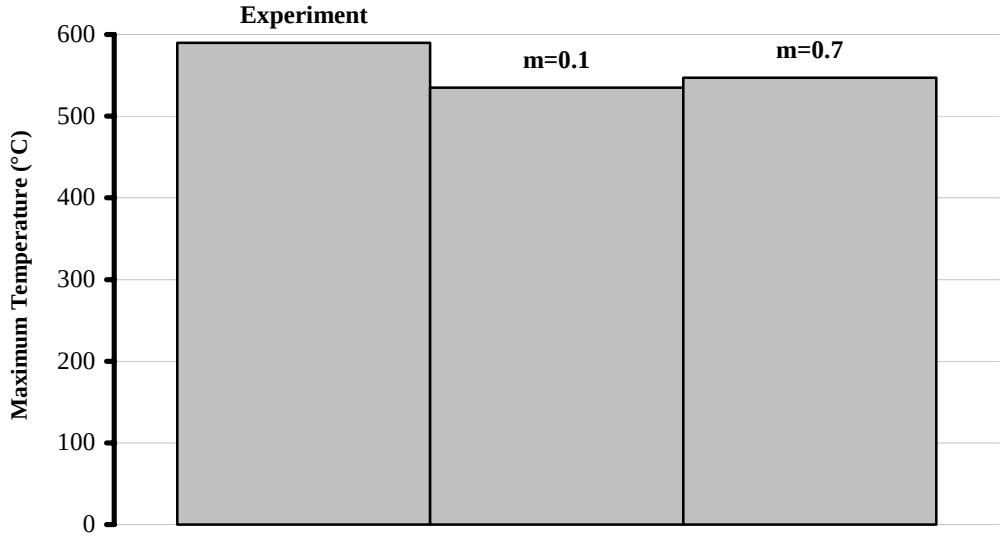

Figure 5.33: Comparison of maximum temperature estimated by MSC.Marc with experiment from literature.

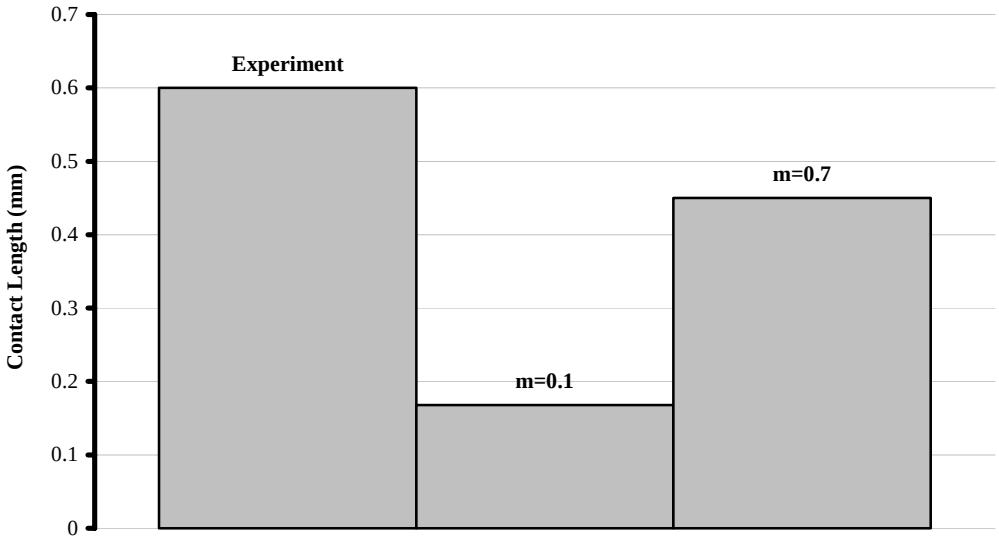

Figure 5.34: Comparison of contact length estimated by MSC.Marc with experiment from literature.

CHAPTER 6

DISCUSSION AND CONCLUSION

6.1 Introduction

In this work, finite element models of plane-strain orthogonal metal cutting operations were presented. Three commercial finite element codes, which are MSC.Marc, Deform2D and Thirdwave AdvantEdge, were used as simulation tools.

Cutting and thrust forces, shear angles, chip thicknesses and contact lengths as well as temperature, stress, strain and strain-rate distributions were predicted by the simulations. Predicted results of cutting and thrust forces were verified with experiments which is the end cutting of a tube on a lathe. In addition, in four of the experiments, chip thicknesses and rake face – chip contact lengths were measured by means of a microscope. Shear angles were calculated from the measured chip thicknesses. These variables were also compared with the simulations of three commercial codes.

In addition, effects of chip separation criterion and friction on the results were examined by running the same simulation several times with either different friction factor or with different chip separation criterion.

Results show that, recent commercial finite element codes are able simulate plane-strain orthogonal metal cutting operations. However there are some important points to mention.

6.2 Effect of Friction

In this work, two types of friction model and several friction factors or coefficients were used and the results were presented in Chapter 5.

It is seen that the friction condition at the interface of chip and tool's rake face has a major effect on the results.

For small friction factors, MSC.Marc and Deform2D predicts the cutting force quite precisely. However, very high normal forces and generally high temperatures are attained in a typical cutting operation. Under these conditions, application of a small friction factor is a not a realistic assumption. This is even more understandable when the thrust forces are examined. At the end of simulations, it is found that assumption of small friction leads to negative values of thrust forces, which means the tool is drawn to the inside of workpiece. However, experiments show that this is not the case, since thrust forces are found to be positive. The reason for this fact is that, for small friction factors, vertical component of normal force exceeds the vertical component of friction force at the rake face and the tool appears to be drawn inside of the workpiece.

Using high friction factors, on the other hand, makes the cutting force results to be overestimated, whereas, the results of chip thickness, shear angle and thrust force converges to the experimental results with increasing friction factor.

In the view of above results, it can be said that excellent results of individual variables can be obtained by tuning the friction parameter. However, since the

mechanics of the process is represented by the shear angle, friction should be tuned according to that variable.

In addition, two different friction models were used in this work. While MSC.Marc and Deform2D uses constant shear friction model, Thirdwave AdvantEdge uses Coulomb friction model by default. From the results, it is perfectly seen that Coulomb friction model leads to higher forces since it uses the contact normal stress, which is generally higher than the shear yield strength of the material, to find the frictional force at the tool-chip interface.

In a typical cutting operation, the most extreme situation of the frictional condition is the sticking of the chip to rake face, in which case the frictional stress is equal to the shear yield stress of the material. However, when using Coulomb friction model, the frictional stress is calculated from the normal contact force. Therefore, at the tool chip interface, where the normal stresses are extremely high, frictional stress may exceed the shear yield stress of the material, which is not possible. Hence, the Coulomb friction model is not very appropriate for machining purposes.

It is also important to note that no matter the type or value of friction condition at the interface of chip and tool's rake face, contact length is significantly underestimated by all of the three commercial codes.

6.3 Effect of Material Modeling

In a typical metal cutting operation, very high strain-rates (in excess of 10^4 s^{-1}) and generally high temperatures are attained at the primary and secondary shear zones while the rest of material is deforming at average strain-rates. This makes the material modeling as one of the most important parts of finite element models.

However, as presented in Chapter 4 – Numerical Modeling, material data of MSC.Marc, for example, is defined up to strain-rate of 40 s^{-1}. This is a potential error source, since in general simulated strain-rates are at the order of 10^4.

Although, the material data is not enough if the strain-rate is considered, it is seen that the results are still in good agreement with experimental measurements. This might be explained by the effects of temperature and strain-rate on the material flow curve. It is already mentioned that both high temperature and high strain-rate is acting at the same time during a cutting operation. Therefore, the material is softening due to high temperatures and hardening due to high strain-rates. Hence, it can be stated that these two effects are compensating each other, or at least they are decreasing the error associated with insufficient material data.

6.4 Effect of Chip Separation Criterion

In this present work two types of chip separation criteria were used. First is the continuous remeshing of the workpiece, which is used by MSC.Marc and Thirdwave AdvantEdge. Second is the erasing of elements at the tool tip due to cumulative damage on the element. Cockroft-Latham damage criterion, which is available as a built-in function in Deform2D, is used.

Results are showing that chip separation criterion is another important factor that should be studied very carefully when developing finite element models of metal cutting operations.

In Chapter 5, it has been shown that the simulated chip geometries by MSC.Marc and Thirdwave AdvantEdge are very similar, while the results of Deform2D are different. The reason for this difference can be related to the different chip separation criteria used in the commercial codes.

In addition, recent experiments have shown that no crack occurs in the workpiece at the tip of the tool. However, erasing of elements inherently generates a crack. On the other hand, MSC.Marc and Thirdwave AdvantEdge is using the remeshing option for the formation of chip claiming that it generates the chip totally by plastic flow. However, Figure-6.1 shows that actually a crack is generated during a remeshing step, although it is not seen before or after the remeshing step. Therefore, it can be stated that a new separation criterion is necessary for the proper modeling of chip formation.

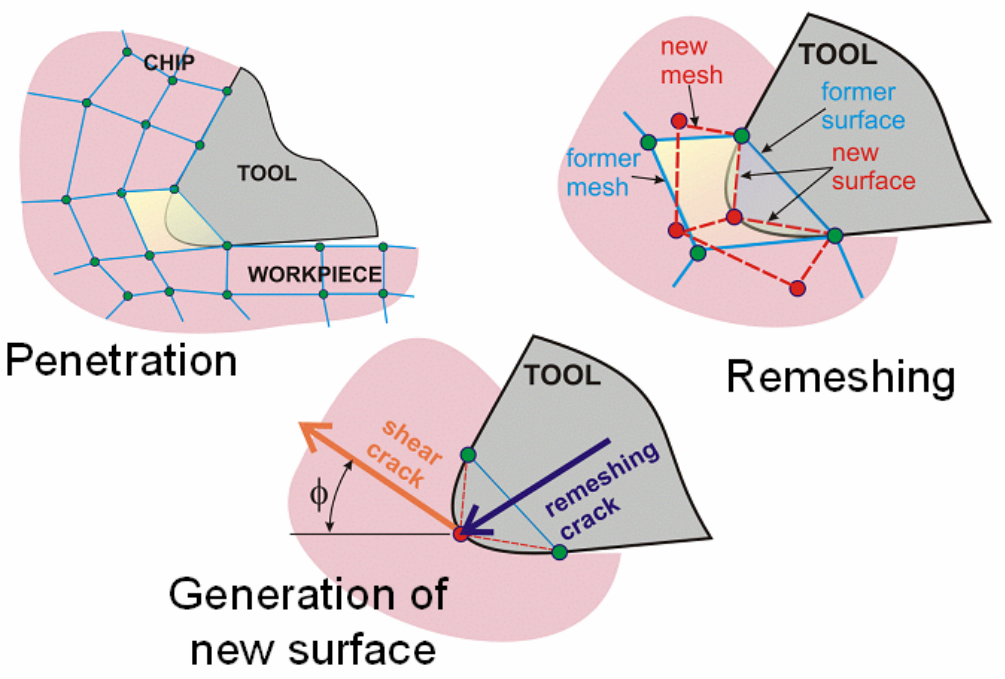

Figure 6.1: Crack generated by remeshing.

6.5 Computational Aspects

The models of MSC.Marc and Deform2D have 4975 bilinear 4-noded elements and it takes about 6-7 hours to simulate a cutting operation for one millimeter of tool stroke. Evolution of more efficient codes and quick developments in computer hardware, on the other hand, will make this kind of simulations to complete much faster and even compute the results in a real time environment.

This can be seen obviously when the computational times of simulations are observed during the thesis. At the beginning (January, 2001), simulations were taking about 2.5 days to complete on a computer with 366 MHz processor. In recent days, on the other hand, 6-7 hours of computation time is enough to complete the same simulation on a computer with 1.5 GHz processor.

Computational time of Thirdwave AdvantEdge, however, is about 2-3 hours. Model has about 2500 quadratic 6-noded triangular elements.

Although the input files are small, the output files are about 100 megabytes depending on the desired cutting length and number of outputs. Therefore, taking the other dummy files required for the simulation into account at least 200 megabytes of disk space is necessary for a similar simulation.

6.6 Conclusion

Finite Element simulations of orthogonal metal cutting operations have been performed and verified with experiments during this work. The following can be concluded according to the observations made during the thesis, which may be seen as a summary.

It is seen that individual variables can be predicted very well by tuning the friction parameter. Therefore, it is very important to assess simulation results by all process parameters, which are shear angle, chip thickness, contact length, temperature and cutting and thrust force. However it should be stated that friction parameter must be tuned according to shear angle since it is directly related with the mechanics of the process.

Another important point is the separation criterion used for the formation of chip. From the results it is seen that damage model of Deform2D is not able predict good results, in addition to the wrongly generated crack due to element erase. On

the other hand, remeshing estimates the process variables well, although it also implies the misconception of crack generation during a remeshing step. Therefore, it is believed that a new separation criterion is necessary for the application of machining simulation.

Another important outcome is that flow curve does not have a major effect on the results. It was shown that flow curves of Thirdwave AdvantEdge and MSC.Marc are different in the sense that one of them is tabulated data which is used without extrapolation, while the other is an analytical formula. However the results of simulations from these two commercial codes are very near.

6.7 Recommendation for Future Work

After the discussions and conclusion, it might be said that the most important parameters affecting the results of process variables are the separation criterion and friction. It has been seen that both are changing the results drastically.

Different separation criterion of Deform2D, for example, gave quite different results from the other two commercial codes. Therefore a powerful separation criterion, which satisfies mechanics of the process and gives good agreement with experiment in terms of measurable variables, is needed to use in machining simulations.

Friction, on the other hand, should be modeled as shear type, since Coulomb friction model is not appropriate for machining purposes.

In addition, although the results imply that workpiece flow curve does not affect the results significantly, a better material modeling may be helpful for future works.

After completing the above mentioned tasks, two dimensional orthogonal cutting simulations can be used for the prediction and optimization of all process variables. Three dimensional simulations might also be done after satisfying above tasks.

REFERENCES

[1] Mallock, A., The Action of Cutting Tool, Proceedings of Royal Society, 1881.

[2] Reuleaux, F., Über den Taylor Whitschen Werkzeugstahl, Vereın zur Beförderung des Gewerbefleissen in Preussen, 1900.

[3] Kick, F., zur Folge der Wirkungsweise des Taylor-White und des Bogler Rapid-Stahlen, Baumaterialkunde, 1901.

[4] Degarmo, E. P., Black, J. T. and Kohser, R. A., Materials and Processes in Manufacturing, Prentice-Hall International Inc., 1997.

[5] Piispanen, V., Lastunmoudostumisen Theoria, Teknillien Aika Kauskelti, 1937.

[6] Ernst, H., Machining of Metals, American Society for Metals, 1938.

[7] Merchant, M. E., Mechanics of Metal Cutting and Type 2 Chip, Journal of Applied Physics, 1945.

[8] Palmer, W. B. and Oxley, P. L. B., Mechanics of Orthogonal Machining, Proceedings of Institute of Mechanical Engineers, 1959.

[9] Okushima, K. and Hitomi, K., An Analysis of the Mechanism of Orthogonal Cutting and Its Application to Discontinuous Chip Formation, Journal of Engineering for Industry, 1961.

[10] Salomon, C., German Patent No: 523594 (February, 1931).

[11] Vaughn, R. L., Recent Developments in Ultra High Speed Machining, American Society of Tool and Manufacturing Engineers, 1960.

[12] Kobayashi, S., Thomsen, E. G., Some Observation of the Shearing Process in Metal Cutting, Journal of Engineering for Industry, 1959.

[13] Lee, E. H. and Shaffer, B. W., Theory of Plasticity Applied to the Problem of Machining, Journal of Applied Mechanics, 1951.

[14] Oxley, P. L. B., A Strain Hardening Solution for the Shear Angle in Orthogonal Metal Cutting, International Journal of Mechanical Sciences, 1951.

[15] Coding, B. N., A Yield Criterion Applied to the Shear Angle Relationship, Microtecnic, 1960.

[16] Sata, T. and Yoshikawa, H., A New Expression for the Shear Angle in Metal Cutting, American Society of Mechanical Engineers, 1963.

[17] R. Hill, The Mechanics of Machining: A New Approach, Journal of Mechanics and Physics of Solids, 1954.

[18] H. Kudo, Some New Slip-Line Solutions for Two Dimensional Steady State Machining, International Journal of Mechanical Sciences, 1965.

[19] P. Dewhurst, On the Non-Uniqueness of the Machining Process, Proceeding of Royal Society, 1978.

[20] Shaw, M. C. and Mamin, P. A., Friction Characteristics of Sliding Surfaces Undergoing Sub-Surface Plastic Flow, Journal of Basic Engineering, 1960,

[21] Thomsen, E. G., Lapsey, J. T. and Grassi, R. C., Deformation Work Absorbed by the Workpiece During Metal Cutting, Transactions of American Society of Mechanical Engineers, 1953.

[22] Takeyama, H. and Usui, E., A Photoelastic Analysis of Machining Stresses, Journal Engineering for Industry, 1960.

[23] Zorev, N. N., Interrelationship Between Shear Process Occuring Along Tool Face and Shear Plane in Metal Cutting, American Society of Mechanical Engineers, 1963.

[24] Wallace, P.W. and Boothroyd, G., Tool Forces and Tool-Chip Friction in Orthogonal Machining, Journal of Mechanical Engineering Science, 1964.

[25] Bridgman, P. W., Flow Phenomena in Heavily Stressed Metals, Journal of Applied Physics, 1937.

[26] Bridgman, P. W., On Torsion Combined with Compression, Journal of Applied Physics, 1943.

[27] Crossland, B., The effect of Fluid Pressure on the Shear Properties of Metals, Proceeding of the Institute of Mechanical Engineers, 1954.

[28] Backer, W. R., Marshall, E. R. and Shaw, M. C., The Size Effect in Metal Cutting, Transactions of American Society of Mechanical Engineers, 1952.

[29] Herring, C. and Galt, J. K., Elastic and Plastic Properties of Very Small Metal Specimens, Phys. Rev., 1955.

[30] Piper, W. W. and Roth, W. L., Perfect Crystals of Zink Sulphide, Phys. Rev., 1953.

[31] Shaw, M. C. and Finnie, I., The Shear Stresses in Metal Cutting, Transactions of American Society of Mechanical Engineers, 1955.

[32] Cotrell, A. H., Conference on the Properties of Metal at High Rates of Strain, Institution of Mechanical Engineers, 1957.

[33] Strenkowski, J.S. and Caroll, J. T., A Finite Element Model of Orthogonal Cutting, Journal Engineering for Industry, 1985.

[34] Strenkowski, J. S. and Mitchum, G. L., An Improved Finite Element Model of Orthogonal Cutting, Proceedings of North American Manufacturing Res. Conf., 1987.

[35] Komvopoulos, K. and Erpenbeck, S. A., Finite Element Model of Orthogonal Metal Cutting, Journal of Engineering for Industry, 1991.

[36] Shih, A. and Yang, H. T. Y., Experimental and Finite Element Predictions of Residual Stresses due to Orthogonal Metal Cutting, International Journal for Numerical Methods in Engineering, 1993.

[37] Shih, A., Finite Element Simulation of Orthogonal Metal Cutting, Journal of Engineering for Industry, 1995.

[38] Ueda, K. and Manabe, K., Chip Formation in Microcutting of an Amorphous Metal, Annals of CIRP, 1992.

[39] Howerton, D. H., Strenkowski, J. S. and Bailey, J. A., Prediction of Built-Up Edge Formation in Orthogonal Cutting of Aluminum, Department of Mechanical and Aerospace Engineering, North Carolina State University, Rayleigh, NC 27695-7910.

[40] Strenkowski, J. S. and Kyoung-Jin Moon, Finite Element Prediction of Chip Geometry and Tool/Workpiece Temperature, Journal of Engineering for Industry, 1990.

[41] Tyan, T. and Yang, W. H., Analysis of Orthogonal Metal Cutting Process, International Journal of Numerical Methods in Engineering, 1992.

[42] Muraka, P. D., Barrow, G. and Hindua, S., Influence of the Process Variable on the Temperature Distribution in Orthogonal Machining Using Finite Element Method, International Journal of Mechanical Science, 1979.

[43] Stevenson, M. G., Wrigt, P. K. and Chow, J. G., Further Development in Applying the Finite Element Method to the Calculation of Temperature Distribution in Machining and Comparison with Experiment, Journal of Engineering for Industry, 1983.

[44] Toshimichi, M., Nabuhiro, S. and Sheng, L., Combined Stress, Material Flow and Heat Analysis of Orthogonal Micromachining of Copper, Annals of CIRP, 1993.

[45] Maekawa, K. and Shirakashi, T., Recent Progress of Computer Aided Simulation Flow and Tool Damage in Metal Cutting, Journal of Engineering Manufacture, 1996.

[46] Iwata, K., Osakada, K. and Terasaka, Y., Process Modelingof Orthogonal Cutting by the Rigid Plastic Finite Element Method, Journal of Engineering Materials and Technology, 1984.

[47] Liu, C. R. and Lin, Z. C., Effect of Shear Plane Boundary Condition on Stress Loading in Orthogonal Machining, International Journal of Mechanical Science, 1985.

[48] Lin, Z. C. and Lin, S. Y., A Coupled Finite Element Model of Thermo Elastic Plastic Large Deformation for Orthogonal Cutting, International Journal of Engineering Materials and Technology, 1992.

[49] Arola, D. and Rumulu, M., Orthogonal Cutting of Fiber Reinforced Composites: A Finite Element Analysis, International Journal of Mechanical Science, 1997.

[50] Caroll, J. T. and Strenkowski, J. S., Finite Element Model of Orthogonal Cutting with Application to Single Point Diamond Turning, International Journal of Mechanical Science, 1988.

[51] Zang, B. and Bagchi, A., Finite Element Simulation of Chip Formation and Comparison with Machining Experiment, Journal of Engineering for Industry, 1994.

[52] A. J. Shih, Finite Element Analysis of Orthogonal Metal Cutting Mechanics, International Journal of Machine Tools and Manufacture, 1996.

[53] E. Ceretti, P. Fallbohmer, W. T. Wu, T. Altan, Application of 2D FEM to Chip Formation in Orthogonal Cutting, Journal of Materials Processing Technology, 1996.

[54] Ceretti, E., Lucchi, M. and Altan, T., FEM Simulation of Orthogonal Cutting: Serrated Chip Formation, Journal of Materials Processing Technology, 1999.

[55] Shatla, M., Kerk, C. and Altan, T., Process Modeling in Machining. Part I: Determination of Flow Stress Data, International Journal of Machine Tools and Manufacture, 2001.

[56] Oxley, P. L. B., Mechanics of Machining, An Analytical Approach to Assessing Machinability, Halsted Press, NewYork, 1989.

[57] Mekawa, K. and Maeda, M., Simulation Analysis of Three Dimensional Chip Formation Process – Fem Formulation and a few Results, Japanese Society of Precision engineering, 1993.

[58] Borouchaki, H., Cherouat, A., Laug, P. and Saanouni, K., Adaptive Remeshing for Ductile Fracture Prediction in Metal Forming, C. R. Mecanique, 2002.

[59] Shi, G., Deng, X. and Shet, C., A Finite Element Study of the Effect of Friction in Orthogonal Metal Cutting, Finite Elements in Analysis and Design, 2002.

[60] Lazoglu, İ., Altıntaş, Y., Prediction of Tool and Chip Temperature in Continuous and Interrupted Machining, International Journal of Machine Tools and Manufacture, 2002.

[61] Shet, C. and Deng, X., Residual Stresses and Strains in Orthogonal Metal Cutting, International Journal of Machine Tools and Manufacture, 2003.

[62] Klocke, F., Messner, G. and Hoppe, S., Simulation of Tool Wear and Workpiece Integrity in Machining, CIRP Workshop on Modeling in Machining Process, Ontario, Canada, 2003.

[63] T. H. C. Childs, Numerical Experiments on Material Properties and Machining Parameters Influencing Normal Contact Stress Between Chip and Tool, University of Leeds School of Mechanical Engineering.